THESIS FOR THE DEGREE OF DOCTOR OF PHILOSOPHY

Nitrous Oxide Formation over Zeolite-based Catalysts during Ammonia-SCR: The Effect of Framework Structure, Acidity, and Copper Content

Ghodsieh Isapour

Department of Chemistry and Chemical Engineering

CHALMERS UNIVERSITY OF TECHNOLOGY

Göteborg, Sweden 2023

Nitrous Oxide Formation over Zeolite-based Catalysts during Ammonia-SCR: The Effect of Framework Structure, Acidity, and Copper Content

Ghodsieh Isapour

ISBN 978-91-7905-806-7

© Ghodsieh Isapour, 2023.

Doktorsavhandlingar vid Chalmers tekniska högskola

Ny serie Nr. 5272

ISSN 0346-718X

Department of Chemistry and Chemical Engineering
Chalmers University of Technology
SE-412 96 Göteborg
Telephone +46 31 772 1000

Cover:
Selective catalytic reduction of NO_x by NH_3 over copper SSZ-13 zeolite. Illustrator of SSZ-13 zeolite cage: Yingxin Feng

Typeset in LaTeX using the kaobook class

Printed by Chalmers Digitaltryck

Göteborg, Sweden 2023

Nitrous Oxide Formation over Zeolite-based Catalysts during Ammonia-SCR: The Effect of Framework Structure, Acidity, and Copper Content

Ghodsieh Isapour
Department of Chemistry and Chemical Engineering
Chalmers University of Technology

Abstract

The emission control of anthropogenic nitrous oxide (N_2O), a by-product formed through fossil- and renewable fuel combustion, agricultural activities, and industrial chemical processes, has attracted large considerations due to its substantial contribution in global warming and ozone layer depletion. Selective catalytic reduction with ammonia (NH_3-SCR) is the most prevailing technology for the abatement of nitrogen oxides (NO_x) in the exhaust gases from lean-burn processes, with the possible formation of N_2O. Therefore, the development of catalysts for efficient NO_x reduction with no or minor N_2O formation is of major importance. Hence, zeolite-based catalysts exchanged with copper have shown to be efficient catalysts for NO_x reduction owing to their high catalytic performance under practical reaction conditions. This work aims to increase the understanding of the N_2O formation during NH_3-SCR, in particular studying the effect of different parameters, from zeolite framework structure, ammonia storage capacity of the zeolites, to Si/Al and Cu/Al molar ratios.

Three different zeolites with varying pore sizes, from small to medium and large pore zeolites (SSZ-13, ZSM-5 and beta), were chosen to investigate their performance as SCR catalysts. A range of SSZ-13 samples with Si/Al molar ratios of 6, 12, and 24 were prepared by hydrothermal crystallization, and exchanged with copper, Cu/Al= 0-0.4 molar ratios, to investigate the effect of the Si/Al and Cu/Al molar ratios on the ammonia storage capacity and the SCR performance of the samples. Furthermore, the role of the sample pretreatment on the SCR performance was investigated for the SSZ-13 sample with Si/Al= 12 molar ratio. The prepared samples were studied by flow reactor experiments and *in situ* diffuse reflectance infrared Fourier transform spectroscopy (DRIFTS) to evaluate the catalytic activity and selectivity, and to monitor the evolution of surface species during reaction.

Copper ions as active sites in the zeolite catalyzing the SCR reaction by NO activation and formation of NO^+ and/or surface nitrate species. During SCR, the nitrate species can subsequently react with NH_3 and form ammonium nitrate (AN) as an intermediate, which partially contributes to N_2O formation upon decomposition.

In order to understand the system in more detail, we have investigated important factors such as Si/Al and Cu/Al molar ratio and temperature on the NH_3 storage capacity of the samples based on SSZ-13. Temperature programmed desorption by NH_3 (NH_3-TPD) carried out to characterize the nature of the different acid sites in the zeolite. It is revealed that the samples with low Si/Al molar ratio provide higher NH_3 storage capacity, which increases with increasing Cu loading. After NH_3-TPD, SCR experiments were subsequently performed resulting in higher NO_x conversion and N_2O formation by increasing the Cu content for all samples. Results from DRIFTS showing vibrational peaks associated with N_2O in accordance with the flow reactor findings. Moreover, the role of pretreatment for the NH_3-SCR performance was evaluated for the sample with Si/Al= 12, and the results show that the pretreatment in NH_3 and NO, in the absence of O_2, reveals higher low-temperature activity for standard SCR compared to the pretreatment including O_2.

Keywords: Zeolites, N_2O, *In situ* IR spectroscopy, Heterogeneous catalysis, SCR, Si/Al molar ratio, Copper content

List of Publications

This thesis is based on the following appended papers, referred to by Roman numerals in the text:

I. *In situ* DRIFT studies on N_2O formation over Cu-functionalized zeolites during ammonia-SCR

Ghodsieh Isapour , Aiyong Wang, Joonsoo Han, Yingxin Feng, Henrik Grönbeck, Derek Creaser, Louise Olsson, Magnus Skoglundh and Hanna Härelind

Catalysis Science & Technology, 12 ***(2022),*** *3921-3936.*

II. N_2O formation during NH_3-SCR over different zeolite frameworks: Effect of framework structure, copper species, and water

Joonsoo Han, Aiyong Wang, Ghodsieh Isapour, Hanna Härelind, Magnus Skoglundh, Derek Creaser and Louise Olsson
Industrial & Engineering Chemistry Research, 60 ***(2021),*** *17826–17839.*

III. Nature of acidic sites in Cu-SSZ-13 probed by NH_3 using *in situ* DRIFT spectroscopy

Ghodsieh Isapour , Yingxin Feng, Henrik Grönbeck, Magnus Skoglundh and Hanna Härelind
In Manuscript.

IV. N_2O formation over copper promoted SSZ-13 catalysts during NH_3-SCR: The role of acidity and reaction atmosphere

Ghodsieh Isapour , Yingxin Feng, Henrik Grönbeck, Magnus Skoglundh and Hanna Härelind
In Manuscript.

V. Role of pretreatment conditions on the evolution of surface species, activity, and selectivity during NH_3-SCR over Cu-SSZ-13

Ghodsieh Isapour , Andreas Schaefer, Magnus Skoglundh and Hanna Härelind
In Manuscript.

My Contributions to the Publications

Paper I

I synthesized the catalyst samples, performed the catalyst characterization (SEM-EDX, XRD, BET) together with my co-authors, conducted the DRIFT spectroscopy experiments, analyzed the data, and interpreted the results together with my co-authors. I wrote the first draft of the manuscript and was responsible for writing and submitting the manuscript.

Paper II

I synthesized the catalyst samples, performed the catalyst characterization (XRD and BET) together with my co-authors, conducted the DRIFT spectroscopy experiments and interpreted the results together with my co-authors, and took part in writing the manuscript.

Paper III

I synthesized the catalyst samples, performed the catalyst characterization (SEM, XRD, BET), conducted the DRIFT spectroscopy and flow reactor experiments, analyzed the data, and interpreted the results together with my co-authors. I wrote the first draft of the manuscript and was responsible for writing the manuscript.

Paper IV

I synthesized the catalyst samples, performed the catalyst characterization (SEM, XRD, BET), conducted the DRIFT spectroscopy and flow reactor experiments, analyzed the data, and interpreted the results together with my co-authors. I wrote the first draft of the manuscript and was responsible for writing the manuscript.

Paper V

I synthesized the catalyst samples, performed the catalyst characterization (SEM, XRD, BET), conducted the DRIFT spectroscopy and flow reactor experiments, analyzed the data, and interpreted the results together with my co-authors. I wrote the first draft of the manuscript and was responsible for writing the manuscript.

Publications not included in the thesis

Enhancing the Stability of Aromatic PCN Pincer Nickel Complexes by Incorporation of Pyridine as the Nitrogen Side Arm

Abdelrazek H. Mousa, Kaushik Chakrabarti, Ghodsieh Isapour, Jesper Bendix, and Ola F. Wendt

European Journal of Inorganic Chemistry, 45 ***(2020),*** *4270-4277.*

Conference Report: YEuCat Better Together – Collaborative Catalysis in a Changing World

Pedro S. F. Mendes, Nemanja Vucetic, Antonio Valverde-González, Maxime Delporte, Liliana P. L. Gonçalves, Ghodsieh Isapour, Mohammad Khatamirad, Marty Kinnaer, Lorenz Lindenthal, Remy Pointecouteau, A. Sofia G. G. Santos, Florian Schrenk, Barbara Thijs, Bahar Ipek, Margot Van der Verren, Xian Wu, and Emanuele Moioli

ChemCatChem, 14 ***(2022),*** *e202200166.*

Conference Contributions

Investigating the Effect of Pore Size in Cu-Zeolite Based SCR Catalysts

Ghodsieh Isapour, Aiyong Wang, Joonsoo Han, Derek Creaser, Louise Olsson, Magnus Skoglundh and Hanna Härelind

Oral presentation in International Conference on Environmental Catalysis (ICEC)
7-9 September 2020, Manchester, UK

Better Together – Collaborative Catalysis in a Changing World

Ghodsieh Isapour, Magnus Skoglundh and Hanna Härelind

Young European Catalysis Network (YEuCat)
6-10 September 2021, Segovia, Spain

***In situ* DRIFTS Studies on N_2O Formation over Cu-Functionalized Zeolites during NH_3-SCR**

Ghodsieh Isapour, Aiyong Wang, Joonsoo Han, Yingxin Feng, Henrik Grönbeck, Derek Creaser, Louise Olsson, Magnus Skoglundh and Hanna Härelind

Poster presentation at the Science and Technology Day at Chalmers
12 May 2022, Gothenburg, Sweden

Investigating the Effect of Various NO/NO_2 Ratio on N_2O Formation over Cu-Functionalized Zeolites during Ammonia-SCR by *In Situ* DRIFTS Studies

Ghodsieh Isapour, Aiyong Wang, Joonsoo Han, Yingxin Feng, Henrik Grönbeck, Derek Creaser, Louise Olsson, Magnus Skoglundh and Hanna Härelind

Oral presentation at The 9th Tokyo Conference on Advanced Catalytic Science and Technology (TOCAT9)
24-29 July 2022, Fukuoka, Japan

Financial suport in form of a travel grant from Nils Philblad fond is gratefully acknowledged

***In situ* DRIFTS Studies on N_2O Formation over Cu-Functionalized Zeolites during Ammonia-SCR: Effect of Various NO_x Ratio**

Ghodsieh Isapour, Aiyong Wang, Joonsoo Han, Yingxin Feng, Henrik Grönbeck, Derek Creaser, Louise Olsson, Magnus Skoglundh and Hanna Härelind

Oral presentation in Twelfth International Congress on Catalysis and Automotive Pollution Control (CAPoC12)
29-31 August, 2022, Brussels, Belgium

Financial support in form of a travel grant from Sven och Gurli Hanssons donationsfond is gratefully acknowledged

Acknowledgements

This research is performed at Competence Centre for Catalysis, at Chalmers University of Technology. The Competence Centre for Catalysis is hosted by Chalmers University of Technology and financially supported by the Swedish Energy Agency (Project No. 52689-1) and the member companies Johnson Matthey, Perstorp, Powercell, Preem, Scania CV, Umicore, and Volvo Group. Parts of the work have been performed at Chalmers Materials Analysis Laboratory (CMAL).

I would also like to thank:

My main supervisor Hanna Härelind and examiner Magnus Skoglundh for all your support and guidance. I would say it was definitely one of my big chances working in your research group.

My Co-supervisor, Louis Olsson, and collaborators Dereck Creaser, Henrik Grönbeck, Yingxin Feng, Joonsoo Han and Aiyong Wang. I really enjoyed having discussion with all of you, and raising up questions which was a starting point for new discussion and figuring out new solutions.

My opponent and defense committee for evaluating my thesis and disputation.

Lasse Urholm and Lennart Norberg, without your help in maintenance of equipment, this research work could not proceed well.

Felix Hemmingsson and Andreas Schaefer, thank you for always being available for any help and generously sharing your knowledge with everyone. I never come back to my office without getting an answer for a problem from you both.

Rojin Feizi, for all the memories we made together and for standing beside me in all stressful moments, sadness and happiness.

Yanyue Feng, thanks for being such a nice colleague and friend with a big heart and enormous support.

Mengqiao Di (Jojo), thanks for all the support and moments we had together.

Lotta Pettersson, Frida Andersson, Carina Jogevik, Anna Oskarsson, for your supports and efforts in administrative work in Applied Chemistry.

All my friends and colleagues at KCK and TYK, I do appreciate for all your help and fun moments we had together. I would like to thank Fatemeh, Christopher, Guido, Pegah, Lynga, and Alexander for all the help and good moments we had together.

Finally, my lovely family for all their support and love throughout my life. You are not only my family but also my best friends. Love you all.

Ghodsieh Isapour, Göteborg, March 2023

Contents

Contents **xiii**

1 Introduction **1**

2 Background **3**
2.1 Selective catalytic reduction (SCR) . . . 3
2.2 Application of zeolites in SCR reactions . . . 4
2.2.1 Acidic properties of zeolites . . . 5
2.3 Evolution of surface and gas phase species during SCR . . . 6
2.3.1 Nitrous oxide (N_2O) formation during SCR . . . 6
2.4 Objectives . . . 9

3 Experimental **11**
3.1 Synthesis of zeolite samples . . . 11
3.1.1 Synthesis of SSZ-13 . . . 11
3.1.2 Copper ion-exchange . . . 12
3.1.3 Monolith preparation . . . 13
3.2 Sample characterization . . . 13
3.2.1 Inductively coupled plasma-sector field mass spectrometry and X-ray fluorescence spectroscopy . . . 13
3.2.2 Nitrogen physisorption . . . 14
3.2.3 Scanning electron microscopy accompanied with energy-dispersive X-ray spectroscopy . . . 15
3.2.4 X-ray diffraction . . . 16
3.2.5 Temperature programmed reduction . . . 17
3.2.6 Temperature programmed desorption . . . 17
3.2.7 Diffuse reflectance infrared Fourier transform spectroscopy . . . 18
3.3 Following surface species by *in situ* DRIFTS . . . 19
3.3.1 Surface species evaluated by diffuse reflectance infrared Fourier transform spectroscopy . . . 19
3.3.2 Gas phase species evaluated by mass spectrometry . . . 21
3.4 Catalytic activity and selectivity in flow reactor . . . 21
3.4.1 Flow reactor setups . . . 21
3.4.2 Outlet gas detection . . . 21
3.4.3 Degreening and pretreatment procedure . . . 22
3.4.4 Catalytic activity and selectivity measurements . . . 23

4 Results and Discussion **25**
4.1 The effect of zeolite framework structure in ammonia SCR 27
4.1.1 N_2O formation during standard and fast SCR 27
4.1.3 The evolution of surface species 30
4.1.4 Ammonia storage capacity in the zeolites with different frameworks . . 37
4.2 The effect of Si/Al molar ratio and copper content in ammonia SCR 37
4.2.1 Ammonia storage over zeolite-based catalysts 38
4.2.2 Catalytic performance and surface species during NH_3-SCR over SSZ-13 catalysts 44
DRIFTS Studies 46
4.3 The role of catalyst pretreatment in NH_3-SCR 47

5 Conclusions **53**

List of Figures

2.1 Framework structure of a) CHA, b) MFI and c) BEA zeolites. 5
2.2 Proposed reaction cycle I and II for low-temperature NH_3-SCR over Cu-CHA. . 7

3.1 The schematic procedure for the synthesis of Cu-SSZ-13. 12
3.2 Monolith sample wash-coated by catalyst. 13
3.3 SEM images with two different magnifications for synthesized SSZ-13 zeolite with Si/Al= 24. 15
3.4 Schematic representation of the bragg's equation. 16
3.5 XRD images for the SSZ-13 synthesized catalysts with Si/Al= 12 and various Cu content. 16
3.6 An illustration of a temperature programmed desorption process used in Paper III. 17
3.7 Schematic of DRIFTS cell's dome from top view. 19
3.8 A background spectrum for a zeolite sample after ambient exposure. 20
3.9 Scheme of the in-line monolithic reactor. 21

4.1 N_2O concentration as a function of catalyst temperature within standard and Fast SCR condition over Cu-based zeolites. 28
4.2 Integrated N_2O peak area from DRIFT spectra after exposing the Cu-SSZ-13, Cu-ZSM-5, and Cu-BEA zeolites to various NO_2/ NO_x ratio at 220, 200, and 180 °C. 29
4.3 *In situ* DRIFT spectra after exposing the Cu-SSZ-13, Cu-ZSM-5 and Cu-BEA samples to NO + O_2 for 15 min at 130 °C. 31
4.4 NO^+ and Nitrate or nitrite peak intensity after exposing the Cu-SSZ-13, Cu-ZSM-5, and Cu-BEA zeolites to NO and O_2 at different temperatures. 32
4.5 *In situ* DRIFT spectra after exposing the Cu-SSZ-13, Cu-ZSM-5 and Cu-BEA samples to Standard SCR condition for 15 min at 180 °C, and 1622/2150 intensity ratio at at different Temperatures. 33
4.6 Steady state *in situ* DRIFT spectra for O-H stretching vibration region for the Cu-SSZ-13, Cu-ZSM-5 and Cu-BEA samples under standard SCR condition for 15 min at different temperatures. 34
4.7 *In situ* DRIFT spectra after exposing the Cu-SSZ-13, Cu-ZSM-5 and Cu-BEA samples to NO, NO_2, O_2 for 15 min at 130 °C. 35
4.8 *In situ* DRIFT spectra peak intensity for pre-adsorbed NH_3 on different acid sites of the Cu-SSZ-13 (top), Cu-ZSM-5 (middle), and Cu-BEA (bottom) zeolites exposed to NO + NO_2 + O_2 at 200 °C. 35
4.9 The population of Cu species in Cu-SSZ-13, Cu-ZSM-5, and Cu-BEA zeolites, based on H_2-TPR measurements (0.2% H_2 in Ar, 10 °C.min^{-1}.) 36
4.10 Ammonia temperature-programmed desorption for the samples with (a) CHA, (b) ZSM-5, and (c) BEA framework structure. 37
4.11 Deconvoluted peaks from the NH_3-TPD experiments carried out for the SSZ-13 samples with three Si/Al molar ratio and Cu/Al molar ratio of 0, 0.1, and 0.4. . 39

4.12 Peak intensities obtained from *in situ* DRIFT spectra during NH_3 adsorption for SSZ-13 catalysts with Si/Al (6, 12, and 24) and Cu/Al (0-0.4) molar ratio after 15 min at 70 °C. . . . 40
4.13 *In situ* DRIFT spectra for NH_3 adsorbed on different acid sites of the Cu-SSZ-13 catalysts with different Si/Al (6, 12, and 24) and Cu/Al (0-0.4) molar ratios at 70 °C. (NH_3= 400 ppm in Ar). . . . 41
4.14 DRIFTS spectra of T-O-T vibrational region perturbed by NH_3 adsorption at 70 °C for Cu-SSZ-13 samples with Si/Al= 6, 12, and 24 and Cu/Al= 0.4 molar ratio. 41
4.15 Peak intensities obtained from *in situ* DRIFT spectra during NH_3 desoprtion after 15 min under Ar flow for SSZ-13 catalysts with different Si/Al (6, 12, and 24) and Cu/Al (0-0.4) molar ratio at 200 °C. . . . 42
4.16 The deconvoluted δ(NH) spectra of NH_4^+ ions at 130 and 200 °C desorption temperature during NH_3-TPD. . . . 43
4.17 Calculated vibrations for O-H stretching and N-H bending of potential species. 44
4.18 Steady-state N_2O formation as a function of temperature for Cu-SSZ-13 with Si/Al= 6, 12, and 24 and Cu/Al= 0.1, and 0.4 molar ratio under standard and fast SCR conditions . . . 45
4.19 The signal intensity obtained from *in situ* DRIFT spectra at 1622 and 1456 cm^{-1} as a function of Cu/Al molar ratio for the Cu-SSZ-13 samples with with different Si/Al (6, 12, and 24) and Cu/Al (0-0.4) molar ratio for steady-state during standard SCR at 130 °C. . . . 46
4.20 DRIFT spectra for the 5th min of the standard SCR over the sample with Si/Al= 12 and Cu/Al= 0.1, and 0.4 molar ratio at 130 °C. . . . 47
4.21 Steady-state NO_x conversions and the corresponding N_2O formation levels as a function of temperature for Cu-SSZ-13 with Si/Al= 12 and Cu/Al= 0.3, and 0.4 molar ratio under standard and fast SCR conditions. . . . 48
4.22 *In situ* DRIFT spectra corresponding to N_2O wavenumber region for Cu-SSZ-13 with Si/Al= 12 and Cu/Al= 0.3 molar ratio under standard and fast SCR conditions, at 130 and 200 °C. . . . 50
4.23 *In situ* DRIFT spectra in NH bending vibration region for Cu-SSZ-13 with Si/Al= 12 and Cu/Al= 0.3 molar ratio under standard SCR condition, at 130 and 200 °C, with the corresponding peak intensities at 1622 and 1452 cm^{-1}. . . . 51

List of Tables

3.1 Chemicals used for the synthesis of SSZ-13 and for the functionalization of the zeolite samples with copper. . . . 13

4.1 The specific surface area (SSA) and the specific pore volume (SPV) . . . 26
4.2 Infrared peak assignments for different species emerged during the reaction in 4000-400 cm^{-1}. . . . 30

4.3 Steady-state NO_x conversions for Cu-SSZ-13 with Si/Al= 6, 12, and 24 and Cu/Al= 0.1, and 0.4 molar ratio under standard and fast SCR conditions. 45

Abbreviations, acronyms and terms

GHG	Green house gas
CAA	Clean Air Acts
NO_x	Nitrogen oxides
SCR	Selective catalytic reduction
LNT	Lean NO_x trap
DRIFTS	Diffuse reflectance infrared Fourier transform spectroscopy
FTIR	Fourier transformed infrared Spectroscopy
SEM	Scanning electron microscopy
EDX	Energy dispersive X-ray
XRD	X-ray diffraction
ICP-SFMS	Inductively coupled plasma sector field mass spectrometry
XRF	X-ray fluorescence
TPD	Temperature programmed desorption
TPR	Temperature programmed reduction
BET	Brunauer-Emmat-Teller
BJH	Barrett-Joyner-Halenda
SSA	Specific surface area
MS	Mass Spectrometryr
MFC	Mass flow controller
CEM	Controlled evaporator and mixer
m/z	Mass to charge ratio
SSZ-13	**S**tandard oil **s**ynthetic **z**eolite-**t**hirteen
ZSM-5	**Z**eolite **s**ocony **m**obil-**f**ive
BEA	Zeolite **be**ta polymorph **A**
BAS	Brønsted acid sites

1 Introduction

A constant tightening of the exhaust emission standards and the global strategies for a sustainable decrease of greenhouse gas (GHG) emissions call for efficient lean-burn combustion processes and development of highly active catalytic systems. An increase in the exhaust filtration procedures obliged by more stringent emission legislation demands adequately higher exhaust gas temperatures. [1] On the contrary, the level of exhaust gas temperature is in general decreasing owing to the consistent improvement in the combustion efficiency.

Air pollution legislations concerning vehicle emissions date back to the 1960s in the USA, where the primary objectives of federal emission regulations were grounded on the Clean Air Acts (CAA)[1]. These acts were initially established in 1967, and later in 1970, pursued by two modifications in 1977 and in 1990. [2]

1: CAA is a comprehensive Federal law that regulates all source off air emissions like NO_x, SO_2, CO, VOC and Pb.

By the compliance of the CAA and the upcoming vehicle emission standards, the commercialization of oxidation catalysts[2] was commenced in the USA in the 1970s in order to control emissions of carbon monoxide (CO) and hydrocarbons (HC) from gasoline engine combustion. Afterwards, suggesting the three-way catalyst[3] technology in the 1980s, expanded the possibility to control nitrogen oxide emissions as well. Eventually, in the 1990s, along with the introduction of the oxidation catalysts for diesel fueled cars in Europe, heavy-duty diesel trucks and diesel busses in the USA started to use these catalysts as well. The catalysts in the above-mentioned applications mostly contain noble metals such as palladium, platinum, and rhodium as their active components. [2]

2: Oxidation of hazardous compounds like CO, VOC, CH_2O, HC to CO_2 and water in the presence of precious metals such as Pt or Pd, with promoters and binders is done by oxidation catalysts.

Oxidation catalysts are less effective on NO_x reduction.

NO_x is a general term for NO and NO_2 both of which are potent in contributing to air pollution and result in forming ozon (O_3), smog and acid rain. [3, 4] The composition of NO_x in combustion process originates from; (i) thermal NO_x; which forms by exceeding the combustion chamber temperature to 2000 K (ii) fuel NO_x; produced via the oxidation of ionized nitrogen compounds in the fuel in advance, and (iii) prompt NO_x; emerges through the combination of N_2 in the air with the fuel.

3: Three-way catalysts (TWC) simultaneously convert three pollutants to harmless emissions:

1. CO to CO_2
2. HC to CO_2 and H_2O
3. NO_x to N_2

The catalyst uses active precious metals such as platinum, palladium and rhodium supported on metal oxides like alumina, ceria and zirconia. By controlling the air to fuel ratio, three-way catalysts can cut CO, HC and NO_x emissions by over 99%.

Different types of catalyst technologies such as lean NO_x trap (LNT), non-selective catalytic reduction (NSCR) of NO_x in rich burn natural gas engines and selective catalytic reduction of NO_x by ammonia (NH_3-SCR) for lean-burn processes, are applied for mobile and stationary engines. Among all, NH_3-SCR of NO_x is an

efficient technology for the abatement of NO_x and works via the continuous selective catalytic reduction of NO_x to nitrogen and water by the reaction with ammonia. This technology was first discovered over a platinum (Pt) catalyst. [5] The drawback with Pt-based catalysts is their poor NO_x reduction at higher temperatures, which makes it applicable only at low temperatures (< 250 °C).

Another group of metal-based SCR catalysts, which were developed at a later stage, are zeolite-based-catalysts.[4] These have wide temperature operation windows with functionality at higher temperatures. Zeolites are applied in many catalytic processes because of their stability, high activity and selectivity. Zeolites are often modified in order to tune their catalytic properties and can be found in different pore sizes, from small to medium and large pore zeolites. [6]

4: Zeolite;

1. Was coined by the Swedish mineralogist Cronstedt, in 1756.
2. The name comes from the Greek meaning 'boiling stone'.
3. Porous crystalline framework materials.
4. Containing pores of molecular size (5–12 A° or 0.5–1.2 nm).
5. Have a crystal structure which is constructed from TO_4 tetrahedral, where T is either Si or Al.

The first zeolite that was identified as an active SCR catalyst was mordenite. [7] Commonly, the ion-exchanged zeolites with transition metals such as Fe and Cu, were found to be beneficial in the SCR application. [8] The disadvantage of available Fe-based zeolites for SCR applications in the stationary system is their performance at temperatures around 600 °C. [9] Therefore, the temperature restriction may be determined by the durability of the catalyst rather than its selectivity. So, the expanded catalysts for mobile engine applications being efficient in both low and high temperatures, are Cu-based zeolites. The Cu-based ZSM-5 zeolite, which was widely known as the comprehensive lean-NO_x catalyst in the 1990s, is active in NO_x reduction during SCR within the temperature range of about 200-400 °C, however with an insufficient thermal durability. [10] Later, the large-pore Cu-beta zeolite catalysts, were developed for lean-burn applications owing to their better durability in a wider temperature range compared to the ZSM-5 zeolites. However, the well-known tendency of the beta zeolite to adsorb hydrocarbons (HCs) from the exhaust, results in catalyst deactivation during a fast oxidation of the HCs. [11]

The drawbacks of medium and large-pore zeolites resulted in the development of another type of Cu-based zeolites formulated for SCR reactions for lean-burn applications These are based on the chabazite framework structure (CHA): SSZ-13 is one type of zeolite with chabazite framework structure. It is a small-pore size zeolite with the capability of not adsorbing HCs from the exhaust gases as these cannot enter the pore structure, active over a wide temperature range and being hydrothermally stable at temperatures above 650 °C. [12]

Background 2

2.1 Selective catalytic reduction (SCR)

Growing environmental awareness in recent decades has resulted in the establishment of more severe and stringent environmental legislation and regulations. The concept 'air pollutant' covers all compounds which potentially are considered detrimental for human beings, animals, vegetation and other substances. [13] The major sources of air pollution are combustion processes utilized in mobile and stationary sources such as power plants, vehicles and other incineration processes. Sulfur oxides (particularly SO_2), particulate matter, hydrocarbons, carbon monoxide, and nitrogen oxides are the key combustion-generated air contaminants. [14] The emergence of acid rain, ozone layer depletion, photochemical smog, and even global warming (correlated with N_2O), mainly produced by atmospheric pollutants such as SO_2 and NO_x, are considered as the most drastic world ecological issues due to creating irreversible changes in the ecosystems both terrestrial and aquatic. [15–18]

In a recent emission scandal [19, 20] the public awareness rose regarding that NO_x emissions from combustion processes both in mobile and stationary sources, are a major threat to human health and environment. The contribution of NO_x from diesel engines, formed by oxidation of atmospheric nitrogen at elevated temperatures (thermal NO_x), is about 75% of the total NO_x emissions from road traffic. [10]

Great efforts have been made to restrict the emission of such pollutants through an extensive application of existing technologies or via the development of new ones. [15] The process to reduce NO_x emissions from lean-burn application, which have been extensively developed over the past few decades, is so-called selective catalytic reduction (SCR)[1] with ammonia. However, this technology that originally was applied in industrial installations and stationary power plants, it is now installed in a multitude of lean-burn applications, ranging from off-road vehicles, light and heavy-duty trucks, and cars, to ships and locomotives. All these applications implicate specific challenges owing to rigorous emission restrictions, alternative fuels and new internal combustion engine technologies.

Until now, tremendous efforts have been made to fulfil these legislative commitments, to optimize the performance of either pre-combustion control or combustion and post-combustion abatement modifications. [13, 14] The reduction of the nitrogen content

1: SCR:

- It is already presented in the late 1970s for stationary sources.
- The main involved reactions in selective catalytic reduction of NO_x by ammonia are:

"Standard-SCR":
$4\,NH_3 + 4\,NO + O_2 \longrightarrow 4\,N_2 + 6\,H_2O$
"Fast-SCR":
$2\,NH_3 + NO + NO_2 \longrightarrow 2\,N_2 + 3\,H_2O$
"NO_2-SCR": $2\,NO_2 + 2\,NH_3 \longrightarrow N_2 + N_2O + 3\,H_2O$
Or:
$3\,NO_2 + 4\,NH_3 \longrightarrow \frac{7}{2}\,N_2 + 6\,H_2O$. [21, 22]

in the fuel via fuel purification, attains pre-combustion control. During combustion, engine modification can help alternating the operational conditions to eliminate or reduce the NO_x formation. It should be considered that pre-combustion and combustion control are merely achieving a modest reduction of NO_2 emissions. [23]

So, for achieving a high NO_x reduction, post-combustion control is required. As the term suggests, post-combustion control deals with reducing the nitrogen oxides after they have been formed in the combustion processes. Many attempts, either by combustion control or by post-combustion control technologies, have been applied to reduce NO_x emissions. Various techniques have been applied for the NO_x abatement and as mentioned earlier the most widely used method is selective catalytic reduction by ammonia [2] (NH_3-SCR) as a reducing agent. [23] The aim of this technology is to decrease the NO_x content in the flue gas and convert it to harmless N_2. [13, 14] This is the most efficient technology for the NO_x reduction from lean exhaust gases which has undergone enormous developments over the past couple of decades.

2: Two forms of ammonia applicable in SCR:

- Anhydrous ammonia:
  toxic
  hazardous
  high vapor pressure
  requires thick-shell pressurized storage tanks and piping.
- Aqueous ammonia:
  less hazardous and easier to handle.

One of the challenges with the SCR technology is the threshold temperature of the urea injection into the hot exhaust gas. The required temperature is of about 200 °C, which for many lean-burn processes, is above the exhaust gas temperature. Furthermore, during the catalytic reaction, the uniform distribution of the reducing agent is a crucial factor for the efficiency of the SCR systems. [23] However, selectivity to nitrogen, cost and fuel efficiency are important properties of SCR catalysts.

2.2 Application of zeolites in SCR reactions

One of the utmost required issues for the sustainable development of the society is appointing cost-effective and environmental-friendly processes to achieve improvement from environmental aspect and renewable energy sources. Catalytic technologies are noteworthy for emission abatement owing to their low costs and high efficiency. [24]

One type of material, which has been widely applied in catalysis, adsorption and separation, is zeolites. Zeolite-based catalysts are of high interest in exhaust gas abatement for instance for lean-burn processes. The outstanding thermal and chemical stabilities of zeolites at different operational temperatures, their high surface area and activity, accessibility, and their adaptable chemical properties result in extensive technological applications.

2.2.1 Acidic properties of zeolites

Zeolites have represented prominent potential for industrial applications by taking advantage of their unique multifunctional Brønsted and Lewis acidic sites. However, the stability, product selectivity and reproducibility of zeolites need further improvement.

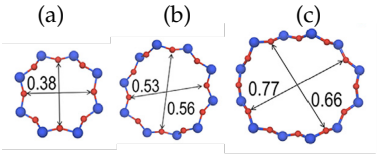

Figure 2.1: Framework structure of a) CHA, b) MFI and c) BEA zeolites.

a) Zeolite SSZ-13 (CHA), 8-membered ring, small-pore, 0.38 × 0.38 nm [27]
b) Zeolite ZSM-5 (MFI), 10-membered ring, medium-pore, 0.53 × 0.56 nm [28]
c) Zeolite beta (BEA), 12-membered ring, large-pore, 0.77 × 0.66 nm. [29]

Brønsted acid sites in zeolite frameworks are highly polarized hydroxyl groups, which have the role as proton donors with high activity to many catalytic reactions. Brønsted acidic zeolites are playing a crucial role in many processes in the oil-refining and petrochemical industries. [25] In addition to Brønsted acid sites, zeolites are interesting scaffold structures for providing Lewis acid properties by substitution of Si atoms in zeolite frameworks with tetrahedrally coordinated Zr, Ti, Sn, or Cu atoms which results in generating Lewis acid sites. Lewis acid sites are electron acceptors from other molecules and are facilitating many conversion processes that will not occur over Brønsted acid sites. [26]

Metal-exchanged zeolite catalysts have played a significant role in the NH_3-SCR technology development compared to base metal catalysts[3] like molybdenum and tungsten, and vanadium oxide-based catalysts as early NH_3-SCR catalysts. The zeolites can be categorized based on their framework structure and pore size ranging from small- to medium-, and large-pore zeolites such as SSZ-13 (CHA), ZSM-5 (MFI), and beta (BEA) zeolites, respectively. [24, 30] A schematic representation of the zeolite framework structure, with the relative pore dimension, is presented in Figure 2.1. Compared to previous NH_3-SCR catalysts, zeolites have the advantages of high activity, easy availability, and high stability at substantially higher temperatures than base metal catalysts. They can also withstand prolonged operation at elevated temperatures, for example 900 °C for small-pore zeolites with chabazite structure. A lower potential for SO_2 oxidation and less corrosion related risks are their further specific properties.

3: Base metal catalysts:

- Less expensive
- Operate well at common temperature ranges used in industrial applications
- Lack high thermal durability
- Potential to oxidize SO_2 into SO_3

Among the different metal-exchanged zeolites, copper-based zeolites are of high interest based on their availability, high stability at different temperatures and high activity for NO_x reduction in a wide range of reaction conditions. Furthermore, Cu zeolites are of high importance as model systems, and aids better understanding of the fundamental aspects of the chemistry and mechanistic pathways of the reactions through the catalytic transformation of the pollutants. [24, 31]

2.3 Evolution of surface and gas phase species during SCR

2.3.1 Nitrous oxide (N_2O) formation during SCR

As mentioned earlier, selective catalytic reduction technology by NH_3 is an efficient technique for the abatement of NO_x. During SCR and the exposure of the catalyst to the gas composition, the compounds react on the catalyst surface and the catalyst surface undergoes a change in its state from reduced to oxidized. This leads to the emergence of different species which can retain on the catalyst surface or desorb to the gas phase. Reduction of NO_x during the aftertreatment process by the SCR reaction can result in the formation of the undesired by-product nitrous oxide. Nitrous oxide has a potential contribution in global warming, hence being one of the pollutants in the list of greenhouse gas contributors.

Different types of catalysts such as diesel oxidation catalysts (DOC)[4], ammonia slip catalysts (ASC)[5] and the selective catalytic reduction catalysts all are potential contributors to N_2O formation, depending on the exhaust gas composition, temperature, type of catalyst, and aftertreatment operation strategy.

The N_2O formation during the SCR process is temperature dependent, and can proceed through different pathways at different temperatures. It has been proposed that at temperatures lower than 200 °C, N_2O forms through the formation and subsequent decomposition of Cu-peroxo complexes. In the temperature range of 230-400 °C, N_2O formation proceeds via the decomposition of surface ammonium nitrates (NH_4NO_3) species and at temperatures higher than 400 °C, non-selective catalytic oxidation of ammonia by oxygen is the source of N_2O formation.

4: DOC is an aftertreatment catalyst designed to oxidize CO and HC into CO_2 and H_2O.

5: ASC is a catalysts which converts unreacted ammonia passing through the SCR catalyst. This may occurs at excess ammonia injection, low temperatures or for poisoned SCR catalysts.

N_2O formation via copper per-oxo complexes

Formation of N_2O via the Cu per-oxo reaction mechanism suggests the formation of H_2NNO and HONO over NH_3-solvated Cu-sites, which later decompose to N_2 and H_2O over Brønsted acid sites. Also, Non-selective N_2O formation proceeds via H_2NNO decomposition over the Cu-sites. [32] Two cycles that takes this mechanism into account are shown in Figure 2.2. [32]

In cycle I in Figure 2.2, NO adsorption on a Cu cation forms NO–OO–*. Later, the coordination of an additional NH_3 molecule to NO–OO–* results in the formation of H_2NNO–OOH–*.

Desorption of H_2NNO from the Cu site follows by its diffusion to a Brønsted acid site. The reaction proceeds by subsequent NO and NH_3 adsorption and H_2NNO–OH–OH formation.

The desorption and diffusion of H_2NNO occurs twice, which enables the adsorption of a third NO in the reaction cycle forming HONO–OH–*. HONO desorbs and further reacts over a Brønsted acid site. After HONO desorption, the remaining *–OH–* can react with NO to produce another HONO. An alternative reaction pathway can be through the adsorption of an additional NH_3, to form NH_3–OH–* and *. Subsequently, NO can be adsorbed on NH_3–OH–*, and form HONO, which desorbs and diffuses to a Brønsted acid site. The additional NH_3 desorption results in the restoration of the linear $[Cu(NH_3)_2]^+$ complex.

A possible path for N_2O formation within cycle I may be a side reaction of direct decomposition of H_2NNO over H_2NNO–OOH–*. After the formation of H_2NNO–OOH–*, it is possible for H_2NNO to transfer two H atoms to the OOH–* intermediate instead of diffusing to the Brønsted acid sites.

In cycle II, each oxygen site *-OO-* can adsorb one NO to form -ONOONO-. The complex separates into two ONO- as adsorbed nitrites (NO_2^-), and the separated complexes subsequently react with NO and NH_3 to form HONO-H_2NNO. The HONO and H_2NNO complexes desorb and later decompose into N_2 and H_2O at the Brønsted acid sites. Here, the Cu sites appear as linear complexes *. As in cycle I, NH_3 may adsorb on *-OO-* and restrict NO adsorption. N_2O formation in cycle II is not considered since H_2NNO cannot decompose by hydrogen transfers in this cycle. [32]

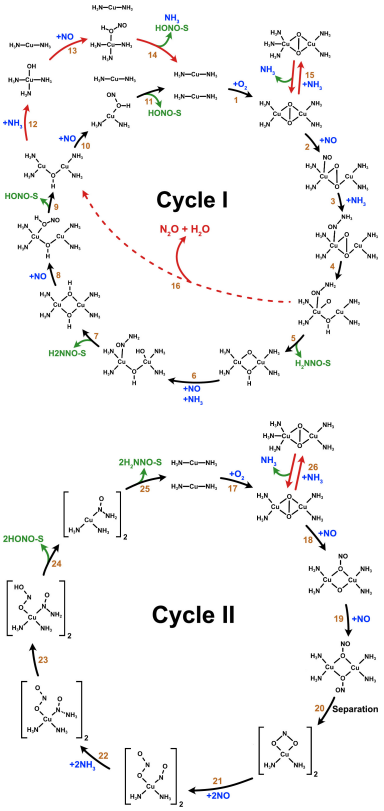

Figure 2.2: Proposed reaction cycle I and II for low-temperature NH_3-SCR over Cu-CHA.

N_2O formation through the ammonium nitrate route

The reaction between NH_3 and surface nitrates species can result in the formation of ammonium nitrate. Decomposition of ammonium nitrate is recognized as one source of N_2O formation during SCR conditions. [33] Two key factors are important for the rate of N_2O formation: the concentration of NO_2 in the gas phase and the stored NH_3 on the catalyst surface.

Based on the discussion in the literature regarding the role of the zeolite structure on NH_3-SCR and, specifically N_2O formation, it is agreed that during the SCR reaction N_2O is formed to a higher extent in the MFI or BEA framework structure, in comparison to the CHA framework. [34, 35]

A number of reaction mechanisms for the N_2O formation under standard SCR reaction conditions are suggested. The most commonly reported one is a Langmuir-Hinshelwood mechanism, in which the reaction between adsorbed NO_x and ammonia species on the catalyst surface results in the formation of adsorbed ammonium nitrate (AN). [36, 37] It is assumed that the AN is formed at low temperature (<200 °C) and subsequently decomposes when the temperature becomes higher than around 230 °C. [38] Hence, at elevated temperatures, the formation and decomposition of AN intermediate proceeds continuously at steady state. [39] Another suggested mechanism for N_2O formation is through the reaction of NO_2 with a pair of NH_4^+ ions, leading to the formation of an active compound, which subsequently decomposes to N_2 or N_2O owing to a rapid reaction with NO or NO_2.

Hence, reaction of ammonium and nitrate species via the Langmuir-Hinshelwood mechanism could explain the generated N_2O at temperatures around 250-350 °C. By further temperature increase to around 550 °C, a considerable decline in the N_2O formation appears, which could be owing to the lack of surface NH_4NO_3 species. [37, 40, 41]

N_2O formation through NH_3 oxidation

Based on previous reports, there is no clear and specific connection between the relevance for the NH_3 oxidation activity and N_2O selectivity for SCR catalysts. It seems that N_2O formation is not particularly connected to the ammonia oxidation, but rather to the surface reactions over the different kinds of catalytic materials, controlled by the chemistry and the specific properties of the catalysts. N_2O formation through NH_3 oxidation is known as non-selective oxidation of NH_3 (eqn. (2.1)). [42] It is revealed that N_2O formation via NH_3 oxidation over Cu-based catalysts mainly occurs at elevated temperatures. [43] In addition, the existence of intermediate species such as NH and NHO, may result in a reaction over transition metal oxides and produce NO, N_2 and N_2O, during the ammonia oxidation. [44]

$$2\,NH_3 + 2\,O_2 \rightleftharpoons N_2O + 3\,H_2O \tag{2.1}$$

Besides, during the fast NH_3-SCR, N_2O formation appears in higher concentrations upon the addition of NO_2 into the inlet gas composition. Two main pathways can be taken into account for N_2O formation during fast SCR; one can be the reaction between NO_2 and the adsorbed surface nitrite intermediate species [33, 45] and the other, can occur through NO_2-SCR , which are shown in eqn. (2.2) and (2.3), respectively;

$$300-450^{\circ}\mathrm{C}\ \ \mathrm{NO_2{-}(NH_4{}^{+})_2} + \mathrm{NO_2} + \frac{1}{2}\,\mathrm{O_2} \longrightarrow 2\,\mathrm{N_2O} + 3\,\mathrm{H_2O} + 2\,\mathrm{H^{+}} \tag{2.2}$$

$$250-300^{\circ}\mathrm{C}\ \ 2\,\mathrm{NO_2} + 2\,\mathrm{NH_3} \longrightarrow \mathrm{N_2} + \mathrm{N_2O} + 3\,\mathrm{H_2O} \tag{2.3}$$

In addition, it is demonstrated via the Eley-Rideal mechanism that the adsorbed NH_3 species can react with gaseous NO and contribute to N_2O formation in the SCR reactions. [37]

2.4 Objectives

The objective of this work is to understand and provide knowledge regarding the effect of the framework structure of zeolites, acidity, and copper content in the formation of by-products during NH_3-SCR. This study has mainly focused on the catalyst performance under various reaction conditions forming N_2O, as one of the major byproducts during NH_3-SCR. The evolution of different surface species during the NH_3-SCR has been evaluated by *in situ* diffuse reflectance infrared Fourier transform (DRIFT) spectroscopy along with catalytic activity studies in flow reactor with a focus on the effect of framework structure in **Papers I** and **II**, respectively. In **Papers III** and **IV** an investigation of the importance of acidity and copper content over zeolites with different Si/Al and Cu/Al molar ratio is presented. The role of pretreatment conditions on the evolution of different surface species during NH_3-SCR has been evaluated in **Paper V**. Additionally, the catalytic activity of the zeolites was followed by flow reactor studies to correlate the catalytic activity to different Cu species.

Experimental 3

This study aims at investigating the influence of the zeolite framework, role of acidity and copper content on the formation of N_2O and surface species during the NH_3-SCR reaction. A detailed description of the experimental procedure applied throughout this thesis project is presented in this chapter. The performance of the zeolite samples was studied by flow reactor measurements and *in situ* DRIFT spectroscopy, followed by detailed sample characterization in order to improve the understanding of the results. Various characterization techniques were applied including scanning electron microscopy with energy-dispersive X-ray spectroscopy (SEM-EDX), X-ray diffraction (XRD), nitrogen and argon physisorption, inductively coupled plasma sector field mass spectrometry (ICP-SFMS), X-ray fluorescence (XRF), Temperature-programmed reduction by hydrogen (H_2-TPR), and Temperature-programmed desorption by ammonia (NH_3-TPD).

3.1 Synthesis of zeolite samples

In all samples, copper was used as the active metal site and introduced by the "incipient wetness impregnation" method to the structure of the zeolite. In **Papers I** and **II** three different zeolites (SSZ-13, ZSM-5, and beta) with Si/Al molar ratios of around 12 with 2 wt% Cu loaded to the zeolite, were used. The SSZ-13 zeolite was synthesized by a sol-gel synthesis procedure followed by hydrothermal crystallization in an autoclave. Both H-ZSM-5 and H-BEA samples are commercially available, and they have been used with no further preparation. In **Papers III-V**, SSZ-13 zeolites were synthesized with Si/Al= 6, 12, and 24 molar ratio and with varying Cu content (Cu/Al= 0, 0.1, 0.2, 0.3, and 0.4 molar ratio or 0, 0.7, 1.4, 2, 2.7 wt%). The synthesis of the Si/Al= 12 and Si/Al= 24 samples is the same as the method used for the samples in **Papers I** and **II**, but the sample with Si/Al= 6 was synthesized with a different route including NH_4-Y zeolite.

3.1.1 Synthesis of SSZ-13

The general synthesis procedure for the samples with Si/Al= 12, and 24 molar ratio started by dissolving 1M sodium hydroxide (Sigma-Aldrich, > 98 %) in Milli-Q water (18 MΩ.cm) and then mixing the solution with the structure directing agent, SDA, (25%

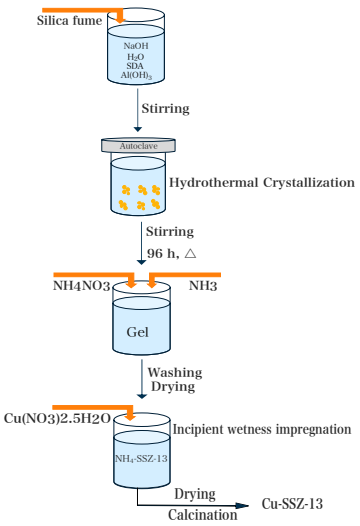

Figure 3.1: The schematic procedure for the synthesis of Cu-SSZ-13.

solution of SDA 2825, Sachem, ZeoGen), $Al(OH)_3$ (Sigma-Aldrich, 50.0-57.5% Al (as Al_2O_3) basis, reagent grade) and fumed silica (Sigma-Aldrich, S5130-500G, standard grade) with an average particle size of 0.007 νm. The obtained homogeneous gel was sealed off in Teflon-lined stainless-steel autoclaves and heated to 160 °C for 96 h under stirring. After hydrothermal synthesis, the autoclaves were cooled down to room temperature and washed and filtered around 10 times with Milli-Q water until reaching pH below 8. Later, the samples were dried at 110 °C and calcined at 600 °C in order to remove the SDA. Then the obtained powder was dissolved in Milli-Q water and ammonium nitrate (Sigma-Aldrich, 98%, hemi(pentahydrate)), and nitric acid (Sigma-Aldrich, 69%) were added to adjust the pH. The solution was stirred for 1 h at 80 °C and then washed with Milli-Q water and centrifuged. This step was repeated twice in order to remove all sodium from the sample. The remaining precipitate was kept at 110 °C overnight to obtain NH_4-SSZ-13. To convert the zeolite to H-form, the samples in NH_4-form were further calcined at 600 °C.

The zeolite sample with Si/Al= 6 molar ratio was prepared by a similar procedure reported by Fickel *et. al.* [46, 47] The water solution of sodium silicate (Sigma-Aldrich, reagent grade) and NaOH (Fisher Scientific) was stirred for 15 min at room temperature. Then, NH_4-Y (Zeolyst CBV100) was added and stirred for 30 min, and the solution was stirred for another 30 min after the addition of SDA. The final solution was collected into Teflon-lined autoclaves and heated at 140 ºC under stirring for 6 days. The product was centrifuged and washed with Milli-Q water and then dried at room temperature. The final solid powder was calcined in air at 550 °C for 8 h. The schematic procedure of the zeolite synthesis is presented in Figure 3.1.

3.1.2 Copper ion-exchange

The preparation of the Cu-promoted samples was performed by the incipient wetness impregnation method. First, a copper nitrate (Sigma-Aldrich, 98%) solution and subsequently ethanol was added to the NH_4-type samples. The slurry was stirred for 15 min and left at room temperature overnight before calcination. The calcination of the Cu-SSZ-13 samples was carried out in two steps, first by increasing the temperature to 600 °C with a rate of 2 °C/min and kept at this temperature for 6 h, and then increased to 750 °C and kept constant for 2 h, followed by a cooling step to room temperature. For the other two zeolites (NH_4-ZSM-5 and NH_4-beta) the calcination was performed in one step at 600 °C for 8 h. The list of applied chemicals for the synthesis are presented in Table 3.1. The samples were pelleted, grinded and sieved to around

Name	Formula	Application
Sodium Hydroxide[a]	NaOH	pH adjustment
Aluminum Hydroxide[b]	$Al(OH)_3$	Al precursor
Trimethyladamantyl ammonium Hydroxide[c]	$C_{13}H_{25}NO$	SDA
Silica Fume[d]	SiO_2	Si source
Nitric Acid[e]	HNO_3	pH adjustment
Ammonium Nitrate[f]	NH_4NO_3	NH_4 exchange
Copper Nitrate[g]	$Cu(NO_3)_2.2.5H_2O$	Cu precursor
Sodium Silicate [h]	Na_2SiO_3	Si source
Zeolite-Y [i]	NH_4-Y	Zeolite source

Table 3.1: Chemicals used for the synthesis of SSZ-13 and for the functionalization of the zeolite samples with copper.

a, f Sigma-Aldrich, > 98% anhydrous;
b Sigma-Aldrich, 50.0-57.5% Al (as Al_2O_3) basis, reagent grade;
c 25% solution of SDA 2825, Sachem, ZeoGen;
d Sigma-Aldrich, S5130-500G, 0.007 νm, standard grade;
e Sigma-Aldrich, 69%;
g Sigma-Aldrich, > 98%;
h Sigma-Aldrich, > 98%;
i Zeolyst CBV100%

350 and 40 microne prior to use for powder reactor experiments and DRIFTS measurements, respectively.

3.1.3 Monolith preparation

Prior to the catalytic activity measurements in the flow reactor in **Paper II**, the samples were washcoated on honey-comb cordierite monolith substrates (cpsi: 400). The dimensions of the monoliths were 20 mm in length and 15 mm in diameter. The monoliths were heated at 550 °C for 2 h in air to remove contaminants. Later, a slurry was prepared with a 90:10 mass ratio of liquid to solid phase. The liquid phase contained the 50:50 mass ratio of water to ethanol, and the solid phase contained the catalyst powder sample and boehmit[1] binder (Dispersal P2) with a mass ratio of 95:5. The monoliths were dipped into the prepared slurry and subsequently dried with a heat gun. This procedure was repeated for a couple of times until reaching the desired loading of washcoat. Finally, the monoliths were calcined at 500 °C for 1 min with heat gun, and subsequently, were calcined at 500 °C for 2 h with a ramp of 2 °Cmin^{-1}. A washcoated monolith sample is shown in Figure 3.2. Detailed procedures for washcoating can be found in **Papers I** and **II**.

1: Boehmite or böhmite is an aluminium oxide hydroxide (γ-AlO(OH)) mineral, a component of the aluminium or bauxite.

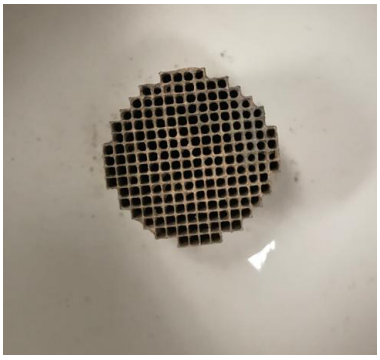

Figure 3.2: Monolith sample washcoated by catalyst.

3.2 Sample characterization

3.2.1 Inductively coupled plasma-sector field mass spectrometry and X-ray fluorescence spectroscopy

The elemental analysis of the zeolite samples was done by ICP-SFMS or XRF to trace element determinations, the Si/Al molar ratio, and the copper content in the zeolite samples. The ICP-SFMS

characterization technique, produces ionized samples in inductively coupled plasma (ICP), which follows by the ion extraction with a mass spectrometer (MS) for determining the elemental compositions both quantitatively and qualitatively. This analysis was performed by ALS Scandinavia AB. XRF is a non-destructive analytical technique applied with the purpose of deducing the composition of some of the studied catalysts. It can determine the chemistry of a sample by measuring the fluorescent (or secondary) X-ray emitted from a sample when it is excited by a primary X-ray source. This analysis was performed using a PANalytical axios spectrometer (Malvern) at KCK Lab, Chalmers.

3.2.2 Nitrogen physisorption

An acronym of the researchers who proposed the BET and BJH theory:

2: Stephen **B**runauer, Paul Hugh **E**mmett and Edward **T**eller.

3: Elliott Pierce **B**arret, Leslie G. **J**oiner and Paul P. **H**alenda

For quantifying the specific surface area (SSA) and pore size distribution of supported catalysts such as zeolites, a commonly used method is that of gas physisorption analysis by N_2. The SSA, which is corresponding to the area occupied by the adsorbed gas, and the pore size distribution of a material can be measured by the BET[2] and BJH[3] methods, respectively, which were proposed in 1938, and 1951. [48] The concept behind this theory is that an inlet gas, generally N_2, generally adsorbs to the sample surface in a layer-by-layer manner and by detecting the volume of one layer, the surface area can be calculated. N_2 is typically applied owing to its availability in high purity and also its weak interaction with almost all solids.

In this work the BET method has been used to measure the SSA and pore volume of the samples. The general concept in the measurements is an initial drying step of the samples at an elevated temperature (normally 220 °C for zeolites) over night, under N_2 flow in order to remove adsorbed water. Owing to the weak interaction between N_2 and solid phases at a low temperature (-196 °C), liquid N_2 is used to cool samples to get detectable amounts of adsorption. N_2 is dosed step-wise (at constant temp) and the physisorbed amount of N_2 is measured after reaching adsorption/desorption equilibrium for each p/p_0. The data is collected by a Micromeritics Tristar 3000 instrument and is presented in the form of a BET isotherm, which depicts the amount of adsorbed gas as a function of the relative pressure. According to IUPAC classification, six types of adsorption isotherms can be distinguished, and typically four of them are found in porous materials, and the isotherm shape depends on the texture of porous solid material. [49]

The BET method is the most extensively applied method to assess the volume of a monolayer (V_m) of adsorbed gas on a solid surface. [50] The relationship between the volume of the monolayer (V_m)

at a certain relative pressure (p/p_0) is demonstrated in the BET equation (eqn. (4.2)), where C is a second parameter connected to the heat of adsorption.

$$[\frac{1}{V[(p_0/p)]-1}] = [\frac{1}{(V_m C + C)}] - [\frac{1}{V_m C(p/p_0)}] \qquad (3.1)$$

However, it is worth noting that this method presents a roughly good estimation of the surface area for microporous and mesoporous compounds with a number of assumptions [4], even though it can be misinterpreted for microporous materials such as zeolites. This is due to the limitations arisen by the small pore volumes resulting in the formation of multilayer adsorption, which cause capillary condensation. [51, 52] Nevertheless, for the zeolite-based materials, BET surface measurements are mainly reported for making comparison, and it should not be considered as the actual surface area but preferably commensurable to the pore volume.

4: BET theory assumptions are as the following:

- Adsorption and desorption rate are equal, regardless of the layer
- Adsorption sites in first layer are equivalent
- no lateral interactions among adsorbed molecules in multilayer
- All available sites have the same energy
- only one adsorbate per adsorption site

In addition, the common method used for the estimation of pore size distribution is based on the obtained data from physisorption, and presented BJH using the t-plot method. This is an appropriate method for the pore size estimation of mesoporous materials and the t-plot is helpful in determining of the volume of micropores. [49] The evaluated values for the surface area and pore size volume are presented in **Papers I-III**.

3.2.3 Scanning electron microscopy accompanied with energy-dispersive X-ray spectroscopy

Scanning electron microscopy (SEM) is a useful well-known technique with very high magnifications which is extensively applied for imaging of surfaces. An SEM projects and scans a focused beam of electrons over a surface of a sample to provide an image. The electrons in the beam interact with the sample, therewith generates various signals that can be applied to obtain information about the surface's topography and composition. The existing of an excellent depth of field in high resolution images of surface topography are produced by a highly focused primary scanning electron beam. The primary electrons create low-energy secondary electrons by entering the surface by an energy of 0.5 – 30 kV. The intensity of the secondary electrons is mostly controlled by the surface topography of the targeted sample. Analysis of the surfaces by SEM can provide information regarding surface structure, microcracks, discoloration, existence of contaminants, and deposits. The SEM images are provided in **Papers I** and **III**. The SEM image of a synthesized Cu-SSZ-13 sample with Si/Al= 24 is shown in Figure

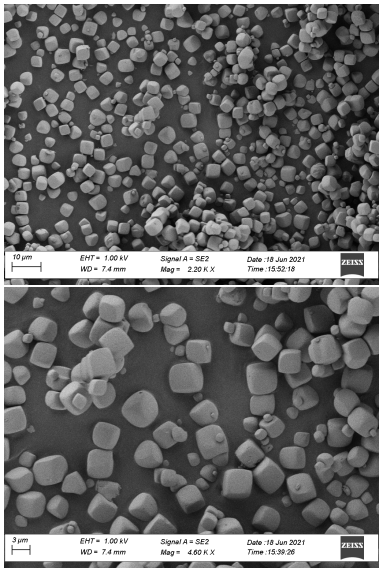

Figure 3.3: SEM images with two different magnifications for synthesized SSZ-13 zeolite with Si/Al= 24.

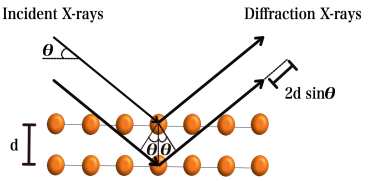

Figure 3.4: Schematic representation of the bragg's equation.

The balls in the graph are schematic illustrations of atoms and correspond to the building blocks of a crystalline material. The atoms are arranged periodically due to the crystalline nature. The incident X-ray beam is scattered at various planes of the material and hence resulting in diffracted X-rays with a different optical path length to travel. The magnitude of the path length solely depends on the distance between the crystal planes and the angle of the incident X-ray beam.

5: $n\lambda = 2d\sin\theta$

d: Interplaner distance

θ: Diffraction angle

n: A positive integer

λ: Wavelength of the refracted light

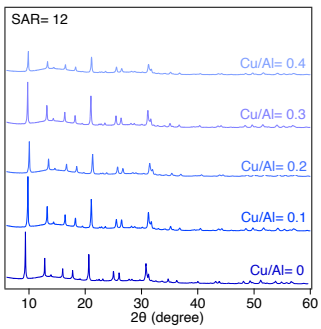

Figure 3.5: XRD images for the SSZ-13 synthesized catalysts with Si/Al= 12 and various Cu content.

3.3. An energy-dispersive X-ray analysis (EDX) accompanied with SEM was used in paper **I** for elemental analysis of the zeolite samples. The EDX mapping, provides information regarding the elemental composition in a specific area.This method depends on the electron excitation from the inner shell after bombarding the target sample with an electron beam.

EDX analysis provided the elemental analysis of Si, Al, O, and Cu in **Paper I** and also a comparison was made with the obtained data from ICP-SFMS analysis.

3.2.4 X-ray diffraction

The X-ray powder diffraction method is a powerful nondestructive technique, which is widely applied to investigate the structural features of crystalline materials owing to its simplicity and availability. This technique can also provide information of the ratio of crystalline to non-crystalline regions, the arrangement of crystals (crystal orientations or texture), average crystal size, and the distance between the planes of the crystal. The application of XRD for the zeolites can help in determining whether the synthesized zeolite has correct crystalline structure or not. Later, an electron from the outer shell begins to fill the hole in the core and results in an energy release as an Auger electron X-ray, and the detector measures the emitted X-ray energies of the existed elements in the sample. [53]

The samples used in all papers were analyzed with XRD to determine the crystalline phase and if the crystalline structure of the synthesized zeolites correspond to the target zeolite structure and is maintained after copper ion-exchange. The diffraction patterns were collected with a Siemens D5000 diffractometer with a 2θ of 0.03°. The sample is placed between the X-ray source and the detector within an angle of 2θ from each other. The XRD measurement is based on Bragg's law[5] [54] and the emergence of the peaks are by the interference of a scattered monochromatic X-ray beam at specific angles with the sample and recorded as reflected X-rays by a detector.

The peak intensities are specified within the lattice planes by the atomic positions. [55] Schematic representation of the bragg's equation and the XRD image of SSZ-13 synthesized zeolite are shown in Figures 3.4 and 3.5, respectively.

The XRD pattern is a characteristic of the investigated substance which is considered as a fingerprint of atomic arrangements in the studied material.

3.2.5 Temperature programmed reduction

For characterizing the surface of metal oxides, mixed metal oxides, and metal oxides dispersed on a support under various thermal conditions, an analytical technique known as Temperature-programmed reduction (TPR) is extensively used. In order to identify the temperature of reduction, the pre-oxidized samples are heated and hydrogen (diluted in Ar) is used as a reducing agent. The detected temperature for hydrogen consumption corresponds to the reducing temperature. The sample is placed in a fixed-bed reactor while the temperature is increased linearly.

In **Paper II**, 50 mg of sample was loaded into the quarts tube and then treated with a low concentration of hydrogen (0.17% H_2 in Ar balance) while increasing the temperature to 800 °C with a ramp of 10 °Cmin^{-1}. The TPR sequences were performed with a scanning differential calorimeter (Sensys DSC, Setaram), and the outlet gas composition was monitored by mass spectrometer (Hiden HPR-20 QUI MS). TPR accompanied with the mass spectrometry equipment can provide information regarding the reducibility of the oxide's surface, both quantitatively and qualitatively, and also the heterogeneity of the reducible surface. However, this technique is intrinsically quantitative and can directly correlate with catalytic behavior, the data obtained regarding the structure of the species is not that straightforward compared to the one obtained by spectroscopic methods. Hence, both methods are applied in combination and are complementary. [56]

3.2.6 Temperature programmed desorption

Temperature programmed (TP) experiments are helpful way to increase the understanding about the interactions between molecules and the catalyst surface, and provide special characteristics of a material. The total surface acid sites of zeolites and their density can be determined using ammonia TPD (temperature programmed desorption). [57, 58] The acid sites in zeolites play a crucial role in catalytic reactions and are consider as active sites. The principle is the pre-adsorption of NH_3 on the catalyst at a specific (low) temperature (e.g. 70 °C) and then physisorbed species are flushed away by purging the sample in Ar flow. Later, the sample is heated in Ar to reach the target temperature. The chemisorbed species start to desorb during the temperature ramp at a certain temperature and the desorbed species can be detected and quantified. Information regarding both numbers and strength of acid sites can be extracted from the data. An illustration of a temperature programmed desorption experiment is given in Figure 3.6. In this

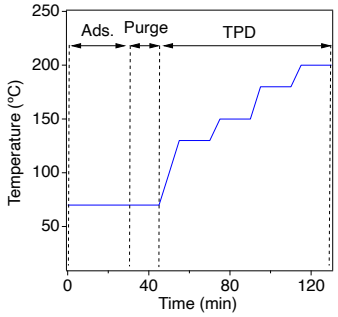

Figure 3.6: An illustration of a temperature programmed desorption process used in Paper III.

thesis work the NH_3-TPD is used to determine the different acid sites and their density for various zeolites.

This information is obtained by studying the DRIFTS spectra of the adsorbed NH_3 and also comparing them with the catalytic activity and selectivity data obtained from flow reactor measurements. Several peaks appear in NH_3-TPD profiles at different desorption temperatures owing to the existence of several types of acid sites distinguished by their strength. Here, TPD profiles were analyzed by fitting Gaussian functions to recognize desorption temperatures and also quantify the population of different acid sites. The obtained peaks are corresponding to weak, medium, strong and sometimes extraframework[6] acid sites.

6: The extra-framework Al species are in the form of octahedral Al_2O_3 and remarkably reduce the zeolites activity since it envelops the actual strong acid sites of the zeolite framework. [59]

NH_3-TPD is applied in **Papers II-III** to gain further insights about the effect of zeolites framework and Si/Al and Cu/Al molar ratio, respectively, on the availability of acid sites and NH_3 storage behavior of the catalysts. For **Paper II**, the monolith samples were used to determine the acid site density, and in **Paper III**, powder samples were used both in DRIFTS and powder reactor measurements. NH_3-TPD experiments in DRIFTS is extensively used to track the acid site density and the acid strength by investigating samples with various Si/Al molar ratio and Cu content. More detailed discussion is given in section 4.1.3, and 4.2.1 for **Paper II** and **Paper III**, respectively.

3.2.7 Diffuse reflectance infrared Fourier transform spectroscopy

Diffuse reflectance infrared Fourier transform (DRIFT) spectroscopy is a spectroscopic method for the identification of adsorbed surface species (e.g. zeolites' surfaces). The method represents scattered spectra from the surface of powder samples [60], allowing analysis of e.g. metallic centers and acid sites and quantification of reaction products, during reaction conditions. [60, 61]

In infrared spectroscopy the sample is irradiated with an infrared beam, and the transmitted or reflected radiation is measured, which provides structural analysis and quantification. The absorbance is wavelength dependent and measures the amount of absorbed radiation by the molecules in the sample. By the atom adsorption, the electron density around the atom will be modified which will result in the appearance of an electric dipole. The modification will increase as the bond between the adsorbed atom and the substrate becomes more ionic and stronger. [62] For infrared light, the absorption is associated with the vibrational and rotational modes of the various functional groups such as -OH, -NH, -NO, etc., in the molecules, [63] which appear at specific wavenumbers.

The wavenumbers are characteristic of chemical absorption bands and functional groups, and the corresponding evolved peaks are analyzed to estimate the structure of the compound. The frequency or absorption band of functional groups is typically reported in wavenumber (cm^{-1}) and depends to the mass of involved atoms in the chemical bonds and the bond strength. [63] Hence, it provides information about the species bonded to the catalyst surface and helps in clarifying the various catalyst sites by using specific probe molecules such as NO or CO.

DRIFTS measurements require a minimum of sample preparation. The sample is typically loaded on a flat surface inside a chamber covered with two IR transparent dome-shaped CaF_2 windows on top. The schematic of DRIFTS cell's dome is shown in Figure 3.7. The DRIFT spectrum strongly relies on the particle size, its distribution and homogeneity, the refractive index of the sample and packing density. [63] It should be considered that to obtain the highest quality DRIFTS spectrum and a more accurate spectrum with a narrow bandwidth, a small and uniform particle size is required. Furthermore, the packing of the loaded sample in the DRIFT's cell needs to be loose in order to increase the IR beam penetration.

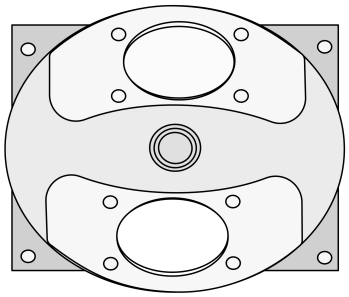

Figure 3.7: Schematic of DRIFTS cell's dome from top view.

In **Paper I**, the DRIFTS analysis was performed to investigate the evolution of various surface species during the step response reaction procedure including NO oxidation, standard SCR, NH_3 adsorption. For this purpose, the initially calcined and degreened zeolite powder samples were pretreated in the DRIFTS cell. The detailed information regarding degreening and pretreatment of the samples are given in **Paper I** and section 3.4. The samples were then cooled in Ar to the target temperature where the background spectra were taken. Thereafter, different inlet gas compositions were provided according to each step at step response reaction and the recorded IR absorbance spectra were collected after 15 min for each step. The procedure for **Papers II-V** is similar to the procedure explained for **Paper I**, with a difference in inlet gas composition depending on the investigated experiment.

3.3 Following surface species by *in situ* DRIFTS

3.3.1 Surface species evaluated by diffuse reflectance infrared Fourier transform spectroscopy

Diffuse reflectance infrared Fourier transform spectroscopy (DRIFTS), is commonly applied method to analyze powders and rough surface solids since it depends on scattering of radiation within the

sample and can provide information of rotational (only gas phase species) and vibrational bonds of one or two stimulated atoms in the examined sample and present it as the collected spectra from powder samples. The radiated IR beam over the sample results in a scattered reflection which is collected by a mirror adjusted outside the DRIFT cell and recorded as a spectra after reaching the detector. There are two general types of reflected light: specular and diffuse. A common example of specular reflection (also called front-surface, regular, or Fresnel reflection) is light reflected from mirrors or other polished surfaces. Specular reflectance occurs at any interface between two materials with different refractive indices. Specularly reflected light is characterized by the rule that the angle of reflection is equal to the angle of incidence. Common examples of diffusely reflecting surfaces are the matte surfaces characteristic of certain types of paper and powders. Diffusely reflected radiation is the light reflected from a diffusely reflecting sample for which the angle of reflection does not equal the angle of incidence. The DRIFT set up includes a beam splitter along with a fixed and moving mirror. The incident light that reaches on a beam splitter will be divided into two equal intensity beams where 50% is reflected to the moving mirror and the other 50% is transmitted to the fixed mirror. Later, the light is reflected back from both mirrors to the beam splitter where 50% is sent to the detector and the other 50% is lost to the source. [64]

The radiated IR beam over the sample results in a scattered reflection which is collected by a mirror adjusted outside the DRIFT cell and recorded as a spectrum after reaching the detector. However, the quantitative analysis of the obtained spectra is intricate and difficult, due to the size and number of particles as well as their orientation in the beam which affect the intensity of the scattered light. Additionally, the overlapping of different spectra resulting in complication in the interpretation and identification of different species.

The pretreatment of the samples before running experiments plays a crucial role to remove the contaminants from the surface, since any kind of contamination can affect the results. It is noteworthy that the pretreatment immediately follows by the reaction procedure in case of starting experiment with an oxidized catalyst and reducing the number of adsorbed surface species. [65] Figure 3.8 shows a spectra of less proper pretreated sample. The bands highlighted in the red dashed line are related to hydrocarbons adsorbed on the surface of the zeolite, which is an indication of a non-proper pretreatment procedure.

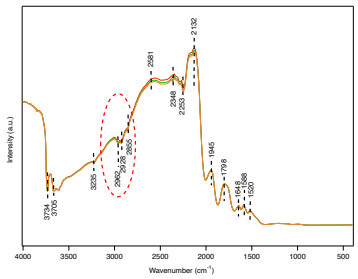

Figure 3.8: A background spectrum for a zeolite sample after ambient exposure.

3.3.2 Gas phase species evaluated by mass spectrometry

Mass spectrometry is an advanced powerful technique for both qualitative and quantitative analysis and is based on ionization followed by separation of ions according to their mass-to-charge ratio. In a mass spectrometer (MS), the detector plays a crucial role for the separated charged ions. The choice of detector mainly depends on the type of experiment and the design of the instrument. A desirable detector in a mass spectrometer can present properties such as high amplification and high collection efficiency, low noise and cost, fast time response with a narrow distribution, long term stability and long life and preferably be mounted outside of the vacuum. In case of inaccurate and unreliable ion detection, any measurements performed previously would be meaningless.

3.4 Catalytic activity and selectivity in flow reactor

3.4.1 Flow reactor setups

In order to evaluate catalytic activity of zeolites, a monolith reactor was used for monolith samples in **Paper II** and a fixed bed reactor was used for powder samples in **Papers III-V**. The washcoated monolith samples were placed in a quartz tube flow reactor accompanied with a heating coil and insulation. The temperature was controlled by two thermocouples; for monolith samples one thermocouple is positioned 10 mm upstream from the inlet of the monolith sample and the other located centrally inside the monolith sample (see Figure 3.9), while for the fixed bed powder reactor one thermocouples is positioned close to the sample and the other is a couple of millimeters away from the sample. The flow of each inlet gas was controlled by separate mass flow controllers (MFCs) (Bronkhorst) and the outlet gas composition was monitored by a Fourier transform infrared (FTIR) spectroscopy (MKS MultiGas 2023 HS) and a mass spectrometer (MS).

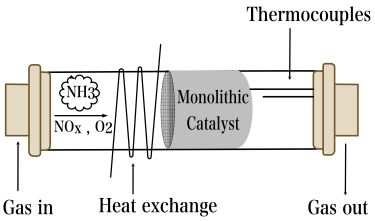

Figure 3.9: Scheme of the in-line monolithic reactor.

3.4.2 Outlet gas detection

The outlet gas composition was detected with both FTIR and mass spectrometry.
IR spectroscopy is an analytical technique which relies on the same principle as DRIFT spectroscopy and measures the interaction between infrared light and material by absorption, emission, or reflection. [51] It is applied to study and identify chemical materials or functional groups in liquid, solid, or gaseous forms. Each

molecule absorbs frequencies of light which are characteristic of their structure. When the frequency of the molecular vibration or rotation matches with the frequency of the incident light, absorption happens. The adsorption of a atom on the surface results in a change in the dipole moment due to the charge seperation and electrone density chane around the atom. [62] Different factors such as molecular potential energy, the mass of the atom in the chemical bond, and the corresponding vibrational coupling can affect their energies, which is expressed in wavenumbers with a typical unit of cm^{-1}.

The visualization of an infrared light absorbance (or transmittance) versus frequency, wavenumber or wavelength results in an IR spectrum. The infrared spectrum is usually divided into three regions; the near, mid and far infrared[5], named with their relation to the visible spectrum.

5: Infrared spectrum regions:

- Near-IR (high energy): 4000–12500 cm^{-1} (2.5–25 νm), for studying the fundamental vibrations and associated rotational–vibrational structure.
- Mid-IR, 4000–400 cm^{-1} (2.5–25 νm)
- Far-IR (low energy), 400–10 cm^{-1} (25–1000 νm), for studying rotational spectroscopy and low frequency vibrations.

Mass spectrometry[6] is another analytical tool applied for measuring the mass-to-charge ratio (m/z) of one or more molecules present in a material. It is extensively used for the monitoring of either pure samples or complex mixtures. The interaction of the ions with an applied electric field is the base of mass selection. A material which can be solid, liquid, or gaseous, is ionized by bombarding with a beam of electrons. This may result in breaking up of some of the molecules in the into positively charged fragments, and then separated according to their mass-to-charge ratio.[7] Results are displayed as spectra of the signal intensity of detected ions as a function of the mass-to-charge ratio. These measurements can also be used for calculating the exact molecular weight of the sample components. Typically, mass spectrometers help in identifying unknown compounds via determining molecular weight, quantifying known compounds.

6: Mass spectrometer consists of at least these three components: ionization source, mass analyzer, and ion detection system.

7: a. For example by accelerating them and subjecting them to an electric or magnetic field.
b.Ions of the same mass-to-charge ratio will undergo the same amount of deflection.

3.4.3 Degreening and pretreatment procedure

All the powder samples were initially degreened at 500 °C for 2 h in standard SCR reaction conditions (400 ppm NO, 400 ppm NH_3, 10% O_2) prior to the activity or other characterization experiments (such as DRIFTS, and NH_3-TPD) in the flow reactor with GHSV of 20,400/24,300 h^{-1}. Furthermore, the monoliths were degreened once more in the same conditions after being washcoated. Subsequently, the pretreatment procedure was performed before each measurement in order to remove potential surface adsorbates. In **Papers I and II**, the pretreatment was carried out in the presence of Ar and 10% O_2, while in **Papers III** and **IV** the pretreatment was done in two steps: first in the presence of Ar and 10% O_2, followed by flowing 400 ppm NO, 400 ppm NH_3 in Ar. In addition, a series

of measurements were performed to investigate the effect of the pretreatment on the catalytic activity and the evolution of surface species. In these experiments(presented in **Paper V** three different pretreatments were used, i) Ar and 10% O_2, ii) Ar and 10% O_2, followed by 400 ppm NO, 400 ppm NH_3 and 10% O_2 in Ar balance, and iii) Ar and 10% O_2, followed by 400 ppm NO, 400 ppm NH_3 in Ar balance.

3.4.4 Catalytic activity and selectivity measurements

The catalytic activity and selectivity of the degreened, pretreated powder and washcoated samples were investigated in flow reactor experiments in the presence of different gas feed composition at different temperatures. In **Paper II**, the prepared monolith samples were exposed to a gas composition corresponding to standard (400 ppm NO, 400 ppm NH_3, 10% O_2) and fast SCR (200 ppm NO, 200 ppm NO_2, 400 ppm NH_3, 10% O_2) conditions with or without water (5%) with a total flow of 1200 ml.min^{-1} (Ar balance). The catalysts were heated in a ramp of 20 °C.min^{-1} to the target temperature and kept at that temperature for 30 min. Also, experiments with varying ratio of NO/NO_2 and with the constant concentration of NH_3, O_2 and H_2O (400 ppm, 10% and 5%, respectively, Ar balance) were done in **Paper II**. In **Paper III** powder samples were used for ammonia adsorption/desorption experiments with 400 ppm NH_3 (Ar balance). Standard (400 ppm NH_3, 400 ppm NO, and 10% O_2) and fast (400 ppm NH_3, 200 ppm NO, 200 ppm NO_2, and 10% O_2) SCR conditions were evaluated for powder samples in **Papers IV** and **V**.

4 Results and Discussion

Selective catalytic reduction with ammonia is an efficient technology to eliminate hazardous NO_x compounds from lean-burn processes. Among the various assayed catalysts for this purpose, copper-containing zeolites have been found to be active with high performance over a wide range of temperatures and conditions. [12, 31]

Different factors such as the zeolite pore size, acidity of zeolite and metal content plays a crucial role in the performance of the zeolite catalysts. The zeolite framework structure has a significant effect in determining the fundamental features of zeolite-based catalysts during NH_3-SCR. Zeolites based on 12- and 10-membered rings such as BEA, [34, 66] or MFI [67] (large and medium-pore size zeolites), respectively, are predominantly reported for application in the SCR process.

Recently, 8-membered ring (small-pore) zeolite catalysts, with CHA framework, were recognized to have remarkable advantages such as improved hydrothermal stability, higher SCR activity, better hydrocarbon tolerance, elevated N_2 selectivity with less N_2O formation, as compared to large- or medium-pore zeolite counterparts. [12, 68] Hence, both **Papers I** and **II** focus on how the framework of the zeolites and their properties affects the emergence of various species and intermediates such as N_2O, during NH_3-SCR. **Paper I** was mainly carried out in dry conditions while in **Paper II** both dry and wet conditions are considered for the activity measurements.

As mentioned, surface acidity is an important factor for SCR catalysis. The evaluation of the acidity, or more specifically the surface acidity, requires the determination of the nature, the strength, and the number of acid sites. Among many techniques, temperature programmed desorption is frequently used, where the catalyst first is saturated with a reactive gas, like NH_3 in a static or dynamic system. Later the catalyst is submitted to a linear temperature ramp in a flow of inert gas, e.g. Ar, to desorb NH_3.

To evaluate the NH_3 storage in the zeolite, NH_3-TPD experiments were performed first for the zeolites with different pore size in **Paper II** in a flow reactor and then investigated for the SSZ-13 zeolites with different Si/Al molar ratio and Cu content in **Paper III** with both *in situ* DRIFT spectroscopy and flow reactor experiments.

The effect of different Si/Al molar ratio and Cu content for the SSZ-13 samples on the formation of various species and particularly N_2O, were evaluated in **Paper IV** with both *in situ* DRIFT spectroscopy and flow reactor. The role of pretreatment as one of the affecting parameters on the performance of the catalyst has been evaluated in **Paper V** for the SSZ-13 samples with Si/Al= 12 molar ratio.

For elemental analysis and to determine the content of Si, Al and Cu in the zeolites ICP-SFMS analysis was used for all studied zeolites in **Papers I-IV**, while XRF analysis was used in **Paper V**. The results for the studied samples with different pore size are provided in Table 2, Section 3.1 in **Paper II** and the obtained results for the samples with different Si/Al and Cu/Al molar ratio are presented in Table S1, in the supplementary information, in **Paper III**. The obtained results correspond to the target values.

Table 4.1: The specific surface area (SSA) and the specific pore volume (SPV) of the samples with different pore sizes.

sample	SSA	SPV
Cu-SSZ-13	540	0.232
Cu-ZSM-5	323	0.124
Cu-BEA	508	0.150
H-SSZ-13	674	0.304
H-ZSM-5	425	0.158
H-BEA	631	0.185

The specific surface area and specific pore volume for all samples were measured applying sorption analysis (BET) by nitrogen or Ar. The results for the samples with three different pore sizes (**Papers I-II** are shown in Table 4.1, and the results for **Papers III-IV** and **Paper V** are shown in the supplementary information for **Paper III** and **Paper V**, respectively.

Based on the results in Table 4.1, it is clear that the samples with CHA framework structure show significantly higher specific pore volume compared to the other two samples, which can be owing to the large cage void of the CHA-type framework. [69] Besides, Cu addition decreases the specific surface area by almost 20% compared to the samples in H-form. The reason can be the accumulation of copper species such as, Cu^{2+} and $[Cu\ (OH)]^{+}$ inside the cages in the zeolite framework and as a consequence block the zeolite surface where the N_2 can be adsorbed. [70] It is also concluded that Cu species are located not only inside but also in the extra framework positions of the zeolite, which can lead to the blockage of the micropores.

For the SSZ-13 samples with different Si/Al molar ratios and Cu content (**Papers III-V**) the decreasing trend in specific surface area does not appear for all the samples by increasing Cu content. To investigate this, the BET measurements were carried out in both N_2 and Ar environment for some of the samples with Si/Al= 12 to study if there is an interaction between N_2 and the zeolite samples. Interestingly, the obtained results from both measurements showed the same trend. So, it can be inferred that for the SSZ-13 zeolite, with a small pore size, either the penetration of the N_2 molecule into the pores of the zeolite is hampered and hence hinder the complete N_2 adsorption or Cu dispersion was done quite well during the Cu-exchange procedure with no blockage of the pores of the zeolites.

However, it needs to be considered that BET measurement is a way to get a rough estimation of the surface area of the zeolites and it does not provide the actual and real surface area.

4.1 The effect of zeolite framework structure in ammonia SCR

In this section, the effect of the framework structure of the zeolite on the formation of different species such as N_2O during NH_3-SCR is in focus. N_2O formation is evaluated based on the flow reactor studies in **Paper II** and the results are correlated with the observations from DRIFT spectroscopy measurements from **Paper I**. In addition, the ammonia storage capacity of three different zeolites is taken into account to achieve information regarding the acidity and the acid strength in the zeolites.

4.1.1 N_2O formation during standard and fast SCR

Catalytic activity tests were performed in flow reactor to investigate the N_2O formation during both standard and fast SCR reaction conditions. The N_2O formation profiles as a function of reaction temperature are presented in Figure 4.1 for all three Cu-SSZ-13, Cu-ZSM-5 and Cu-BEA samples during both standard and fast SCR reaction conditions. Although, the results depict that the Cu-BEA sample result in higher N_2O formation in the entire temperature range compared to the Cu-ZSM-5 and Cu-SSZ-13 samples, there is two different trends at low and high temperature for N_2O formation.

As mentioned earlier in Section 2.3, N_2O formation can proceed through different pathways depending on the reaction temperature. During SCR reaction conditions at temperatures below 200 °C, N_2O formation will not occur via the formation and decomposition of NH_4NO_3, since the temperature is too low for the NH_4NO_3 decomposition, which starts above 230 °C. Ammonium nitrate forms through the reaction of ammonia with surface nitrate species in the zeolite during NH_3-SCR. [37, 71, 72]

Hence, the N_2O formation through the NH_4NO_3 decomposition can proceed at temperatures above 230 °C, which appears with two maximum peaks below 350 °C and the other high-temperature regions around 350-500 °C. The NH_4NO_3 decomposition continues until it is consumed and by a further temperature elevation to around 350 °C, a considerable decline in the N_2O formation appears, which could be owing to the lack of surface NH_4NO_3

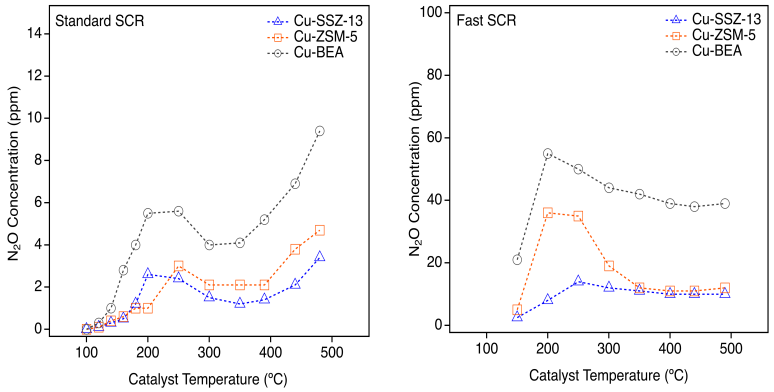

Figure 4.1: N_2O concentration as a function of catalyst temperature within standard and Fast SCR condition over Cu-based zeolites.

species. The second peak for N_2O formation appears at temperatures above 350 °C and reaches the highest N_2O formation at 500 °C. Here, at higher temperatures, N_2O originates from the non-selective oxidation of NH_3. However, for all samples, the N_2O formation is quite low with less than 10 ppm during standard SCR conditions.

Moreover, upon the addition of NO_2 during fast SCR reaction conditions higher N_2O formation is achieved for all samples in comparison to standard SCR reaction conditions. This reveals the crucial role of NO_2 on the SCR activity at lower temperatures, [38, 73] which is probably owing to the higher activity of NO_2 compared to O_2 in re-oxidization of Cu(I) to Cu(II). Figure 4.1 shows the highest formation of N_2O for the fast SCR reaction conditions for Cu-BEA, followed by Cu-ZSM-5 and Cu-SSZ-13 at 130 °C and 150 °C. An investigation of N_2O formation at lower temperatures reported by Devadas et al., [45] revealed that the N_2O formation over Fe-ZSM-5 can be due to the NH_4NO_3 decomposition. In addition, the influence of NO_2 on the NH_3-SCR reaction has been investigated [74] and it is proposed that the introduction of NO_2 has a major contribution in the production of N_2O in the lower temperature range (150-250 °C).

4.1.2 N_2O formation over varying NO_2/NO_x ratio

To determine the contribution of fast and NO_2 SCR on N_2O formation, the effect of NO_2/NO_x ratio was investigated for the Cu-SSZ-13, Cu-ZSM-5 and Cu-BEA samples at three different bed temperatures (220, 200, 180 °C). The zeolite samples were exposed to 400 ppm NH_3 and varying NO_2/NO_x ratio as follow; NO_2/NO_x; 0, 50, 60, 75, 80, and 100%.

The spectra are recorded after 15 min of exposing the catalysts to the corresponding gas composition of each step. The obtained value for N_2O integrated peak area is shown in Figure 4.2. The

peak around 2230 cm^{-1} attributed to N_2O formation, shows larger peak area for the Cu-SSZ-13 compared to the other two zeolites, and most pronounced at the lowest temperature. The Cu-ZSM-5 and Cu-BEA show the same trend at low temperature, as well. The same observation is seen for the NO^+ integrated peak area for the band around 2120 cm^{-1} at the lowest temperature. The higher amount of NO^+ and N_2O formation at low temperature can be related to the NO^+ coverage which decreases with increasing temperature.

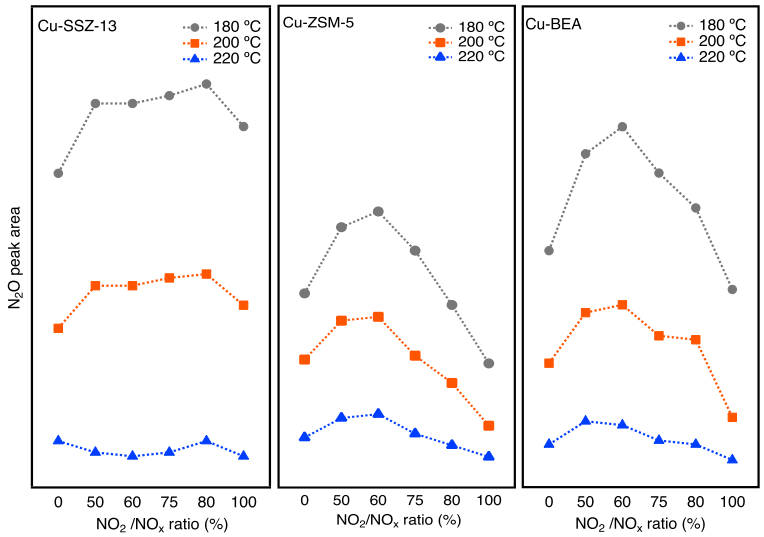

Figure 4.2: Integrated N_2O peak area from DRIFT spectra after exposing the Cu-SSZ-13, Cu-ZSM-5, and Cu-BEA zeolites to various NO_2 / NO_x ratio at 220, 200, and 180 °C.

Studies reported by Liu et al. [74] revealed that N_2O formation is temperature dependent and shows different behaviour at temperatures above or below 250 °C. The results show that below 250 °C there should be maximum N_2O formation with less NO_2 concentration. This is in line with our study where at temperatures below 250 °C, N_2O shows higher integrated peak area when NO_2 has less concentration. Also, further increase in NO_2 concentration results in a drop in N_2O formation. A possible reason can be that at high NO_2 concentration ammonium nitrate forms in a higher amount and consequently blocks the surface of the catalyst, which results in lower conversion and subsequently lower N_2O formation. At higher temperatures, no surface blocking happens and the maximum N_2O formation is achieved for 100% NO_2.

Furthermore, it is notable that the trend of the produced amount of AN is correlated with the NO^+ peak intensity within the NO oxidation step from the *in situ* DRIFTS results in **Paper I**. This indicates that the amount of surface nitrates can determine the amount of produced AN. Also, at higher temperatures the formation of species such as N_2O_4 [75] is of less interest, it can explain the lower amount of surface nitrate groups at low temperature. Based on the literature, it is commonly accepted that at low temperatures, the

large-pore zeolites represent higher N_2O formation. [76] It can be assumed that, at low temperatures, the rate of AN decomposition and subsequently N_2O formation is higher for Cu-BEA and the main part of AN is decomposed in the large-pore zeolites.

Additionally, the integrated peak area attributed to nitrate species (1530–1700 cm^{-1}) has demonstrated a similar trend as seen for NO^+ and N_2O for all three zeolites, with the highest value of nitrate species at low temperature and low NO_2 concentrations.

At NO_2/NO_x= 0%, corresponding to standard SCR reaction conditions, the highest peak area can be originated from the lower reaction rate. On the other hand, increasing the NO_2/NO_x ratio from 0% to 50%, promotes the fast SCR reaction, resulting in the consumption of surface nitrate species appearing as a sharp decline in the related peak area. Later, a further NO_2 addition cause a gradual increase for the related peak area. This agrees with the lowest amount of NO^+ and N_2O formation when we have the highest amount of nitrate species.In a nutshell, the zeolite framework structure and reaction temperature play a crucial role on the formation of surface species and also undesired by-products during NO_x reduction by ammonia-SCR. The results obtained from DRIFTS and flow reactor studies reveal major contributions of NO^+ and nitrate species during NO oxidation. Moreover, by varying the NO_2/NO_x-ratio, the higher formation of NO^+ and N_2O species occurs at lower temperatures and higher N_2O formation for the large-pore zeolite (Cu-BEA) compared to medium- (Cu-ZSM-5) and small-pore (Cu-SSZ-13).

Table 4.2: Infrared peak assignments for different species emerged during the reaction in 4000-400 cm^{-1}.

ν [cm^{-1}]	Ref.
NO on Cu^{2+}	
1902	[76]
1907 (6MR)	[76]
1945 (8MR)	[77]
NO on Cu^{+}	
1812	[76]
NO^+ on M^{n+} or BAS	
2144 Cu-CHA	[78]
2123 Cu-ZSM-5	[79]
2134 Cu-BEA	[80]
NO^{3-}, NO^{2-}	
1550-1650	[81]
NH Stretching	
3300-3500	[76]
NH Bending	
1400-1650	[76]
NH^{4+} on BAS	
1430, 3000	[82]
Cu^{n+}... NH_3	
3352, 3182, 1620	[80]
NH_3 on EFAl	
1327	[83]
$[Cu(NH_3)NH_2]^{2+}$	
1619, 1278	[83]
Si(OH)Si, Silanol OH	
3740-3760	[84]
Si(OH)Al, Brønsted AS	
3600-3650	[85]

The position of the peaks may vary between different zeolite samples and/or in one type of sample with different exchanged metal.

4.1.3 The evolution of surface species

This section concerns the evolution of surface species that emerge during the step response experiments carried out over three Cu-based catalysts under dry conditions (in the absence of water vapor), which is investigated in **Paper I** and **Paper II**. The aim is to correlate the effect of zeolite framework structure to the formed surface species. It should be noted that the same samples, with the same Si/Al= 12 molar ratio and Cu content (2wt%), were used in both **Paper I** and **Paper II**, with the same degreening and pretreatment procedures.

NO Oxidation

In situ DRIFTS measurements, where three zeolites (Cu-SSZ-13, Cu-ZSM-5, and Cu-BEA) were exposed to NO and O_2 at 130 °C for 15 min (Figure 4.3), identifies two types of adsorbed surface species, which possibly participate in the SCR reactions. [12] Two

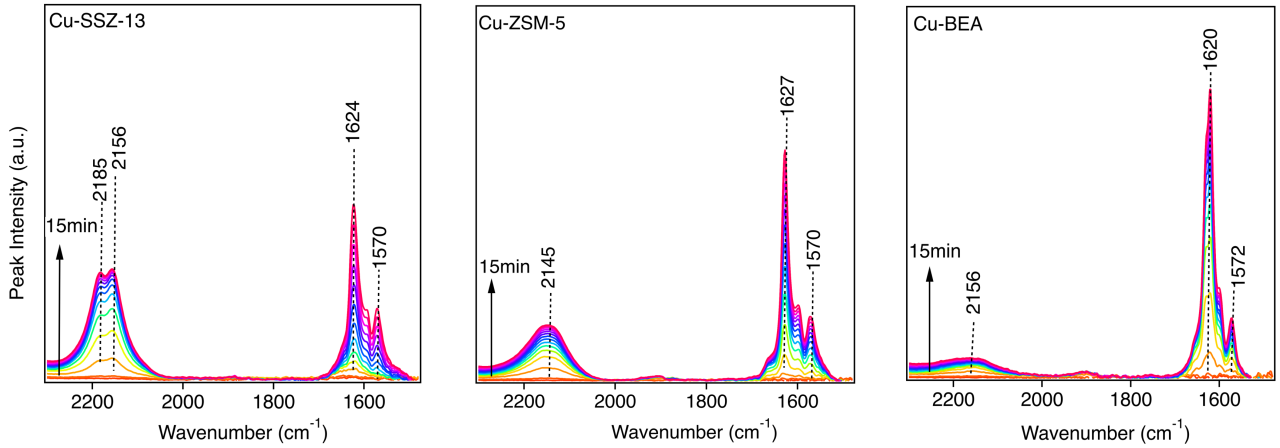

Figure 4.3: *In situ* DRIFT spectra after exposing the Cu-SSZ-13, Cu-ZSM-5 and Cu-BEA samples to NO + O_2 for 15 min at 130 °C.

vibrational bands in the 1560-1630 cm^{-1} wavenumber region could be ascribed to various configurations of surface nitrates. Another relatively broad band also appears, centered around 2154 cm^{-1} for Cu-BEA, 2145 cm^{-1} for Cu-ZSM-5 and 2156 cm^{-1} with a shoulder at 2185 cm^{-1} for Cu-SSZ-13. The band around 2150 cm^{-1} is attributed to NO^+ at the exchange sites of the zeolite (Cu^{2+}) and the shoulder (at 2185 cm^{-1} for Cu-SSZ-13) is related to N-O stretching vibrations of NO^+ adsorbed on Brønsted acid sites. [86, 87]

It has been proposed that copper can exist in two different sites in zeolite-based catalysts and based on the location of Cu in the zeolite they can be considered as isolated Cu ions or multi-nuclear Cu clusters. [76] Although the SCR reaction proceeds through different reaction pathways over different Cu species, both types of Cu ions and clusters can catalyze SCR reactions. The step response experiments initiated with NO oxidation, in which NO can be activated by isolated Cu sites and form surface NO^+ intermediate species with an oxidation state of +3 for N, or by multinuclear Cu sites, which results in the formation of intermediates with higher N oxidation states like +4 or +5, contributing in the evolution of surface nitrates or nitrites. [12]

Of the two mentioned Cu sites, isolated Cu ions are the preferred active centers for the SCR reaction, which represent excellent N_2 selectivity and high SCR activity. [12] However, in the SCR reaction, multinuclear Cu sites are involved as less active sites, in comparison with isolated Cu sites. In addition, they contribute to the formation of undesirable byproducts, such as N_2O. [12] The framework structure of the zeolite presents high importance and strong effect on the distribution of Cu sites. In small-pore zeolites, isolated Cu sites are the dominant, while multinuclear Cu sites are detected in low levels in large or medium-pore size zeolites. [12] It shows that the NO molecule originally adsorbs on an isolated

Cu^{2+} site, and, donate one electron to the Cu^{2+} ion, to reduce it to Cu^{+}. Simultaneously, the oxidation state of the N atom in the NO increases from +2 to +3 and forms NO^{+}.

An alternative assignment has been suggested for the two mentioned bands which are based on the two cationic positions in the zeolite. [86] The existence of two Cu^{2+} species in Cu-SSZ-13 zeolite with different reducibility has been reported by Kwak et al. [88] Cu ions can either occupy the six-membered rings in the zeolite framework or can be located in the cationic positions in the larger cages of the zeolite framework. Based on their observations, the peak at low wavenumber ascribes to NO^{+} placed in the six-membered ring, whereas the high wavenumber band that appeared as a shoulder, features the NO^{+} located in the larger cages of the SSZ-13 framework.

All three zeolites represent similar spectra regarding the peak positions with a difference in the peak intensities, proportional to the amounts of surface species during the NO oxidation. It is considerable that the reported peak intensity values can merely be remarked as a trend for comparison of different IR bands. The illustrated peak intensities in Figure 4.4 reveals two different trends depending on the temperature. At low temperature the Cu-BEA sample shows a higher nitrate or nitrite peak intensity with lower intensity for the NO^{+} peak in comparison to the other two zeolites, while Cu-SSZ-13 zeolite reveals a higher peak intensity for NO^{+} at lower temperature. This results in a high value of nitrate or nitrite/NO^{+} intensity ratio for the Cu-BEA zeolite, which correspond to the lower number of Cu^{2+} species in the Cu-BEA zeolite, while the Cu-SSZ-13 sample provides high abundance of Cu^{2+} species due to the higher peak intensity of NO^{+}. In the reduction cycle of the SCR, Cu^{2+} is reduced to Cu^{+}, which occurs by the adsorption of NO on Cu^{2+} sites, thus forming Cu^{+} and NO^{+}. [89]

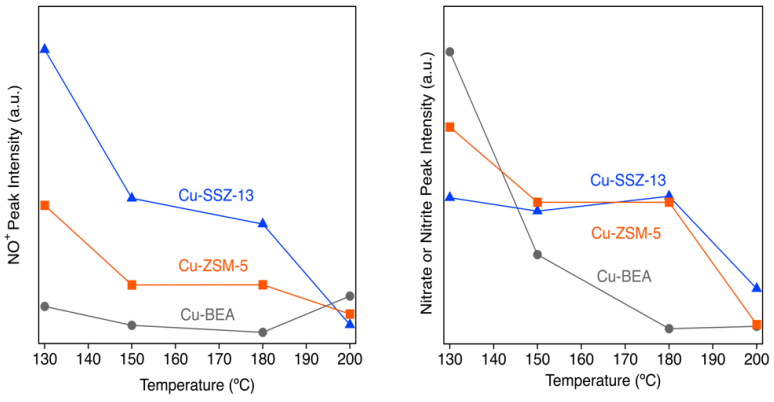

Figure 4.4: NO^{+} and Nitrate or nitrite peak intensity after exposing the Cu-SSZ-13, Cu-ZSM-5, and Cu-BEA zeolites to NO and O_2 at different temperatures.

NH_3-SCR

The surface nitrate groups on all three zeolite samples are reactive to NH_3. From Figure 4.3, the observed band around 1620 cm^{-1}, 1627 cm^{-1}, and 1624 cm^{-1} for Cu-BEA, Cu-ZSM-5, and Cu-SSZ-13, respectively, gradually disappears after exposure to a gas composition corresponding to standard SCR conditions (400 ppm NO + 400 ppm NH_3 + 10% O_2). The spectra for standard SCR are shown in Figure 4.5. Meanwhile, new bands appear in the 3100-3700 cm^{-1} and 2100–3000 cm^{-1} wavenumber region. The first bands are attributed to two series of species on the surface of the zeolite. The ones around 3100-3370 cm^{-1} is ascribed to N-H stretching vibrations of NH_3 or NH_4^+ and the ones at 3400-3700 cm^{-1} are associated with O-H stretching vibrations. However, the broad bands in the 2100–3000 cm^{-1} region, complicate the correlation between these bands and the nature of the surface species. However, this band can be generally assigned to ammonium nitrates on the catalyst surface. [47, 76, 78]

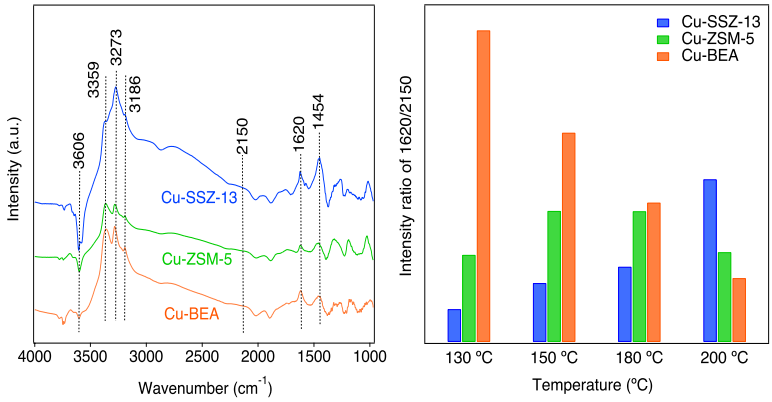

Figure 4.5: *In situ* DRIFT spectra after exposing the Cu-SSZ-13, Cu-ZSM-5 and Cu-BEA samples to Standard SCR condition for 15 min at 180 °C, and 1622/2150 intensity ratio at at different Temperatures.

Interestingly, under the standard NH_3-SCR reaction conditions at low-temperature, Cu ions are solvated by NH_3. For the solvation of a Cu^+, two NH_3 ligands are needed to form monometallic [Cu-$(NH_3)_2]^+$ complexes, while for Cu^{2+} species four-fold coordinated complexes such as $[Cu(NH_3)_4]^{2+}$, $[Cu(OH)(NH_3)_3]^+$, and complexes containing a mixture of NH_3 and NO_x can form. The [Cu-$(NH_3)_2]^+$ complexes appear abundantly over isolated Cu sites [47, 90] and very likely diffuse across zeolite pores to generate transient [CuI $(NH_3)_2]^+$-O_2-[CuI $(NH_3)_2]^+$ dimers which play a role in activation of O_2 via re-oxidation of Cu^+ ions to Cu^{2+}. [91, 92]

Hence, evaluating the emergence of surface species from adsorption of NH_3 on Cu-based zeolites is of high importance to connect their involvement in the NH_3-SCR. Interactivity between Cu and NH_3 depends on some factors such as; the nature of Cu ions (Cu^+,

Cu^{2+} or $[Cu(OH)]^{+}$) and their environment, gas phase composition, and temperature.

The redox nature of the standard SCR reaction is confirmed by the observation of both Cu(I) and Cu(II) in operando experiments, [89, 93, 94] which therefore makes it possible to correlate the activity of the catalysts with the observed reducibility. It is indicated that for attaining the Cu(II) → Cu(I) reduction half-cycle, both NO and NH_3 are required, [89, 95] and as soon as NO^+ or surface nitrite species emerge, a rapid reaction between them and NH_3 occurs under SCR condition, which subsequently results in producing water and nitrogen according to eqn. (4.2):

$$NO^+ + NH_3 \rightleftharpoons N_2 + H_2O + H^+ \tag{4.1}$$

Unluckily, the surface nitrites vibrational bands appear at fairly low wavenumbers, with the higher possibility of overlapping with the zeolite framework vibrations, which makes the interpretation of observations very difficult.

However, at the same reaction time and conditions, Cu-SSZ-13 shows higher NH_3 storage in its cages, which requires more time and NO_2 to consume all the adsorbed NH_3. The higher ammonia storage can also be confirmed from the strongly bonded NH_3 on Brønsted acid sites, which appear as the sharp negative band in the OH stretching region as in Figure 4.6. The negative peaks appeared at 3579 and 3604 cm^{-1} after NH_3 adsorption for Cu-SSZ-13 and are assigned to O–H stretching vibrations from Brønsted acid sites (-Al-O(H)-Si-) in the zeolite framework. An analogous trend is observed for the Cu-ZSM-5 and Cu-BEA samples with the values at 3602 and 3606 cm^{-1}, respectively. This indicates the existence of two types of Brønsted acid sites for Cu-SSZ-13 with higher negative intensity and one type of Brønsted acid sites for Cu-ZSM-5 and Cu-BEA. The appearance of another type of band above 3700 cm^{-1}, are attributed to O–H stretching vibrations of Al (OH) or Si (OH) surface species that can happen upon the NH_3 adsorption on silanol groups. [96]

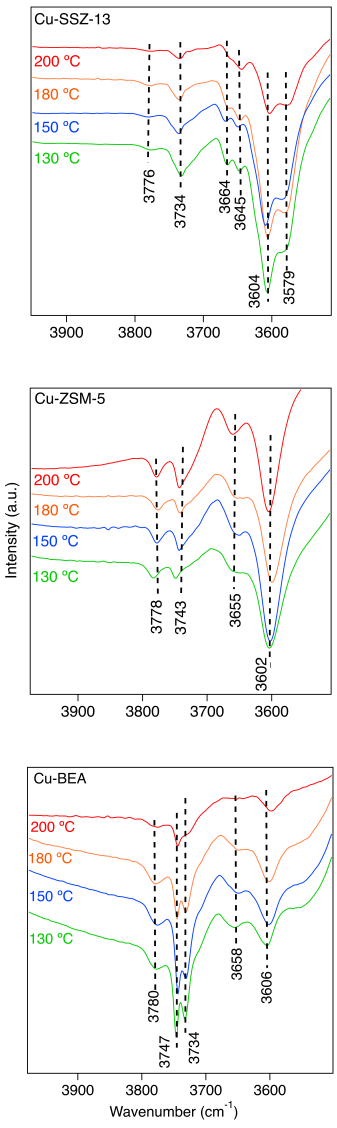

Figure 4.6: Steady state *in situ* DRIFT spectra for O-H stretching vibration region for the Cu-SSZ-13, Cu-ZSM-5 and Cu-BEA samples under standard SCR condition for 15 min at different temperatures.

NO_2 SCR reaction over pre-adsorbed NH_3

The introduction of NO and NO_2 after NH_3 adsorption consumes all pre-adsorbed NH_3 in all three zeolite samples, faster for the large-pore zeolite. This can result in higher and faster AN formation and subsequent release, during SCR condition, which facilitates the formation of N_2O at higher temperatures.

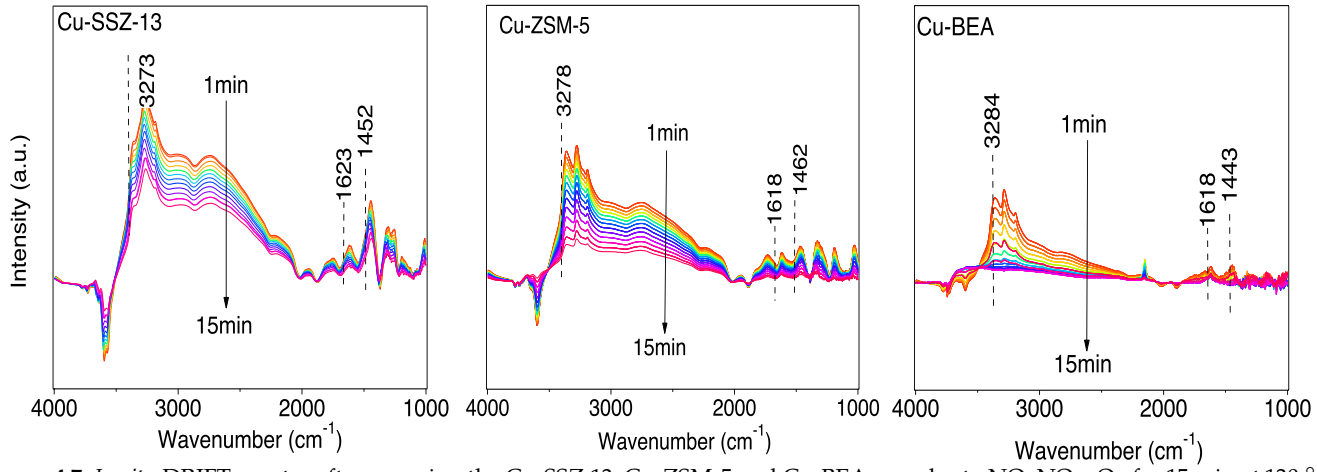

Figure 4.7: *In situ* DRIFT spectra after exposing the Cu-SSZ-13, Cu-ZSM-5 and Cu-BEA samples to NO, NO_2, O_2 for 15 min at 130 °C.

In order to study the interaction of ammonia and NO_2 over the catalysts, step response experiments with pre-adsorbed NH_3 were performed. During the experiments the amount of surface NH_3 species decreases as function of NO_2 exposure time. Figure 4.7 shows the *in situ* DRIFTS spectra obtained during the exposure of Cu-SSZ-13, Cu-ZSM-5 and Cu-BEA to NO_2 and NO (200 ppm each) and 10% O_2. Exposing the catalysts to the mentioned gas composition for 15 min shows a decline in the peak intensity corresponding to ammonia species adsorbed on acid sites (both N-H stretching and N-H bending region). The reaction between NO_2 in the gas feed and the pre-adsorbed NH_3 proceeds according to the following overall reaction in eqn. (4.2): [97]

$$4NH_3 + 3NO_2 \rightleftharpoons 3.5N_2 + 6H_2O \tag{4.2}$$

An interesting observation is a faster peak intensity drop for the Cu-BEA sample compared to the Cu-ZSM-5 and Cu-SSZ-13 samples within 15 min of exposure time. It seems that the degree of NH_3 consumption is connected to the framework structure of the zeolite, and the large-pore Cu-BEA zeolite has a lower capacity to accumulate NH_3 compared to Cu-ZSM-5 and Cu-SSZ-13, and within 15 min the pre-adsorbed NH_3 is almost consumed, while the higher amount and strongly bonded NH_3 in the Cu-SSZ-13 sample requires more NO_2 and longer exposure time to be able to consume the pre-adsorbed NH_3. For making this clear, three different peaks corresponding to the ammonia species adsorbed on the different acid sites of the zeolites have been chosen and the intensity of these peaks illustrated versus the gas exposure time in Figure 4.8. This observation agrees with the trends in the OH stretching region in Figure 4.6, in which demonstrates the intense negative peak in the OH stretching region for the Cu-SSZ-13 sample indicates larger amount of strongly bonded NH_3 on the sample

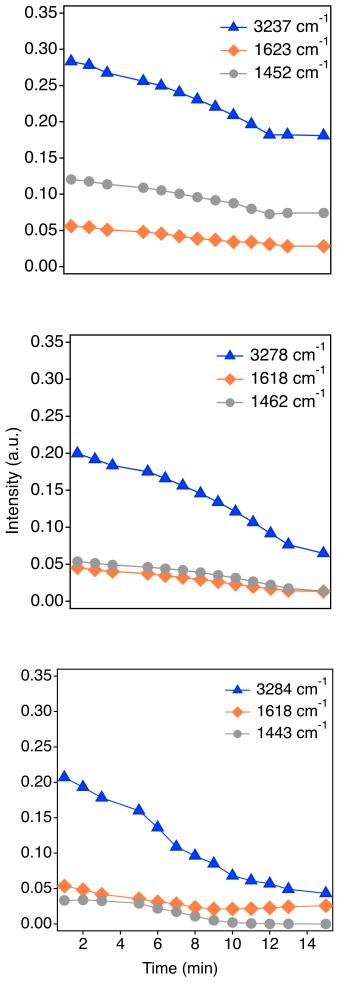

Figure 4.8: *In situ* DRIFT spectra peak intensity for pre-adsorbed NH_3 on different acid sites of the Cu-SSZ-13 (top), Cu-ZSM-5 (middle), and Cu-BEA (bottom) zeolites exposed to NO + NO_2 + O_2 at 200 °C.

surface. Furthermore, it can be concluded that NO_2 represents a higher reactivity compared to NO, due to the consumption of accumulated NH_3 on the zeolite surface by NO_2.

Copper Species

The reducibility of the oxidized Cu-SSZ-13, Cu-ZSM-5, and Cu-BEA samples was evaluated by H_2-TPR analysis to achieve an insight regarding the existence of various types of Cu species over the zeolites. The results, which are discussed in **Paper II**, demonstrates the presence of different Cu species; Cu^{2+}, Cu^{+}, $[Cu(OH)]^{+}$, and CuO. It is worth noting that the SSZ-13 sample possesses relatively higher amount of Cu^{2+} compared to the other two counterparts. These results are in agreement with *in situ* DRIFTS observations during the NO oxidation step in Figures 4.3 and 4.4, which show a higher peak intensity for NO^{+} (vibration of NO adsorbed on Cu^{2+}) for the small-pore zeolite sample compared to the other two zeolites. The distribution of the main copper species obtained from H_2-TPR measurements are presented in Figure 4.9. It shows that the Cu-SSZ-13 zeolite has the highest Cu^{2+} populations while the higher amount of $[Cu(OH)]^{+}$ species appears for the Cu-BEA zeolite. Besides the H_2-TPR measurements, further investigation of the Cu species in connection to the zeolite framework structure, the perturbation of T-O-T vibrations of the zeolite framework by NH_3 has been evaluated and the data are presented in Figure 2, **Paper II**. The investigation of structural vibrations of T-O-T bonds (Si-O-Si and Si-O-Al) is a way of quantifying the obtained Cu species from H_2-TPR. The antisymmetric T-O-T vibration of the framework oxygen (O_{fw}) is susceptible to the interaction with Cu cations. So, the binding of NH_3 to the Cu cations results in further modification in the interaction between cation and O_{fw}. As a consequence, IR band displacement from the unperturbed position (1020-1100 cm^{-1}) occurs due to the existence of Cu cations. [88, 98, 99] IR features at 901 and 948 cm^{-1} for Cu-SSZ-13, are assigned to asymmetric T-O-T vibrations perturbed by Cu ions in the form of Cu^{2+} and $[Cu(OH)]^{+}$, respectively. [88]

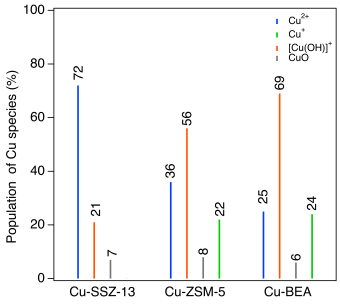

Figure 4.9: The population of Cu species in Cu-SSZ-13, Cu-ZSM-5, and Cu-BEA zeolites, based on H_2-TPR measurements (0.2% H_2 in Ar, 10 °C.min^{-1}.)

The percentages are calculated based on the integration of deconvoluted peak area of H_2 consumption during H_2-TPR.

While both IR bands were detected for all samples, their corresponding intensities varied for the different samples suggesting diverse populations of Cu^{2+} and $[Cu(OH)]^{+}$ within these catalysts. It has been found that the Cu^{2+} species located inside large pores of the zeolite can become hydrated to some extent by residual H_2O formed during the cooling of the DRIFTS cell. The totally dehydrated Cu^{2+} species inside the large cages of CHA were reported to give rise to a peak at 901 cm^{-1} with a band shift of 119 cm^{-1} owing to the interaction with water. [99, 100] In the case of Cu-BEA and Cu-ZSM-5, the position of the peak corresponding to

Cu^{2+} species is around 924 and 914 cm^{-1} with a band shift of 96 and 106 cm^{-1}, respectively. Also, the intensity of the peak attributed to the Cu^{2+} species is seen to be higher for the Cu-SSZ-13 sample compared to the other Cu-ZSM-5 and Cu-BEA, which supports the presence of Cu^{2+} species in small-pore zeolite rather than in medium- and large-pore zeolites. So, the ammonia storage capacity and reducibility of the zeolite have a crucial effect in proceeding the SCR process. It leads us to take a closer look at the acidity of the zeolites and to investigate how it changes by altering the pore size of the zeolite which is discussed in section 4.1.4.

4.1.4 Ammonia storage capacity in the zeolites with different frameworks

For obtaining information regarding the interaction of ammonia and zeolites and determining the concentration of acid sites and acid strength in each zeolite sample, NH_3-TPD experiments were carried out for the washcoated monolith samples. The illustrated results in Figure 4.10 shows the emergence of two distinct peaks for the H-type zeolites. The peak at lower temperature is attributed to weakly bonded NH_3 and the one at higher temperature is related to strongly bonded NH_3 on the Brønsted acid sites. Among the three different zeolites, H-SSZ-13 contains higher number of strong Brønsted acid sites, shown as a peak at 390 °C, followed by H-ZSM-5 and H-BEA with peaks at 310 °C and 270 °C, respectively.

Upon the addition of copper, an extra peak develops at intermediate temperature for the Cu-SSZ-13 sample, while the intermediate temperature peak cannot be seen for the Cu-ZSM-5 or Cu-BEA samples. The reason for this can be due to the higher strength of the Brønsted acid sites compared to that of the Lewis acid sites in the Cu-SSZ-13 sample. For the Cu-BEA and Cu-ZSM-5 samples, the medium temperature peak cannot be observed but might be embeded in the other two peaks due to the overlap of the ammonia desorption peak from Lewis acid sites with the one from Brønsted acid sites. In addition, the NH_3-TPD results show a clear ammonia storage capacity for the Cu-BEA and Cu-ZSM-5 samples, specifically for Cu-ZSM-5 with a remarkable amount of ammonia desorption compared to similar conditions for the H-ZSM-5 sample.

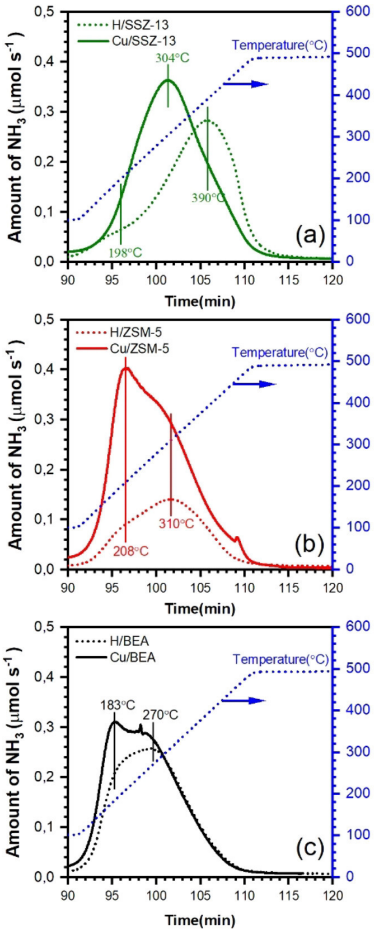

Figure 4.10: Ammonia temperature-programmed desorption for the samples with (a) CHA, (b) ZSM-5, and (c) BEA framework structure. Gas inlet during adsorption: 400 ppm NH_3 , 5% H_2O in Ar for 1 h at 100 °C, flow rate: 1200 mL.min $^{-1}$, heating rate: 20 °C.min^{-1}.

4.2 The effect of Si/Al molar ratio and copper content in ammonia SCR

Typically, the nature and location of Cu species are affected by two features: the Si/Al molar ratio and the synthesis method.

[58, 101–103] The Si/Al molar ratio has also been found to play a role in determining the number of acid sites in zeolites, which further remarkably affects the deNO$_x$ performance. [58, 102, 103] However, in recent years many metal-promoted zeolites have shown acceptable NH$_3$-SCR activity. It has been reported that Cu-based zeolites with SSZ-13 framework exhibit a superior catalytic activity and higher hydrothermal stability compared to other zeolites especially with a lower Al content. In addition to the active Cu species, the general framework acidity of the zeolites has been proposed as a decisive factor for NH$_3$-SCR activity. However, the role of different types of acid sites in NH$_3$-SCR is still not fully understood.

Hence, this section mainly focuses on the effect of Si/Al molar ratio and copper content in the SSZ-13 zeolite on the ammonia storage behavior and also the formation of different species and correlate them to the deNO$_x$ performance in the NH$_3$-SCR over the zeolites. **Paper III** investigates the surface acidity over samples with different Si/Al and Cu/Al molar ratio to obtain a helpful information regarding the type and strength of acid sites and correlate them to the behavior of the catalysts. The same samples have been applied in **Paper IV** to study the NO$_x$ conversion and N$_2$O formation in the flow reactor and correlate with the spectroscopic findings. In **Paper V**, the samples with Si/Al= 12 is in focus to evaluate the role of pretreatment on the zeolites SCR performance.

4.2.1 Ammonia storage over zeolite-based catalysts

In section 4.1.4, the effect of framework structure of the zeolite on the ammonia storage capacity of the zeolite has been investigated and the results showed that ammonia storage has a dependency on the type of zeolite framework and plays a crucial role in NO$_x$ abatement. These observations brought us to the point to evaluate the role of ammonia storage capacity in the NH$_3$-SCR system, with regard to the NO$_x$ conversion efficiency. For this purpose, small-pore size zeolite (SSZ-13) with higher hydrothermal stability has been used and the ammonia storage capacity has been investigated on this zeolite with varying Si/Al and Cu/Al molar ratio.

Temperature-programmed desorption of ammonia

The concern in zeolite acidity is motivated by the significance of zeolites as solid acid catalysts. Typically, the interaction between the acid sites of the zeolite and basic probe molecules helps to recognize Lewis and Brønsted-type acid sites and also distinguish the amount together with the acidic strength. Temperature-programmed desorption (TPD) with NH$_3$ is one of the most widely used methods

for characterization of acid sites in catalysts. The method is uncomplicated and relies on measuring the desorption profile of pre-adsorbed NH_3 during a controlled temperature ramp. It has been extensively accepted that the Si/Al molar ratio has a pronounced effect on the acidity of zeolites, and thus influences the NH_3-SCR performance. [58, 101]

In order to examine the effect of different Si/Al molar ratio on the acidity of the SSZ-13 zeolite, NH_3-TPD experiments were carried out for SSZ-13 samples with three Si/Al molar ratio and Cu/Al molar ratio of 0, 0.1, and 0.4. The results are displayed in Figure 4.11. Moreover, the pretreatment of the samples is crucial and should be considered. The pretreatment was done in two steps: first in the presence of Ar and 10% O_2 at 550 °C for 1 h, followed by exposing the samples to a mixture of 400 ppm NO, 400 ppm NH_3 in Ar, at three different temperatures (250, 200, and 150 °C, for 30 min each). Based on the pretreatment, different types of Cu species can be formed, like Cu^+, $[Cu\text{-}(NH_3)_2]^+$, and $[Cu\text{-}NH_3]^+$ complexes, which are decomposed at high temperature and form framework-bond Cu^+ species. This is discussed in detail in Section 3.2 in **Paper III**.

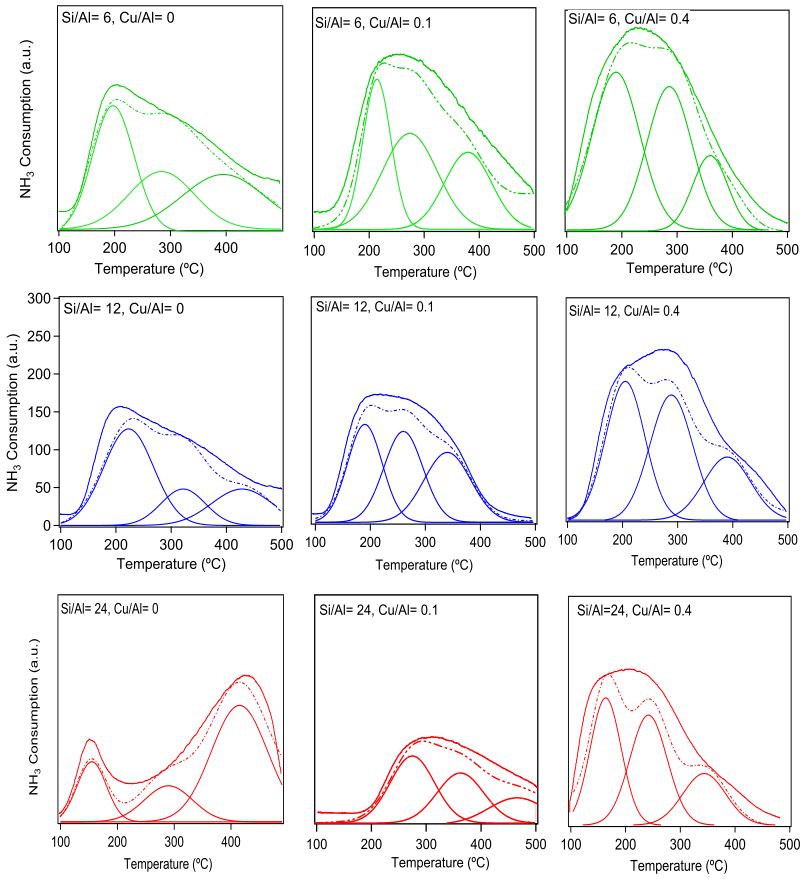

Figure 4.11: Deconvoluted peaks from the NH_3-TPD experiments carried out for the SSZ-13 samples with three Si/Al molar ratio and Cu/Al molar ratio of 0, 0.1, and 0.4.

In the TPD profiles it can be seen that the NH_3 desorption peak can be fitted to three NH_3 desorption peaks. A low-temperature (LT) desorption peak at around 180 °C ascribed to the weakly

adsorbed NH_3 on the weak Lewis acid sites or the physisorbed NH_3 on the surface or zeolite framework, a medium-temperature (MT) desorption peak owing to the NH_3 adsorbed on the strong Lewis acid sites developed by the isolated Cu^{2+} ions at around 250-350 °C and a high-temperature (HT) desorption peak above 350 °C assigned to the NH_3 desorption from the Brønsted acid sites. [58, 104]

As anticipated, the total amount of acid sites in the sample with Si/Al= 6 molar ratio is remarkably larger than that of the samples with Si/Al= 12, and Si/Al= 24 molar ratio, rendering that the increase in Si/Al molar ratio, results in a decline in the acidity. Particularly, for the weak Lewis acid sites, which are connected to extra-framework Al, the sample with Si/Al= 6 molar ratio favors the adsorption of NH_3 on the Lewis acid sites. [58] In addition, the disparity of Brønsted acidity between the catalysts with the lowest and highest Si/Al molar ratio is remarkable, which is owing to the less content of Brønsted acidity and framework Al in the sample with Si/Al= 24. In addition, the total acid quantity of the samples with higher Cu content was obviously larger than that of lower Cu (or no) content, which can be attributed to the noticeable increase in the number of isolated Cu^{2+} ions with an increase in the Cu/Al molar ratio. [104]

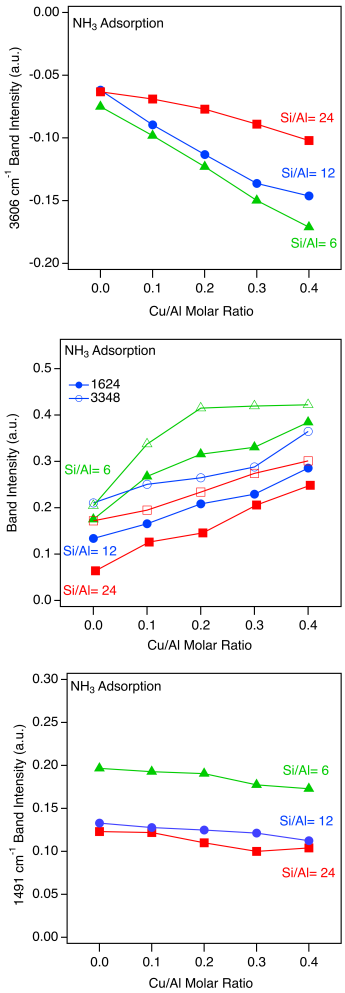

Figure 4.12: Peak intensities obtained from *in situ* DRIFT spectra during NH_3 adsorption for SSZ-13 catalysts with Si/Al (6, 12, and 24) and Cu/Al (0-0.4) molar ratio after 15 min at 70 °C.

Nature of acidic sites in Cu-SSZ-13 followed by *in situ* DRIFTS

In situ DRIFT-NH_3 adsorption experiments were carried out to investigate the NH_3 adsorption properties of the zeolites. As mentioned earlier, the zeolites acidity and the acid sites could be estimated applying NH_3 as a probe molecule. NH_3 can adsorb on both Lewis and Brønsted acid sites in the zeolites. The intensity of the band at 3606 cm^{-1} together with the bands at 3348, 1624 and 1491 cm^{-1} vs Cu/Al molar ratios are depicted in Figure 4.12, and the corresponding DRIFTS-NH_3 adsorption spectra of the zeolite samples are depicted in Figure 4.13. The NH_3 adsorption spectra over the SSZ-13-zeolites show some negative bands around 3606, and 3656 cm^{-1} which are generally assigned to the NH_3 adsorption on these OH bands resulting in the blockage of OH sites. The results reveal a decreasing trend for the band at 3606 cm^{-1} by elevating Cu loading, with the highest decrease for the sample with low Si/Al molar ratio. Generally, it is considered that upon copper exchange in the zeolite framework through ion exchange, the positive charge of Cu^{2+} ions should be neutralized by two negative charges, probably two aluminum atoms in the nearby proximity.

Based on the applied pretreatment in **Paper III**, the Cu^{2+} species have less possibility to exist in the zeolite. The results simply display

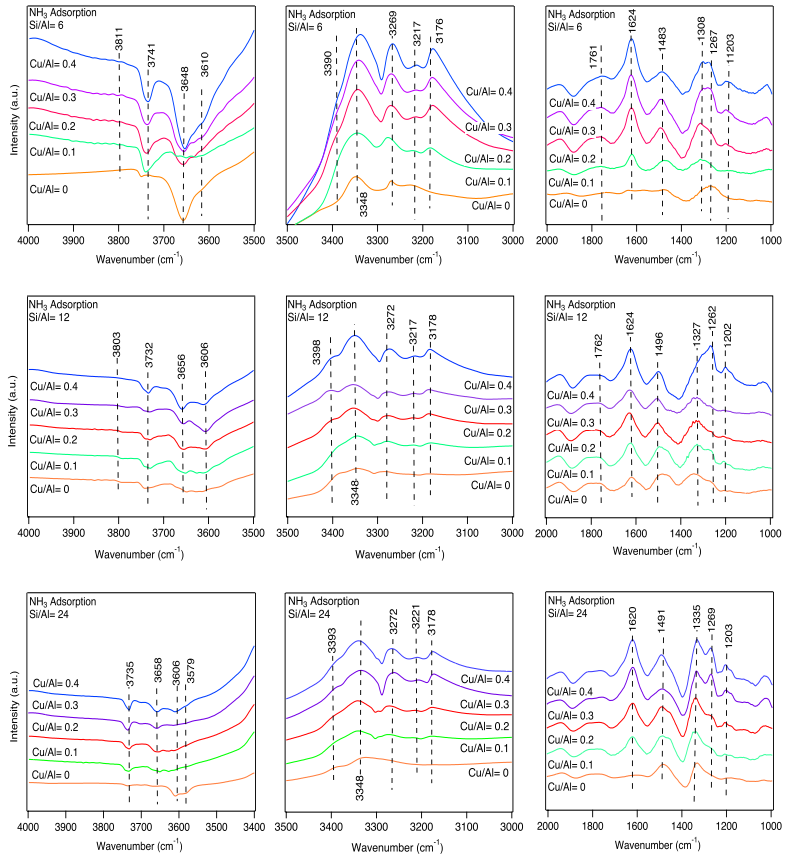

Figure 4.13: *In situ* DRIFT spectra for NH_3 adsorbed on different acid sites of the Cu-SSZ-13 catalysts with different Si/Al (6, 12, and 24) and Cu/Al (0-0.4) molar ratios at 70 °C. (NH_3= 400 ppm in Ar).

the presence of a constant concentration of non-exchanged Brønsted sites, even at copper contents close to the stoichiometric exchange level. This indicates that via Cu ion exchange, Cu^{2+} appears in the form of $[Cu–OH]^+$, and result in the partial exchange of Brønsted acid sites with this complex. This is confirmed with observations of an intense negative band around 960 cm^{-1} in Figure 4.14, attributed to the T-O-T stretching vibrations of NH_3 adsorption on the copper sites, and reveals the dominant populations of $[Cu–OH]^+$ species in the zeolites, as well.

The bands associated with NH_3 adsorption at 3500 to 3000 cm^{-1} are ascribed to the N–H stretching vibrations of ammonia. In addition, the small band around 1624 cm^{-1} are related to the NH_3 adsorption on the Lewis acid sites, while the band at 1449 cm^{-1} occurs from the bending vibration of NH_4^+ ions on the Brønsted acid sites.

Adsorption step followed by NH_3-TPD experiments measured by *in situ* DRIFTS for targeting the effect of different Si/Al molar ratio for the acidity of SSZ-13 zeolites. The desorption peak intensities around 3601, 1620, and 1450 cm^{-1} for the steady state at 200 °C are shown in Figure 4.15. The peak intensity of the desorption peak at 3601 cm^{-1} presents a very slight change in the intensity by increasing the temperature, and has almost the same intensity as the adsorption step. This observation can be due to the required

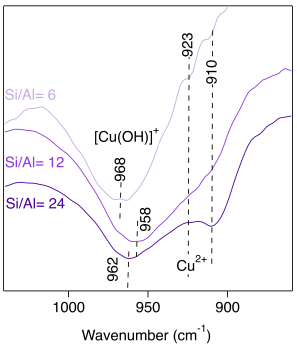

Figure 4.14: DRIFTS spectra of T-O-T vibrational region perturbed by NH_3 adsorption at 70 °C for Cu-SSZ-13 samples with Si/Al= 6, 12, and 24 and Cu/Al= 0.4 molar ratio.

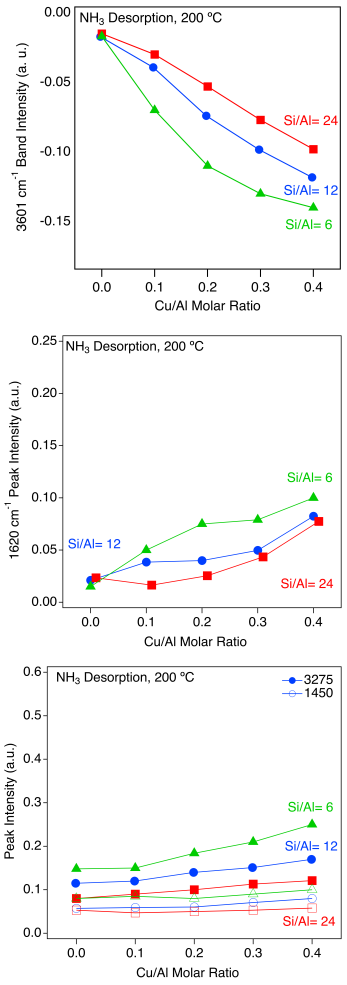

Figure 4.15: Peak intensities obtained from *in situ* DRIFT spectra during NH_3 desoprtion after 15 min under Ar flow for SSZ-13 catalysts with different Si/Al (6, 12, and 24) and Cu/Al (0-0.4) molar ratio at 200 °C.

desoprtion temperature of NH_3 from the Brønsted acid sites which is higher than the applied temperature in our study, exhibiting an intensity decline by elevating temperature to around almost 50% in the band at 1624 cm^{-1} compared to the one at 1450 cm^{-1} which shows a slight decrease. This infers that at 200 °C weakly bonded ammonia on Lewis acid sites (the band at 1624 cm^{-1}) can easily be desorbed compared to the ones strongly adsorbed on Brønsted acid sites (the band at 1450 cm^{-1}).

Thus, the NH_3 desorption from the weak Lewis acid sites proceeds faster. A decrease in the intensity of the complicated signal at the 1550-1300 cm^{-1} region at 200 °C indicates less thermal stability of the ammonium species.

For more clarification, the bands at the 1550-1300 cm^{-1} region were deconvoluted for the Cu-SSZ-13 sample with SAR= 24 and the results are presented in Figure 4.16. At a lower Si/Al molar ratio with higher Al content, disordered peaks appear upon deconvolution due to the Al distribution which result in many configurations of NH_3 species. Considering the spectra at 130 °C, the signal intensity attributed to the NH_4^+ species on Brønsted acid sites decreases during the desorption process for all the samples.

Elevating the temperature to 200 °C, results in a slight red shift of the component at 1475 cm^{-1} for the sample with Si/Al= 24 to around 1470 cm^{-1}, with a further decrease for the peak intensity at 1470 cm^{-1} accompanied by an increase of the peak intensity at 1447 cm^{-1}. This behavior simply shows that during the desorption procedure, the species are connected to the band at 1470 cm^{-1} are transformed into species related to the 1447 cm^{-1} band. The shifts in the vibration modes of NH_4^+ ions are most probably owing to the NH_3 coordinated to NH_4^+. The band around 1470 cm^{-1} could also originate from the $NH_4^+.nNH_3$ associations. It is notable that a higher temperature could restrict the amount of solvated NH_3 molecules. Therefore, at different desorption temperatures the band at 1437 cm^{-1} is composed of two main components at 1410 and 1447 cm^{-1}, and these bands could be plainly assigned to the antisymmetric and symmetric bending vibrations of not-solvated NH_4^+.

Additionally, at higher Cu content, less decrease in the peak intensity is observed compared to the samples with lower Cu/Al molar ratio, which renders higher desorption possibility at lower Cu loadings. However, it is worth noting that the NH_3 adsorption is lower at higher Cu loading for the peak at 1491 cm^{-1} and there is not a drastic change in the desorption peak at 130 °C.

To further clarify the changes of the species during the NH_3 adsorption and NH_3-TPD process over different SSZ-13 catalysts, DFT calculations were performed. This also provides a guide for

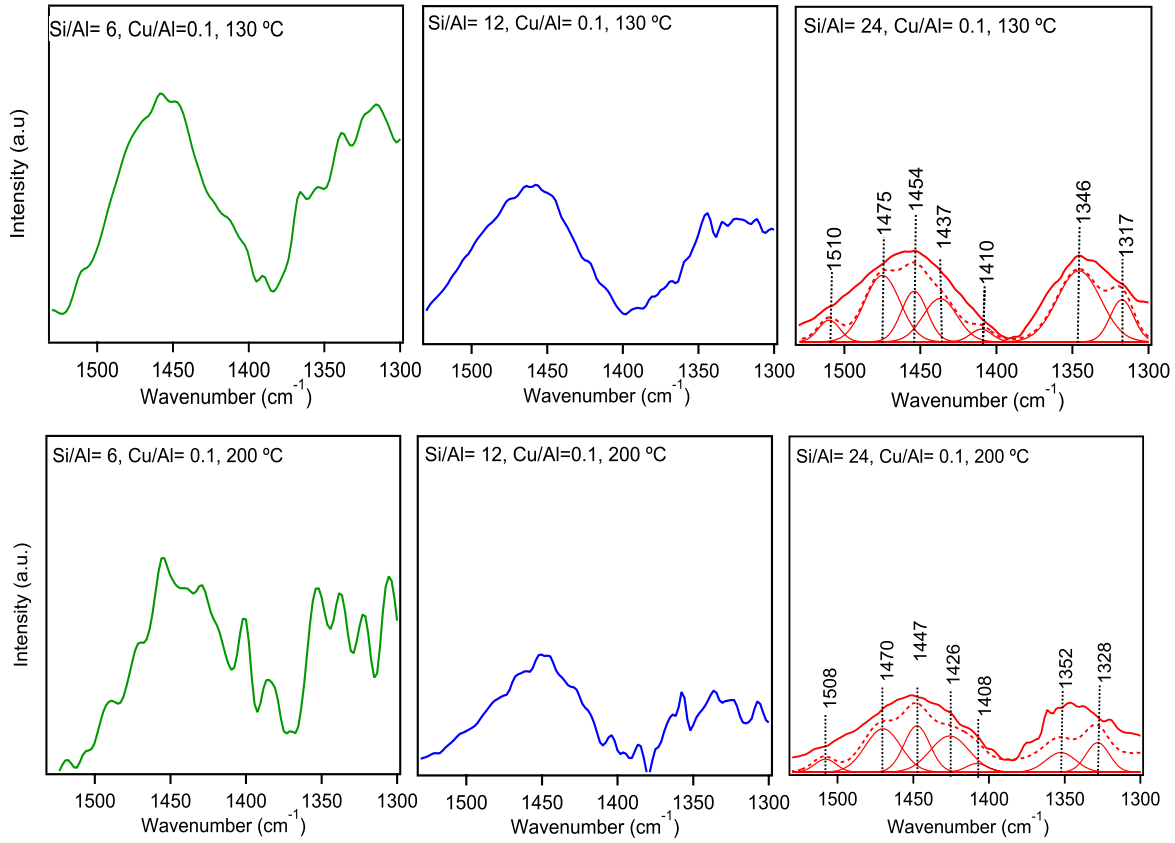

Figure 4.16: The deconvoluted δ(NH) spectra of NH_4^+ ions at 130 and 200 °C desorption temperature during NH_3-TPD.

identification of the various IR bands. The structures and relevant vibrations of the potential species are illustrated in Figure 4.17

Comparing the measured DRIFT spectra with the simulated infrared spectra for different species, presents an acceptable match between the simulated infrared spectra of $[Cu(NH_3)_2]^+$, and $NH_4^+.NH_3$ and the experiments.

These findings indicate that for the unpromoted SSZ-13 catalysts, $NH_4^+.NH_3$ species predominately appear after NH_3 adsorption at 70 °C, with contribution to the band at 3348 cm^{-1} that loses intensity for increasing Si/Al molar ratio. At lower Si/Al molar ratio, $[Cu(NH_3)_4]^{2+}$ species appear, which result in the emergence of multiple peaks, with the low wavenumber at 3185 cm^{-1} in Figure 10, **Paper III**. At elevated Si/Al molar ratio, however, copper exists essentially as Cu^+, hence $[Cu(NH_3)_2]^+$ appears which gives relatively simple spectra (corresponding to the orange curve in Figure 10, **Paper III**) and sustains the peaks around 3185 cm^{-1}.

It is obvious from Figure 4.13 that the band at 3176 cm^{-1} correlates positively with the Cu content, and negatively with the Si/Al molar ratio, with a slight shift to a higher wavenumber with increasing Si/Al molar ratio. This observation is consistent with the results

Structure	Wavenumber (cm^{-1})
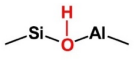	3601
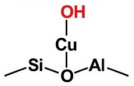	3678
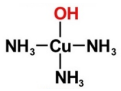	3759
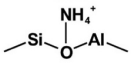	3192, 1477
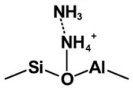	3329, 1524
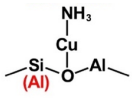	1 Al: 1627, 1223 2 Al: 1638, 1222
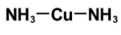	1 Al: 3284, 1606, 1239

Figure 4.17: Calculated vibrations for O-H stretching and N-H bending of potential species.

of DFT calculations, supporting that the amount of $[Cu(NH_3)_2]^+$ rises with increasing Si/Al molar ratio.

4.2.2 Catalytic performance and surface species during NH_3-SCR over SSZ-13 catalysts

It is commonly assumed that NH_3 is activated on the Brønsted acid sites of the zeolite in the form of ammonium (NH_4^+) ions, which later react with NO_x species to form N_2 and H_2O. However, it has also been proposed that Brønsted acid sites may not be needed for NH_3 adsorption or activation, and the support mainly works as an NH_3 reservoir, for facile migration of NH_3 to the active site.

In general, NH_3 storage capacity plays a crucial role in the NH_3-SCR reaction, in which NO_x conversion efficiency, especially at low temperatures, to a large extent is determined by the amount of stored NH_3. Hence, zeolites present an exceptional NH_3 storage capacity and an optimal performance of the NH_3-SCR system can merely be achieved by adopting and controlling NH_3 storage capacity of zeolites.

NH_3-TPD experiments followed by standard and fast SCR reactions, which were carried out for the SSZ-13 samples studied in **Paper III**. The obtained results for the NO_x conversion and corresponding N_2O yields for the samples with Si/Al= 6, 12, and 24 are exhibited for one low and one high Cu content in Table 4.3 and Figure 4.18, respectively. An elevated NO_x conversion during both standard and fast SCR reaction conditions is seen by increasing Cu content which overlaps for the samples with higher Cu/Al molar ratio than 0.2. This infers that the selectivity in the NH_3-SCR reaction for these samples reaching almost 90%. The activity develops from 130 °C to 250 and 230 °C during standard and fast SCR, respectively. Hence, not only the Cu content but also the reaction temperature plays a role for the SCR activity changes. It is worth noting that the presence of NO_2 in fast SCR promotes NO_x conversion and N_2O formation.

Furthermore, at temperatures below 300 °C, N_2O forms to higher extent at elevated Cu content. In this study, the main focus is the N_2O formation at temperatures below 350 °C. From Figure 4.18, it is obvious that N_2O formation is promoted for the highest Cu containing samples. The lowest amount of N_2O is formed over the Cu/Al= 0 catalyst via standard SCR conditions (data for all Cu loadings are shown in **Paper III**). This is possibly related to the lack of $[Cu(OH)]^+$ species. As discussed earlier regarding the different N_2O formation pathways, at lower temperatures N_2O originates from the formation of H_2N_2O and HONO intermediates over copper peroxo complexes and their subsequent decomposition on

Brønsted acid sites. [105] Hence, it is debatable that Cu can play a crucial role in the N_2O formation under standard SCR conditions. Also, the content of Cu^{2+} species at low temperatures, can be the reason for a change in the N_2O formation trend at lower Cu contents, which needs further investigation. Moreover, N_2O formation occurs to a high extent over samples with Cu/Al= 0 and Cu/Al= 0.1 molar ratio under fast SCR conditions. It infers that N_2O formation over unpromoted (or lower Cu content) samples can happen through NH_4NO_3 formation and its subsequent decomposition without activating Cu sites.

NO_x conversion above 90% during standard SCR could be obtained for all samples with Cu/Al= 0.4 molar ratio at 250 °C, and is observed to be promoted with increasing Cu loading. However, the sample with Si/Al= 24 and Cu/Al= 0.4 presents a lower NO_x conversion in the same temperature range. In order to understand the reason, the nature of Cu catalytic centers in SSZ-13 zeolites and the effect of Si/Al molar ratio needs to be evaluated.

Overall, the interplay between Cu ion content, its mobility and reaction temperature make a complicated NH_3-SCR system. Doubtlessly, SCR catalysis is further influenced by the Si/Al molar ratio of the SSZ-13 zeolite, and it affects both the Cu ion locations and considerably also altering Brønsted acidity and, NH_3 storage of the zeolites. One of the beneficial aspects of lower Si/Al molar ratio

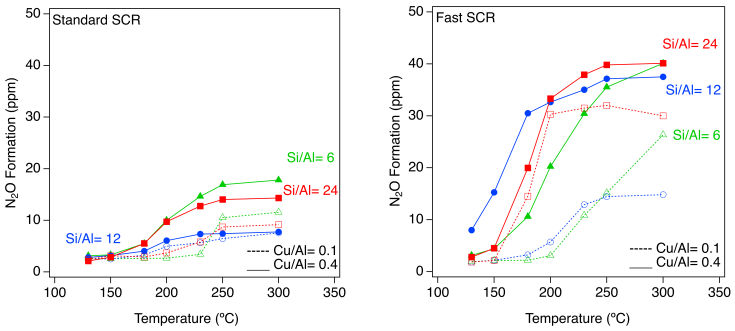

Figure 4.18: Steady-state N_2O formation as a function of temperature for Cu-SSZ-13 with Si/Al= 6, 12, and 24 and Cu/Al= 0.1, and 0.4 molar ratio under standard and fast SCR conditions

of zeolite-based SCR catalysts, is providing more NH_4^+ species owing to the existence of more Brønsted acid sites. [58] However, a few recent studies on SSZ-13 catalysts exhibit less reactivity of NH_4^+ species towards NO_x conversion compared to the molecular NH_3 adsorbed on Lewis acid sites. [58, 78] Brønsted acidity is expected to affect the SCR reaction by affecting Cu ion distribution and NH_3 storage capacity of the zeolites rather than the formation of reactive NH_4^+ species.

Numerous studies have been reported on the nature of Cu catalytic centers in Cu-SSZ-13, [47, 88, 106] and it has been suggested that Cu predominately appears as isolated Cu^{2+} ions in SSZ-13; and preferably reside near the windows of 6MR and bind with 2 Al

Table 4.3: Steady-state NO_x conversions for Cu-SSZ-13 with Si/Al= 6, 12, and 24 and Cu/Al= 0.1, and 0.4 molar ratio under standard and fast SCR conditions at 150 and 250 °C.

Si/Al	Standard	Fast
150 °C		
Cu/Al= 0.1		
6	28.9%	33.2%
12	16.2%	35.8%
24	25.3%	31.9%
Cu/Al= 0.4		
6	32.6%	42.6%
12	58.7%	56.3%
24	35.4%	39.9%
250 °C		
Cu/Al= 0.1		
6	40%	82.8%
12	73.7%	83.2%
24	57.2%	73.6%
Cu/Al= 0.4		
6	98.7%	97.8%
12	98.8%	97.9%
24	96.8%	92.9%

T-sites under dry conditions. [46, 107] On the contrary, at relatively high Si/Al molar ratio with less possibility of finding 2 Al sites in a 6MR, isolated Cu ions charge balance only one Al sites further apart for example in a 8MR. For this case, $[Cu(OH)]^+$ and Cu^+ species are required in order to properly balance the negative framework charge. [108]

DRIFTS Studies

The evolution of different species during standard SCR (400 ppm NO, 400 ppm NH_3, 10% O_2) over zeolite samples with different Si/Al and Cu/Al molar ratio was followed by *in situ* FTIR. The outlined results for the 1000-2200 cm^{-1} wavenumber region in Figure 4.19, shows an increasing trend for the band at around 1622 cm^{-1} while a decline is seen in the intensity of the band at 1456 cm^{-1} by elevating Cu loading. A decrease in the intensity of the band at 1456 cm^{-1}, attributed to NH_3 adsorbed on Brønsted acid sites, originates from a drop in Brønsted acid sites, which can be owing to the coordination of Cu with Al at higher Cu loadings. [109]

Furthermore, the reaction of NH_4^+ species is almost complete for the samples with Si/Al= 12 and 24 with Cu/Al= 0.4 molar ratio after 15 min at 200 °C, while for the Cu/Al= 0.1 the reaction needs longer time to be completed, demonstrating the important role of the Cu^{2+} ions in the SCR reaction. [83]

The results obtained for the Cu-SSZ-13 zeolite with different Si/Al molar ratio show different reactivities for NH_3 species under SCR conditions; the spectrum recorded after 15 min shows the disappearance of the NH_3 species adsorbed over Lewis acid sites (Al or Cu^{2+} ions) to be almost complete, whereas the disappearance of NH_4^+ species formed over the Brønsted acid sites is much slower.

These results indicate the established view that the NH_4^+ ions on the Brønsted acid sites hardly contribute to the SCR process and may not be essential for the NH_3-SCR reaction. However, they function predominantly as NH_3 storage sites, as previously inferred within NH_3-TPD experiments. [96, 110]

N_2O formation was also investigated during standard and fast NH_3-SCR for all the samples at different temperatures. The obtained spectra during standard and fast SCR for the sample with Si/Al= 12 containing Cu/Al= 0.1, and 0.4 at 130 and 200 °C are shown in Figure 4.20. The evolution of two bands around 2230 and 2123 cm^{-1}, corresponding to N_2O and NO^+ adsorbed on Lewis acid sites, are clearly seen. The elevated peak intensity for N_2O by increasing Cu loading can be attributed to the higher content of $[Cu(OH)]^+$

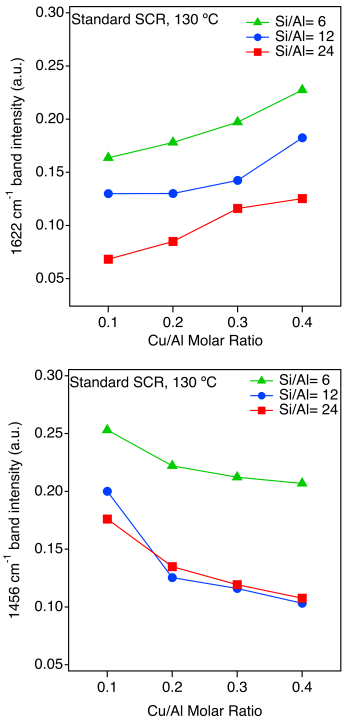

Figure 4.19: The signal intensity obtained from *in situ* DRIFT spectra at 1622 and 1456 cm^{-1} as a function of Cu/Al molar ratio for the Cu-SSZ-13 samples with with different Si/Al (6, 12, and 24) and Cu/Al (0-0.4) molar ratio for steady-state during standard SCR at 130 °C.

species, which consequently elevate the oxidative ability of the catalysts. [109]

Accordingly, the higher Cu content improves the formation of NO_3^- species and enhances the oxidative ability of the catalyst in oxidizing nitrite to nitrate species. This in line with our findings in Figure 4.19, in which an increase in the Cu content results in a rise in the band intensity around 1622 cm^{-1}, ascribable to ammonia and nitrate species adsorbed on Lewis acid sites. Moreover, oxidation of NO to NO_2 is probable in the catalysts with high Cu loading, which leads to the formation of nitrate and nitrite species by NO_2 disproportionation on the acid site [73, 111] which can develop the formation of nitrous oxide.

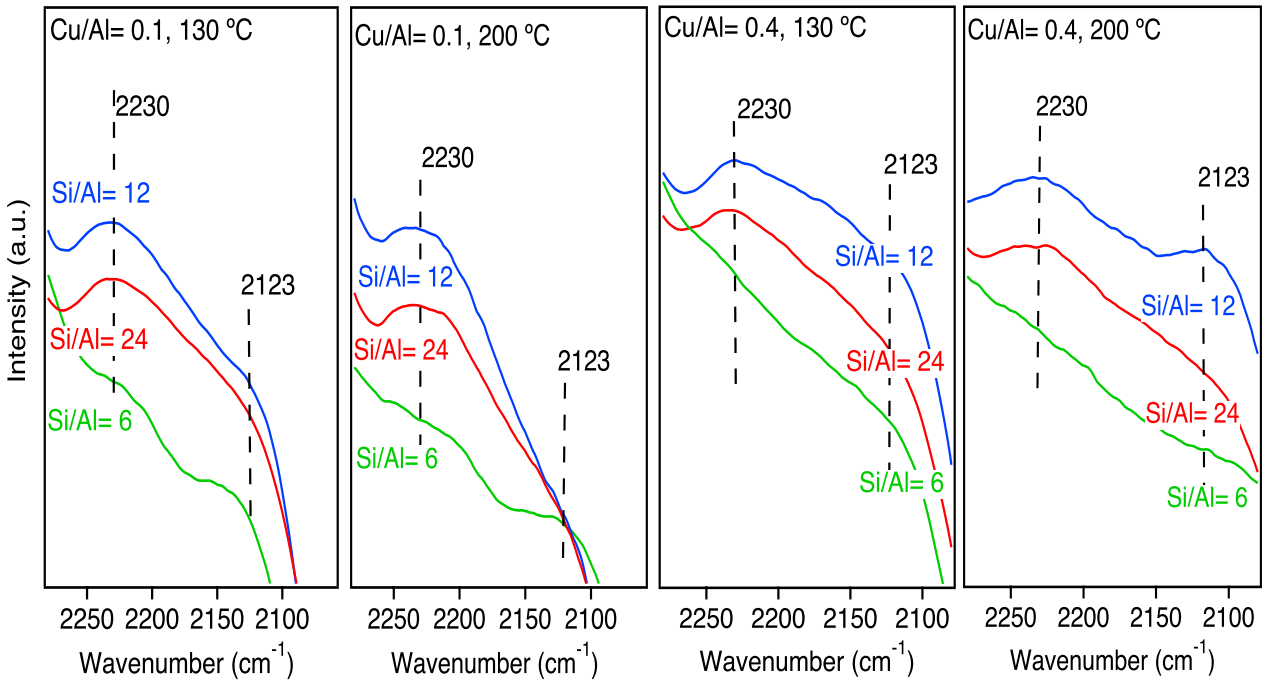

Figure 4.20: DRIFT spectra for the 5th min of the standard SCR over the sample with Si/Al= 12 and Cu/Al= 0.1, and 0.4 molar ratio at 130 °C.

4.3 The role of catalyst pretreatment in NH_3-SCR

A series of NH_3-SCR experiments were carried out for the samples with Si/Al= 12 pretreated at three different conditions as follow: (i) Ar and 10% O_2 for 1 h exposure at 550 °C, (ii) Ar and 10% O_2 for 1 h exposure at 550 °C, followed by Ar flush for 2 h and 400 ppm NH_3, 400 ppm NO, 10% O_2 exposure in Ar balance at 250, 200, and 150 °C for 30 min for each temperature, and (iii) Ar and 10% O_2 for 1 h exposure at 550 °C, followed by Ar flush for 2 h and 400 ppm NH_3, 400 ppm NO, exposure in Ar balance at 250, 200,

and 150 °C for 30 min for each temperature. In all cases, the total flow is 200 mL.min^{-1}.

The activation and dissociation of O_2 is a crucial step in NH_3-SCR. [89, 92, 112] The comprehension of this step is associated with the understanding of the active sites under reaction conditions. Recently, it has been indicated that Cu^+ species is solvated by NH_3 at temperatures below 250 °C and form $[Cu(NH_3)_2]^+$ complex which is dominant over a wide range of NH_3 partial pressures. [89, 113, 114] The mobility and weakly bonding nature of this complex to the zeolite framework, [115] results in NH_3 desorption and direct Cu coordination to the zeolite framework at higher temperatures, which cause a loss in the mobility of this complex. [92, 113]

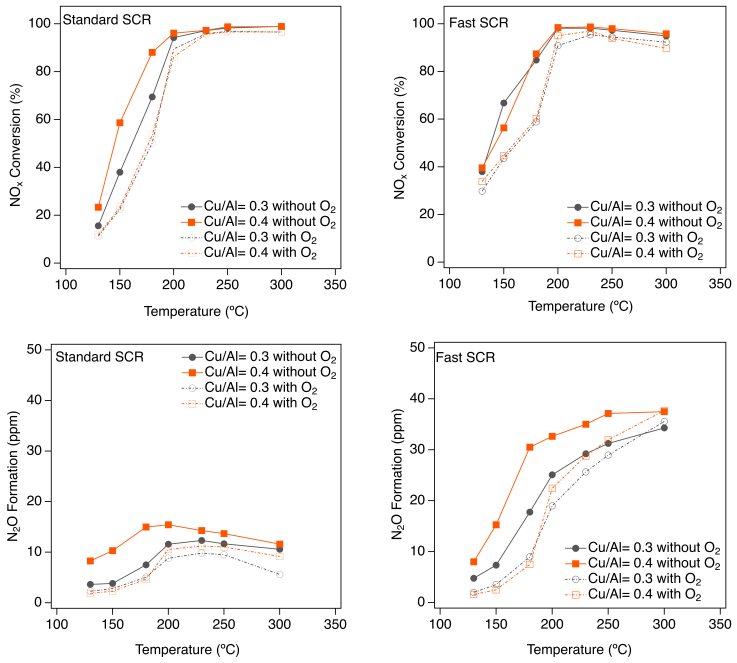

Figure 4.21: Steady-state NO_x conversions and the corresponding N_2O formation levels as a function of temperature for Cu-SSZ-13 with Si/Al= 12 and Cu/Al= 0.3, and 0.4 molar ratio under standard and fast SCR conditions.

The samples were pretreated in 400 ppm NO, 400 ppm NH_3, and 10% O_2 (dashed line) and 400 ppm NO, 400 ppm NH_3, (solid line).

The steady-state NO_x conversions and the corresponding N_2O formation is shown in Figure 4.21 as a function of temperature for Cu-SSZ-13 with the sample with Si/Al= 12 and Cu/Al= 0.3, and 0.4 molar ratio under standard and fast SCR reaction conditions, for pretreatment (ii) and (iii).

The results show the effect of O_2 absence in the feed stream during pretreatment on catalytic performance over the Cu-SSZ-13 sample, in which during standard SCR, NO_x conversion of Cu/Al= 0.3 and 0.4 samples peaked at 180 °C which is a considerable difference compared to the results for the pretreatment in the presence of O_2. By elevating temperature, the achieved NO_x conversion for all the samples show almost the same values with a negligible difference for both pretreatment conditions. This interestingly infers the dependence of the catalytic performance on the oxygen existence in the pretreatment procedure, and the NO_x conversion

has similar selectivity for these samples.

During fast SCR conditions, increasing the temperature from 230 to 300 °C follows by a continuous decrease to almost 3%. In addition to standard SCR, fast SCR illustrates promoted NO_x conversion by the presence of NO_2, indicating the crucial role and higher reactivity of NO_2 compared to NO in the reduction of NO_x.

Comparing N_2O formation during standard and fast SCR conditions reveals a higher N_2O concentration via fast SCR with both pretreatments. However, pretreatment in the absence of O_2 presents higher values compared to the one with O_2. The samples with Cu/Al= 0.4 molar ratio show N_2O formation specifically at temperatures lower than 230 °C and 250 °C during standard and fast SCR conditions, respectively. This can be due to the abundance of $[Cu(OH)]^+$ species at elevated Cu contents.

It is well known that N_2O formation partially originated from the formation and decomposition of NH_4NO_3 at temperatures ranging from 230-280 °C. For the temperatures lower than 230, the N_2O formation originates from the formation of copper peroxo complexes. [105] Therefore, it can be inferred that Cu may play a crucial role in the N_2O formation under standard SCR conditions. Furthermore, as with standard SCR condition, N_2O formation likewise increases with elevating Cu loading under fast SCR conditions.

A recent study by Lomachenko *et al.*, [113] revealed that the mobile Cu(II) and Cu(I) sites solvated by NH_3 as the primary Cu sites at 150 °C. They reported that the most probable Cu-containing moiety is a linear $[Cu(NH_3)_2]^+$ species which transport between unit cells with reasonable energy barriers. It is also proposed that the oxidation half-cycle of standard NH_3-SCR at low temperature only takes place with the participation of two $[Cu(NH_3)_2]^+$ centers, resulting in the formation of a transient $[Cu(NH_3)_2]^+$-O_2-$[Cu(NH_3)_2]^+$ intermediate which play a role as the rate-limiting step at low Cu content. On the other hand, as Cu loading increases to intermediate and high exchange levels the formation of the $[Cu(NH_3)_2]^+$-O_2-$[Cu(NH_3)_2]^+$ intermediate is not the rate-limiting step.

Hence, the NO_x conversion profile displayed in Figure 4.21 explains that as reaction temperature rises above almost 300 °C, stable Cu-NH_3 complexes at lower temperatures start to dissociate at elevated temperatures. In this state, Cu ions will migrate to the zeolite framework ion-exchange sites and will stabilize by coordinating with the lattice O_2. In other words, the oxidation half-cycle at low temperature is no longer possible through the formation of intermediates that contain two isolated Cu ions. However, the oxidation half-cycle will have to be carried out by single isolated Cu ions. [91]

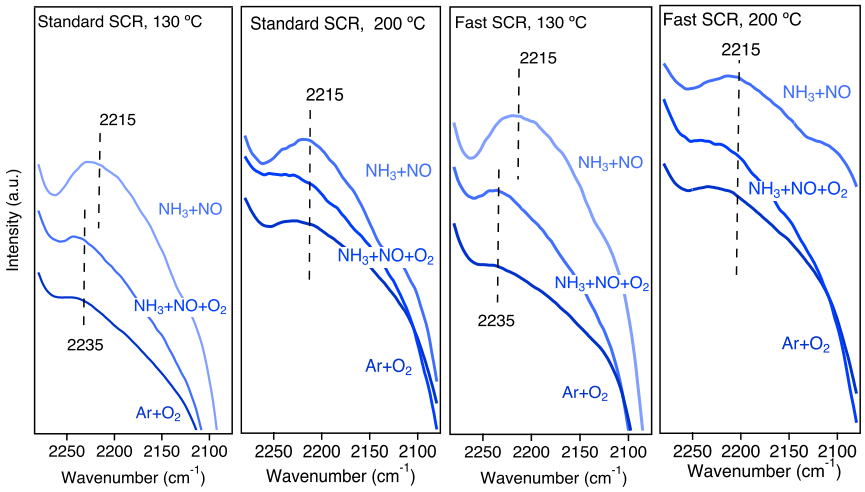

Figure 4.22: *In situ* DRIFT spectra corresponding to N_2O wavenumber region for Cu-SSZ-13 with Si/Al= 12 and Cu/Al= 0.3 molar ratio under standard and fast SCR conditions, at 130 and 200 °C.

Pretreated in: (a) Ar and 10% O_2 for 1 h exposure at 550 °C, (b) Ar and 10% O_2 for 1 h exposure at 550 °C, followed by Ar flush for 2 h and 400 ppm NH_3, 400 ppm NO, 10% O_2 exposure in Ar balance at 250, 200, and 150 °C for 30 min for each temperature, and, (c) Ar and 10% O_2 for 1 h exposure at 550 °C, followed by Ar flush for 2 h and 400 ppm NH_3, 400 ppm NO, exposure in Ar balance at 250, 200, and 150 °C for 30 min for each temperature.

The pretreatments of the samples with Ar and 10% O_2, or with NO, NH_3, and 10% O_2, provide the continuous Cu reduction-oxidation cycle which ensures the presence of both Cu^+, and Cu^{2+} species. This results in the formation of Cu^+, Cu^{2+}, and $[Cu(OH)]^+$ species in the pretreatment with Ar and O_2, while in the one with NO, NH_3 and O_2, different species such as $[Cu(OH)]^+$, $[Cu(NH_3)_2]^+$, $[Cu(NH_3)_4]^{2+}$, $[Cu(NH_3)_3(OH)]^+$ can form. The decomposition and formation of these species occur at high temperature and during the NH_3 adsorption step, respectively, with a subsequent decomposition at high temperature of NH_3-TPD experiments, to form framework-bonded Cu^+ species before the SCR initiation.

On the contrary, the samples pretreatment under NO and NH_3 with no O_2 are lacking a Cu reduction-oxidation cycle, and the Cu^+, Cu^+-NH_3, and the existence of merely Cu^+ species results in the formation of $[Cu(NH_3)_2]^+$ complex. The decomposition of $[Cu(NH_3)_2]^+$ complex starts from 200 °C, corresponding to the highest studied temperature during our NH_3-TPD experiments. Therefore, the standard SCR initiates with this complex which provides a facile oxygen activation at lower temperature. The oxygen activation is well studied over the $[Cu(NH_3)_2]^+$ complex and framework bonded Cu^+ by Wang *et al.* [116] and the results revealed the easier and faster activation of O_2 at low temperatures over $[Cu(NH_3)_2]^+$ complexes compared to framework-bonded Cu^+ due to the lower barrier for O_2 activation.

However, O_2 activation occurs at both low and high temperatures for the samples pretreated with or without oxygen, which results in a Cu reduction-oxidation cycle, the pace of O_2 activation and subsequently the amount of produced various species such as $[Cu(OH)]^+$, $[Cu(NH_3)_2]^+$, $[Cu(NH_3)_4]^{2+}$, $[Cu(NH_3)_3(OH)]^+$, and Cu^+-NH_3 is different at the studied temperature range.

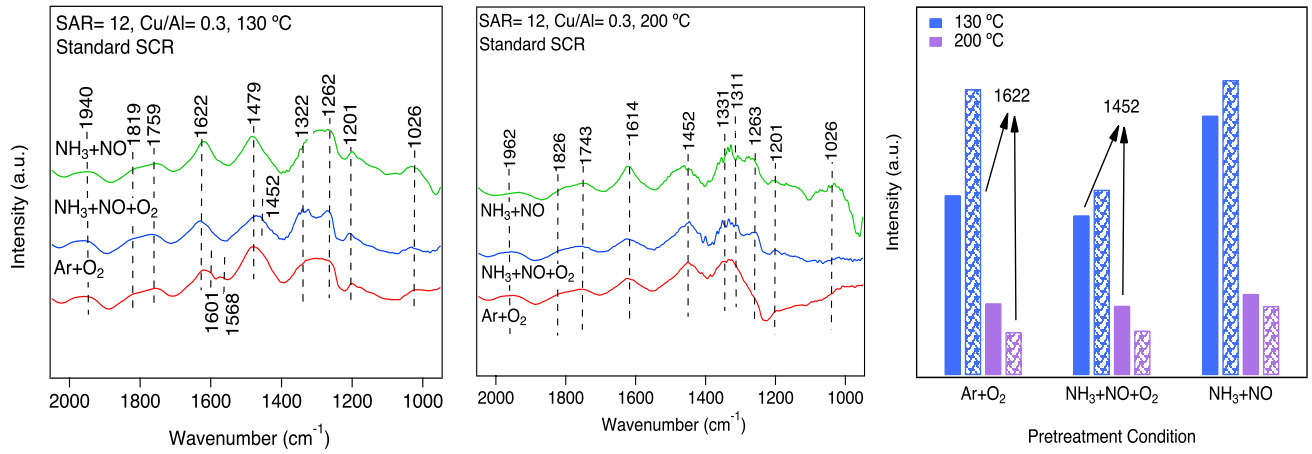

Figure 4.23: *In situ* DRIFT spectra in NH bending vibration region for Cu-SSZ-13 with Si/Al= 12 and Cu/Al= 0.3 molar ratio under standard SCR condition, at 130 and 200 °C, with the corresponding peak intensities at 1622 and 1452 cm^{-1}.

The DRIFT spectra for both standard and fast SCR procedure were compared for three pretreatments at 130 and 200 °C and the data are shown for the corresponding N_2O wavenumber region in Figure 4.22. It is interestingly seen that the sample pretreated under the environment without oxygen, provides higher N_2O peak intensity, which is well in agreement with the findings from flow reactor experiments. For investigating the reason, the spectra at 1000-2000 cm^{-1} are evaluated in detail for the samples under three different pretreatments with the corresponding spectra illustrated in Figure 4.23.

DRIFT spectra for the 1000-2000 wavenumber region clearly show the existence of the bands at 1620 cm^{-1} that corresponds to asymmetric bending vibrations of $[Cu(NH_3)_4]^{2+}$ together with the weakly adsorbed NH_3 on Lewis acid sites. Another band ascribed to the symmetric bending vibrations of $[Cu(NH_3)_4]^{2+}$ arose at 1262 cm^{-1}, accompanied with a shoulder at 1322 cm^{-1} attributed to strongly adsorbed NH_3 on extra framework Al (EFAl), [83] representing almost the same peak intensity at 130 °C. The intensities of these bands are higher for the samples pretreated under oxygen-poor environment at lower temperature, which can be related to the higher number of different species which forms due to the easier activation. Elevating the temperature to 200 °C resulted in a decrease in the band intensity at 1262 cm^{-1} with an increase in the 1322 cm^{-1} band, but with almost similar intensity for all the samples regardless of pretreatment conditions. These data are well agreed with finding from flow reactor experiments and support the affect of the $[Cu(NH_3)_2]^{+}$ complex on the activation of O_2 during standard SCR.

5 Conclusions

The final chapter is dedicated to the summary of what my studies have shown and conclude the proposed hypotheses. To deal with the abatement of NO_x and decreasing the N_2O formation one should figure out the role of different factors contributing in the N_2O formation.

The objective of this study was to understand the N_2O formation as a byproduct during NH_3-SCR over zeolite-based catalysts, by investigating the effect of different parameters, such as zeolite framework structure, ammonia storage capacity of the zeolites, Si/Al molar ratio, copper loading, temperature, gas composition, and pretreatment conditions.

N_2O formation can occur through different pathways depending on the catalyst properties and/or reaction conditions. Considering the effect of pore-size of the zeolites, the highest N_2O formation is shown for the Cu-BEA sample, which is a large-pore zeolite, followed by the Cu-ZSM-5, and Cu-SSZ-13 zeolites with medium- and small-pores, respectively. The DRIFTS spectra obtained during NO oxidation over the samples show the highest peak intensity for nitrate/nitrite species for the Cu-BEA zeolite at lower temperature. This is likely related to the presence of multinuclear Cu clusters that efficiently activates NO, forming surface nitrate species. The higher number of $[Cu(OH)]^+$ species observed for the Cu-BEA zeolite during H_2-TPR measurements show, together with DRIFTS results, that Cu species contributes in the N_2O formation by catalyzing the reaction between nitrate species and ammonia, forming ammonium nitrate that subsequently decompose to N_2O at high temperatures. The Cu-SSZ-13 zeolite showed the highest populations of monometallic Cu-NH_3 complexes, compared to the other samples, that can form over isolated Cu sites under the standard SCR reaction conditions. These complexes can diffuse in the micropores of the zeolite, form transient $[Cu(NH_3)_2]^+$-O_2-$[Cu(NH_3)_2]^+$ dimers and consequently activate O_2 via the re-oxidation of Cu^+ ions to Cu^{2+}.

The results from flow reactor and DRIFTS studies over the Cu-SSZ-13 samples with different Si/Al and Cu/Al molar ratios showed that the N_2O formation is influenced by the zeolite acidity and the Cu loading, especially at lower temperatures. Further, the results show the highest NH_3 storage capacity for the samples with lower Si/Al molar ratio and higher Cu content, corresponding to the

highest Al content and higher number of Lewis acid sites in the zeolite.

Additionally, deconvolution of a feature in the wavenumber region corresponding to the NH_3 adsorbed on the Brønsted acid sites (1390-1520 cm^{-1}), illustrate the existence of three main peaks, which could be attributed to the antisymmetric and symmetric bending vibrations of non-solvated NH_4^+. It is also found that elevating the temperature during ammonia desorption, results in a shift in the peak positions along with an intensity change, which may indicate the transformation of one type of species at higher wavenumbers to another at lower wavenumbers. It can be concluded that these peaks are related to different types of NH_3 species with varying acidic strength. The band at higher wavenumber can be attributed the N-H bending vibrations of weakly bonded NH_3 in $NH_4^+.nNH_3$ associations, while the band at lower wavenumber is ascribable to the N-H bending vibrations of NH_4^+. Hence, an increased temperature could limit the amount of solvated NH_3 molecules.

The flow reactor data during standard SCR over the samples pretreated in NH_3 and NO, revealed the highest N_2O formation for the samples with Si/Al= 6 molar ratio followed by the samples with Si/Al= 12, and 24 molar ratio, which agrees with the DRIFTS results showing the highest peak intensity corresponding to N_2O for the samples with Si/Al= 6 molar ratio. Comparing the differently pretreated samples showed that, at low temperature, the samples pretreated with NH_3 and NO and in the absence of O_2 show higher NO_x conversion and N_2O formation compared to the samples pretreated in the presence of NH_3, NO and O_2 and O_2, which seems to be relevant to the O_2 activation at lower temperature. The pretreatment in the O_2-poor environment results in the formation of $[Cu(NH_3)_2]^+$ complexes, which leads to a facile activation of O_2 at lower temperature, while the pretreatment of the samples in O_2-rich environment results in the formation of framework-bonded Cu^+ species with higher barrier for O_2 activation. Hence, with an easier activation of O_2 the SCR reaction proceeds much faster at low temperatures and results in higher NO_x conversion and N_2O formation. However, at high temperatures the differently pretreated zeolites show similar NO_x conversion and N_2O formation as the O_2 activation barrier is overcome.

In conclusion, it seems that not only the pore size of the zeolite has a considerable effect on the N_2O formation, due to the higher NH_3 storage capacity and higher formation of nitrate species, also the acidity of the small-pore zeolite plays a significant role for the NH_3 storage capacity of the SCR activity. Further, the amount of Cu and the type of Cu species, have a crucial effect on the activation of O_2 and hence the activity and selectivity of the SCR reaction.

Bibliography

[1] Th Körfer et al. 'Advanced, combined exhaust aftertreatment systems for light-duty diesel engines to meet next emission regulations'. In: *Internal Combustion Engines: Performance, Fuel Economy and Emissions*. Elsevier, 2013, pp. 205–217 (cit. on p. 1).

[2] Michael R McHale et al. 'Trends in precipitation chemistry across the US 1985–2017: Quantifying the benefits from 30 years of Clean Air Act amendment regulation'. In: *Atmospheric Environment* 247 (2021), p. 118219 (cit. on p. 1).

[3] A Fritz and Veronique Pitchon. 'The current state of research on automotive lean NOx catalysis'. In: *Applied Catalysis B: Environmental* 13.1 (1997), pp. 1–25 (cit. on p. 1).

[4] Diane Bailey and Gina Solomon. 'Pollution prevention at ports: clearing the air'. In: *Environmental impact assessment review* 24.7-8 (2004), pp. 749–774 (cit. on p. 1).

[5] Martyn V Twigg. 'Catalytic air pollution control: commercial technology'. In: *Platinum Metals Review* 54.3 (2010), pp. 180–183 (cit. on p. 2).

[6] Redouane Hajjar et al. 'Two kinds of framework Al sites studied in BEA zeolite by X-ray diffraction, Fourier transform infrared spectroscopy, NMR techniques, and V probe'. In: *The Journal of Physical Chemistry C* 112.51 (2008), pp. 20167–20175 (cit. on p. 2).

[7] JP Chen, MC Hausladen and RT Yang. 'Delaminated Fe_2O_3-pillared clay: its preparation, characterization, and activities for selective catalytic reduction of NO by NH_3'. In: *Journal of catalysis* 151.1 (1995), pp. 135–146 (cit. on p. 2).

[8] Hanna Sjövall et al. 'Selective catalytic reduction of NO_x with NH_3 over Cu-ZSM-5—The effect of changing the gas composition'. In: *Applied Catalysis B: Environmental* 64.3-4 (2006), pp. 180–188 (cit. on p. 2).

[9] RM Heck, JM Chen and BK Speronello. 'Operating characteristics and commercial operating experience with high temperature SCR NO_x catalyst'. In: *Environmental Progress* 13.4 (1994), pp. 221–225 (cit. on p. 2).

[10] Sandro Brandenberger et al. 'The state of the art in selective catalytic reduction of NO_x by ammonia using metal-exchanged zeolite catalysts'. In: *Catalysis Reviews* 50.4 (2008), pp. 492–531 (cit. on pp. 2, 3).

[11] Alexandre Westermann et al. 'Evolution of unburnt hydrocarbons under "cold-start" conditions from adsorption/desorption to conversion: On the screening of zeolitic materials'. In: *Applied Catalysis B: Environmental* 158 (2014), pp. 48–59 (cit. on p. 2).

[12] Hai-Ying Chen et al. 'Formation of NO^+ and its possible roles during the selective catalytic reduction of NO_x with NH_3 on Cu-CHA catalysts'. In: *Catalysis Today* 320 (2019), pp. 61–71 (cit. on pp. 2, 25, 30, 31).

[13] Kinga Skalska, Jacek S Miller and Stanislaw Ledakowicz. 'Trends in NO_x abatement: A review'. In: *Science of the total environment* 408.19 (2010), pp. 3976–3989 (cit. on pp. 3, 4).

[14] Xingxing Cheng and Xiaotao T Bi. 'A review of recent advances in selective catalytic NO_x reduction reactor technologies'. In: *Particuology* 16 (2014), pp. 1–18 (cit. on pp. 3, 4).

[15] Guido Busca et al. 'Chemical and mechanistic aspects of the selective catalytic reduction of NOx by ammonia over oxide catalysts: a review'. In: *Applied Catalysis B: Environmental* 18.1-2 (1998), pp. 1–36 (cit. on p. 3).

[16] Kinga Skalska, Jacek S Miller and Stanisław Ledakowicz. 'Intensification of NO_x absorption process by means of ozone injection into exhaust gas stream'. In: *Chemical Engineering and Processing: Process Intensification* 61 (2012), pp. 69–74 (cit. on p. 3).

[17] Xingfu Tang et al. 'Origination of N_2O from NO reduction by NH_3 over β-MnO_2 and α-Mn_2O_3'. In: *Applied Catalysis B: Environmental* 99.1-2 (2010), pp. 156–162 (cit. on p. 3).

[18] Vasile I Pârvulescu, Paul Grange and Bernard Delmon. 'Catalytic removal of NO'. In: *Catalysis today* 46.4 (1998), pp. 233–316 (cit. on p. 3).

[19] Thomas Aichner et al. 'Did the volkswagen emissions scandal harm the "made in Germany" image? A cross-cultural, cross-products, cross-time study'. In: *Corporate Reputation Review* 24 (2021), pp. 179–190 (cit. on p. 3).

[20] Krzysztof Jerzy Gruszczyński. 'German made Dieselgate'. In: *Społeczeństwo i Edukacja. Międzynarodowe Studia Humanistyczne* 1 (28 (2018), pp. 43–64 (cit. on p. 3).

[21] Marie-Laure Tarot et al. 'Influence of the sodium impregnation solvent on the deactivation of Cu/FER-exchanged zeolites dedicated to the SCR of NO_x with NH3'. In: *Catalysts* 8.1 (2018), p. 3 (cit. on p. 3).

[22] Masaoki Iwasaki and Hirofumi Shinjoh. 'A comparative study of "standard","fast" and "NO2" SCR reactions over Fe/zeolite catalyst'. In: *Applied Catalysis A: General* 390.1-2 (2010), pp. 71–77 (cit. on p. 3).

[23] Sounak Roy, MS Hegde and Giridhar Madras. 'Catalysis for NO_x abatement'. In: *Applied Energy* 86.11 (2009), pp. 2283–2297 (cit. on p. 4).

[24] Yi Li, Lin Li and Jihong Yu. 'Applications of zeolites in sustainable chemistry'. In: *Chem* 3.6 (2017), pp. 928–949 (cit. on pp. 4, 5).

[25] Thijs Ennaert et al. 'Potential and challenges of zeolite chemistry in the catalytic conversion of biomass'. In: *Chemical Society Reviews* 45.3 (2016), pp. 584–611 (cit. on p. 5).

[26] Martin Spangsberg Holm, Shunmugavel Saravanamurugan and Esben Taarning. 'Conversion of sugars to lactic acid derivatives using heterogeneous zeotype catalysts'. In: *Science* 328.5978 (2010), pp. 602–605 (cit. on p. 5).

[27] Zhiqiang Xu et al. 'Size control of SSZ-13 crystals with APAM and its influence on the coking behaviour during MTO reaction'. In: *Catalysis Science & Technology* 9.11 (2019), pp. 2888–2897 (cit. on p. 5).

[28] W Widayat and AN Annisa. 'Synthesis and characterization of ZSM-5 catalyst at different temperatures'. In: *IOP Conference Series: Materials Science and Engineering*. Vol. 214. 1. IOP Publishing. 2017, p. 012032 (cit. on p. 5).

[29] Rogéria Bingre, Benoît Louis and Patrick Nguyen. 'An overview on zeolite shaping technology and solutions to overcome diffusion limitations'. In: *Catalysts* 8.4 (2018), p. 163 (cit. on p. 5).

[30] Runduo Zhang et al. 'Selective transformation of various nitrogen-containing exhaust gases toward N_2 over zeolite catalysts'. In: *Chemical reviews* 116.6 (2016), pp. 3658–3721 (cit. on p. 5).

[31] Andrew M Beale et al. 'Recent advances in automotive catalysis for NO_x emission control by small-pore microporous materials'. In: *Chemical Society Reviews* 44.20 (2015), pp. 7371–7405 (cit. on pp. 5, 25).

[32] Yingxin Feng et al. 'First-principles microkinetic model for low-temperature NH3-assisted selective catalytic reduction of NO over Cu-CHA'. In: *ACS Catalysis* 11.23 (2021), pp. 14395–14407 (cit. on pp. 6, 7).

[33] Magdalena Jabłońska and Regina Palkovits. 'It is no laughing matter: nitrous oxide formation in diesel engines and advances in its abatement over rhodium-based catalysts'. In: *Catalysis Science & Technology* 6.21 (2016), pp. 7671–7687 (cit. on pp. 7, 8).

[34] Ja Hun Kwak et al. 'Excellent activity and selectivity of Cu-SSZ-13 in the selective catalytic reduction of NO_x with NH3'. In: *Journal of Catalysis* 275.2 (2010), pp. 187–190 (cit. on pp. 7, 25).

[35] Kirsten Leistner et al. 'Comparison of Cu/BEA, Cu/SSZ-13 and Cu/SAPO-34 for ammonia-SCR reactions'. In: *Catalysis Today* 258 (2015), pp. 49–55 (cit. on p. 7).

[36] Shijian Yang et al. 'Mechanism of N_2O formation during the low-temperature selective catalytic reduction of NO with NH_3 over Mn–Fe spinel'. In: *Environmental science & technology* 48.17 (2014), pp. 10354–10362 (cit. on p. 8).

[37] Dong Zhang and Ralph T Yang. 'N_2O formation pathways over zeolite-supported Cu and Fe catalysts in NH_3-SCR'. In: *Energy & fuels* 32.2 (2018), pp. 2170–2182 (cit. on pp. 8, 9, 27).

[38] Manfred Koebel, Giuseppe Madia and Martin Elsener. 'Selective catalytic reduction of NO and NO_2 at low temperatures'. In: *Catalysis Today* 73.3-4 (2002), pp. 239–247 (cit. on pp. 8, 28).

[39] John Eng and Calvin H Bartholomew. 'Kinetic and Mechanistic Study of NO_x Reduction by NH_3 over H-Form Zeolites'. In: *Journal of Catalysis* 171.1 (1997), pp. 27–44 (cit. on p. 8).

[40] Xin Liu et al. 'Theoretical study of N_2O decomposition mechanism over binuclear Cu-ZSM-5 zeolites'. In: *Journal of Molecular Catalysis A: Chemical* 396 (2015), pp. 181–187 (cit. on p. 8).

[41] Wei Zou et al. 'Catalytic decomposition of N_2O over Cu-ZSM-5 nanosheets'. In: *Journal of Molecular Catalysis A: Chemical* 394 (2014), pp. 83–88 (cit. on p. 8).

[42] Malcolm Yates et al. 'N_2O formation in the ammonia oxidation and in the SCR process with V_2O_5-WO_3 catalysts'. In: *Catalysis today* 107 (2005), pp. 120–125 (cit. on p. 8).

[43] Xiongbo Chen et al. 'Design strategies for SCR catalysts with improved N 2 selectivity: the significance of nano-confining effects by titanate nanotubes'. In: *Environmental Science: Nano* 4.2 (2017), pp. 437–447 (cit. on p. 8).

[44] Silvia Suárez et al. 'Influence of NH_3 and NO oxidation on the SCR reaction mechanism on copper/nickel and vanadium oxide catalysts supported on alumina and titania'. In: *Catalysis Today* 75.1-4 (2002), pp. 331–338 (cit. on p. 8).

[45] Mukundan Devadas et al. 'Influence of NO_2 on the selective catalytic reduction of NO with ammonia over Fe-ZSM5'. In: *Applied Catalysis B: Environmental* 67.3-4 (2006), pp. 187–196 (cit. on pp. 8, 28).

[46] Dustin W Fickel and Raul F Lobo. 'Copper coordination in Cu-SSZ-13 and Cu-SSZ-16 investigated by variable-temperature XRD'. In: *The Journal of Physical Chemistry C* 114.3 (2010), pp. 1633–1640 (cit. on pp. 12, 46).

[47] Dustin W Fickel et al. 'The ammonia selective catalytic reduction activity of copper-exchanged small-pore zeolites'. In: *Applied Catalysis B: Environmental* 102.3-4 (2011), pp. 441–448 (cit. on pp. 12, 33, 45).

[48] Jean-François Pommaret. *Partial differential equations and group theory: new perspectives for applications*. Vol. 293. Springer Science & Business Media, 2013 (cit. on p. 14).

[49] G Leofanti et al. 'Surface area and pore texture of catalysts'. In: *Catalysis Today* 41.1-3 (1998), pp. 207–219 (cit. on pp. 14, 15).

[50] Matthias Thommes et al. 'Physisorption of gases, with special reference to the evaluation of surface area and pore size distribution (IUPAC Technical Report)'. In: *Pure and applied chemistry* 87.9-10 (2015), pp. 1051–1069 (cit. on p. 14).

[51] Anthony Haynes. 'Concepts of Modern Catalysis and Kinetics'. In: *Synthesis* 2005.05 (2005), pp. 851–851 (cit. on pp. 15, 21).

[52] Olaf Deutschmann et al. 'High temperature catalysis: role of heterogeneous, homogeneous, and radical chemistry'. In: *Catalysis; Beller, M.; Renken, A.; van Santen, RA, Eds* (2012), pp. 365–389 (cit. on p. 15).

[53] C Barry Carter and David B Williams. *Transmission electron microscopy: Diffraction, imaging, and spectrometry*. Springer, 2016 (cit. on p. 16).

[54] William Lawrence Bragg. 'The structure of some crystals as indicated by their diffraction of X-rays'. In: *Proceedings of the Royal Society of London. Series A, Containing papers of a mathematical and physical character* 89.610 (1913), pp. 248–277 (cit. on p. 16).

[55] DL Dorset. 'X-ray diffraction: a practical approach'. In: *Microscopy and microanalysis* 4.5 (1998), pp. 513–515 (cit. on p. 16).

[56] F Kapteijn, JA Moulijn and A Tarfaoui. 'Temperature programmed reduction and sulphiding'. In: *Studies in Surface Science and Catalysis* 79.1 (1993), pp. 401–401 (cit. on p. 17).

[57] Ferenc Lónyi and József Valyon. 'On the interpretation of the NH3-TPD patterns of H-ZSM-5 and H-mordenite'. In: *Microporous and Mesoporous materials* 47.2-3 (2001), pp. 293–301 (cit. on p. 17).

[58] Feng Gao et al. 'Effects of Si/Al ratio on Cu/SSZ-13 NH3-SCR catalysts: Implications for the active Cu species and the roles of Brønsted acidity'. In: *Journal of catalysis* 331 (2015), pp. 25–38 (cit. on pp. 17, 38–40, 45).

[59] Poonam Rani and Rajendra Srivastava. 'Extra-Framework Aluminum Species of Zeolite that Surrogate the Growth of Metal Organic Framework from Zeolite Matrix'. In: *Chemistry–An Asian Journal* 14.15 (2019), pp. 2598–2603 (cit. on p. 18).

[60] Janusz Ryczkowski. 'IR spectroscopy in catalysis'. In: *Catalysis Today* 68.4 (2001), pp. 263–381 (cit. on p. 18).

[61] Johannes A Lercher and Andreas Jentys. 'Infrared and Raman spectroscopy for characterizing zeolites'. In: *Studies in surface science and catalysis* 168 (2007), pp. 435–476 (cit. on p. 18).

[62] JK Roberts. 'Some effects of dipole interactions on heats of adsorption'. In: *Transactions of the Faraday Society* 34 (1938), pp. 1342–1346 (cit. on pp. 18, 22).

[63] Peter Larkin. *Infrared and Raman spectroscopy: principles and spectral interpretation*. Elsevier, 2017 (cit. on pp. 18, 19).

[64] Peter R Griffiths. 'Fourier transform infrared spectrometry'. In: *Science* 222.4621 (1983), pp. 297–302 (cit. on p. 20).

[65] Ida Friberg, Aiyong Wang and Louise Olsson. 'Hydrothermal Aging of Pd/LTA Monolithic Catalyst for Complete CH_4 Oxidation'. In: *Catalysts* 10.5 (2020), p. 517 (cit. on p. 20).

[66] Feng Gao et al. 'Current understanding of Cu-exchanged chabazite molecular sieves for use as commercial diesel engine DeNO$_x$ catalysts'. In: *Topics in Catalysis* 56.15-17 (2013), pp. 1441–1459 (cit. on p. 25).

[67] Feng Gao et al. 'Understanding ammonia selective catalytic reduction kinetics over Cu/SSZ-13 from motion of the Cu ions'. In: *Journal of catalysis* 319 (2014), pp. 1–14 (cit. on p. 25).

[68] Lin Chen et al. 'A Complete Multisite Reaction Mechanism for Low-Temperature NH_3-SCR over Cu-CHA'. In: *ACS Catalysis* 10.10 (2020), pp. 5646–5656 (cit. on p. 25).

[69] Jie Liang et al. 'CHA-type zeolites with high boron content: Synthesis, structure and selective adsorption properties'. In: *Microporous and mesoporous materials* 194 (2014), pp. 97–105 (cit. on p. 26).

[70] Xueting Wang et al. 'Methane adsorption and methanol desorption of copper modified boron silicate'. In: *RSC advances* 8.63 (2018), pp. 36369–36374 (cit. on p. 26).

[71] Joseph M Fedeyko, Bin Chen and Hai-Ying Chen. 'Mechanistic study of the low temperature activity of transition metal exchanged zeolite SCR catalysts'. In: *Catalysis Today* 151.3-4 (2010), pp. 231–236 (cit. on p. 27).

[72] Oana Mihai et al. 'The effect of Cu-loading on different reactions involved in NH_3-SCR over Cu-BEA catalysts'. In: *Journal of catalysis* 311 (2014), pp. 170–181 (cit. on p. 27).

[73] Hiroe Kubota et al. 'Formation and Reactions of NH_4NO_3 during Transient and Steady-State NH_3-SCR of NO$_x$ over H-AFX Zeolites: Spectroscopic and Theoretical Studies'. In: *ACS Catalysis* 10.3 (2020), pp. 2334–2344 (cit. on pp. 28, 47).

[74] Biao Liu et al. 'Experimental investigation on N2O formation during the selective catalytic reduction of NOx with NH3 over Cu-SSZ-13'. In: *Industrial & Engineering Chemistry Research* 58.45 (2019), pp. 20516–20527 (cit. on pp. 28, 29).

[75] Young Hoon Yeom et al. 'The role of NO in the mechanism of NO$_x$ reduction with ammonia over a BaNa–Y catalyst'. In: *Journal of Catalysis* 231.1 (2005), pp. 181–193 (cit. on p. 29).

[76] Hai-Ying Chen et al. 'A comparative study of N_2O formation during the selective catalytic reduction of NO$_x$ with NH_3 on zeolite supported Cu catalysts'. In: *Journal of Catalysis* 329 (2015), pp. 490–498 (cit. on pp. 30, 31, 33).

[77] Kirsten Leistner et al. 'Ammonia desorption peaks can be assigned to different copper sites in Cu/SSZ-13'. In: *Catalysis Letters* 147.8 (2017), pp. 1882–1890 (cit. on p. 30).

[78] Haiyang Zhu et al. 'In situ DRIFTS-MS studies on the oxidation of adsorbed NH_3 by NO$_x$ over a Cu-SSZ-13 zeolite'. In: *Catalysis today* 205 (2013), pp. 16–23 (cit. on pp. 30, 33, 45).

[79] Bjorn Moden et al. 'The uses and challenges of zeolites in automotive applications'. In: *Topics in Catalysis* 53.19 (2010), pp. 1367–1373 (cit. on p. 30).

[80] G Mul et al. 'N_2O decomposition over liquid ion-exchanged Fe-BEA catalysts: correlation between activity and the IR intensity of adsorbed NO at 1874 cm- 1'. In: *Catalysis letters* 93.1 (2004), pp. 113–120 (cit. on p. 30).

[81] Feng Gao et al. 'Fe/SSZ-13 as an NH_3-SCR catalyst: a reaction kinetics and FTIR/Mössbauer spectroscopic study'. In: *Applied Catalysis B: Environmental* 164 (2015), pp. 407–419 (cit. on p. 30).

[82] Li Cao et al. 'TRA and DRIFTS studies of the fast SCR reaction over CeO_2/TiO_2 catalyst at low temperatures'. In: *Applied Catalysis A: General* 557 (2018), pp. 46–54 (cit. on p. 30).

[83] Ines Lezcano-Gonzalez et al. 'Determining the storage, availability and reactivity of NH 3 within Cu-Chabazite-based Ammonia Selective Catalytic Reduction systems'. In: *Physical Chemistry Chemical Physics* 16.4 (2014), pp. 1639–1650 (cit. on pp. 30, 46, 51).

[84] Bo Kou et al. 'Mathematical model and parameter estimation for gas-phase ethylene homopolymerization with supported metallocene catalyst'. In: *Industrial & engineering chemistry research* 44.8 (2005), pp. 2428–2442 (cit. on p. 30).

[85] Scott M Auerbach, Kathleen A Carrado and Prabir K Dutta. *Handbook of zeolite science and technology*. CRC press, 2003 (cit. on p. 30).

[86] Maria Pia Ruggeri et al. 'In-situ DRIFTS measurements for the mechanistic study of NO oxidation over a commercial Cu-CHA catalyst'. In: *Applied Catalysis B: Environmental* 166 (2015), pp. 181–192 (cit. on pp. 31, 32).

[87] K Hadjiivanov et al. 'FT-IR study of NO + O_2 co-adsorption on H-ZSM-5: re-assignment of the 2133 cm^{-1} band to NO^+ species'. In: *Catalysis letters* 52.1 (1998), pp. 103–108 (cit. on p. 31).

[88] Ja Hun Kwak et al. 'Two different cationic positions in Cu-SSZ-13?' In: *Chemical Communications* 48.39 (2012), pp. 4758–4760 (cit. on pp. 32, 36, 45).

[89] Ton VW Janssens et al. 'A consistent reaction scheme for the selective catalytic reduction of nitrogen oxides with ammonia'. In: *ACS catalysis* 5.5 (2015), pp. 2832–2845 (cit. on pp. 32, 34, 48).

[90] Philip G Blakeman et al. 'The role of pore size on the thermal stability of zeolite supported Cu SCR catalysts'. In: *Catalysis Today* 231 (2014), pp. 56–63 (cit. on p. 33).

[91] Feng Gao et al. 'Selective catalytic reduction over Cu/SSZ-13: linking homo-and heterogeneous catalysis'. In: *Journal of the American Chemical Society* 139.13 (2017), pp. 4935–4942 (cit. on pp. 33, 49).

[92] Christopher Paolucci et al. 'Catalysis in a cage: condition-dependent speciation and dynamics of exchanged Cu cations in SSZ-13 zeolites'. In: *Journal of the American Chemical Society* 138.18 (2016), pp. 6028–6048 (cit. on pp. 33, 48).

[93] J-S McEwen et al. 'Integrated operando X-ray absorption and DFT characterization of Cu–SSZ-13 exchange sites during the selective catalytic reduction of NOx with NH3'. In: *Catalysis Today* 184.1 (2012), pp. 129–144 (cit. on p. 34).

[94] Tobias Günter et al. 'Structural snapshots of the SCR reaction mechanism on Cu-SSZ-13'. In: *Chemical Communications* 51.44 (2015), pp. 9227–9230 (cit. on p. 34).

[95] Christopher Paolucci et al. 'Isolation of the copper redox steps in the standard selective catalytic reduction on Cu-SSZ-13'. In: *Angewandte Chemie International Edition* 53.44 (2014), pp. 11828–11833 (cit. on p. 34).

[96] Di Wang et al. 'In situ-DRIFTS study of selective catalytic reduction of NO x by NH3 over Cu-exchanged SAPO-34'. In: *Acs Catalysis* 3.5 (2013), pp. 871–881 (cit. on pp. 34, 46).

[97] Manfred Koebel et al. 'Enhanced reoxidation of vanadia by NO_2 in the fast SCR reaction'. In: *Journal of Catalysis* 209.1 (2002), pp. 159–165 (cit. on p. 35).

[98] Aiyong Wang et al. 'Investigation of the robust hydrothermal stability of Cu/LTA for NH_3-SCR reaction'. In: *Applied Catalysis B: Environmental* 246 (2019), pp. 242–253 (cit. on p. 36).

[99] Yasser Jangjou et al. 'Nature of Cu active centers in Cu-SSZ-13 and their responses to SO_2 exposure'. In: *ACS Catalysis* 8.2 (2018), pp. 1325–1337 (cit. on p. 36).

[100] Ja Hun Kwak et al. 'Following the movement of Cu ions in a SSZ-13 zeolite during dehydration, reduction and adsorption: A combined in situ TP-XRD, XANES/DRIFTS study'. In: *Journal of catalysis* 314 (2014), pp. 83–93 (cit. on p. 36).

[101] Chi Fan et al. 'The influence of Si/Al ratio on the catalytic property and hydrothermal stability of Cu-SSZ-13 catalysts for NH3-SCR'. In: *Applied Catalysis A: General* 550 (2018), pp. 256–265 (cit. on pp. 38, 39).

[102] Jun Wang et al. 'The influence of silicon on the catalytic properties of Cu/SAPO-34 for NOx reduction by ammonia-SCR'. In: *Applied Catalysis B: Environmental* 127 (2012), pp. 137–147 (cit. on p. 38).

[103] Tie Yu et al. 'NH 3-SCR over Cu/SAPO-34 catalysts with various acid contents and low Cu loading'. In: *Catalysis Science & Technology* 3.12 (2013), pp. 3234–3241 (cit. on p. 38).

[104] Shuai Han et al. 'Effect of the hydrothermal aging temperature and Cu/Al ratio on the hydrothermal stability of CuSSZ-13 catalysts for NH 3-SCR'. In: *Catalysis Science & Technology* 7.3 (2017), pp. 703–717 (cit. on p. 40).

[105] Yingxin Feng et al. 'The Role of H+-and Cu+-Sites for N2O Formation during NH3-SCR over Cu-CHA'. In: *The Journal of Physical Chemistry C* 125.8 (2021), pp. 4595–4601 (cit. on pp. 45, 49).

[106] Ja Hun Kwak et al. 'A common intermediate for N2 formation in enzymes and zeolites: side-on Cu–nitrosyl complexes'. In: *Angewandte Chemie International Edition* 52.38 (2013), pp. 9985–9989 (cit. on p. 45).

[107] Upakul Deka et al. 'Confirmation of isolated Cu2+ ions in SSZ-13 zeolite as active sites in NH3-selective catalytic reduction'. In: *The Journal of Physical Chemistry C* 116.7 (2012), pp. 4809–4818 (cit. on p. 46).

[108] Patrick Da Costa et al. 'Spectroscopic and chemical characterization of active and inactive Cu species in NO decomposition catalysts based on Cu-ZSM5'. In: *Physical Chemistry Chemical Physics* 4.18 (2002), pp. 4590–4601 (cit. on p. 46).

[109] Dongwei Yao et al. 'N2O Formation Mechanism During Low-Temperature NH3-SCR over Cu-SSZ-13 Catalysts with Different Cu Loadings'. In: *Industrial & Engineering Chemistry Research* 60.28 (2021), pp. 10083–10093 (cit. on pp. 46, 47).

[110] Sandro Brandenberger et al. 'The role of Brønsted acidity in the selective catalytic reduction of NO with ammonia over Fe-ZSM-5'. In: *Journal of Catalysis* 268.2 (2009), pp. 297–306 (cit. on p. 46).

[111] Lei Ma et al. 'In situ DRIFTS and temperature-programmed technology study on NH3-SCR of NOx over Cu-SSZ-13 and Cu-SAPO-34 catalysts'. In: *Applied Catalysis B: Environmental* 156 (2014), pp. 428–437 (cit. on p. 47).

[112] Lin Chen et al. 'Effect of Al-distribution on oxygen activation over Cu–CHA'. In: *Catalysis Science & Technology* 8.8 (2018), pp. 2131–2136 (cit. on p. 48).

[113] Kirill A Lomachenko et al. 'The Cu-CHA deNO x catalyst in action: temperature-dependent NH3-assisted selective catalytic reduction monitored by operando XAS and XES'. In: *Journal of the American Chemical Society* 138.37 (2016), pp. 12025–12028 (cit. on pp. 48, 49).

[114] Filippo Giordanino et al. 'Interaction of NH3 with Cu-SSZ-13 catalyst: a complementary FTIR, XANES, and XES study'. In: *The journal of physical chemistry letters* 5.9 (2014), pp. 1552–1559 (cit. on p. 48).

[115] Lin Chen et al. 'Mechanism for solid-state ion exchange of Cu+ into zeolites'. In: *The Journal of Physical Chemistry C* 120.51 (2016), pp. 29182–29189 (cit. on p. 48).

[116] Xueting Wang et al. 'Direct measurement of enthalpy and entropy changes in NH3 promoted O2 activation over Cu- CHA at low temperature'. In: *ChemCatChem* 13.11 (2021), pp. 2577–2582 (cit. on p. 50).